1948 *20 Years of Research Progress* *1968*

ARL 68-0023
FEBRUARY 1968

Aerospace Research Laboratories

EXPERIMENTAL STUDY OF A TRANSPIRATION-COOLED, CONSTRICTED ARC

G. G. GRUBER
E. PFENDER
E. R. G. ECKERT
THE UNIVERSITY OF MINNESOTA
MINNEAPOLIS, MINNESOTA

Contract No. AF 33(657)-7380 and F 33615 67-C-1353
Project No. 7063

OFFICE OF AEROSPACE RESEARCH
United States Air Force

NOTICES

When Government drawings, specifications, or other data are used for any purpose other than in connection with a definitely related Government procurement operation, the United States Government thereby incurs no responsibility nor any obligation whatsoever; and the fact that the Government may have formulated, furnished, or in any way supplied the said drawings, specifications, or other data, is not to be regarded by implication or otherwise as in any manner licensing the holder or any other person or corporation, or conveying any rights or permission to manufacture, use, or sell any patented invention that may in any way be related thereto.

Agencies of the Department of Defense, qualified contractors and other government agencies may obtain copies from the

Defense Documentation Center
Cameron Station
Alexandria, Virginia 22314

This document has been released to the

. . . . . .

CLEARINGHOUSE
U.S. Department of Commerce
Springfield, Virginia 22151

for sale to the public.

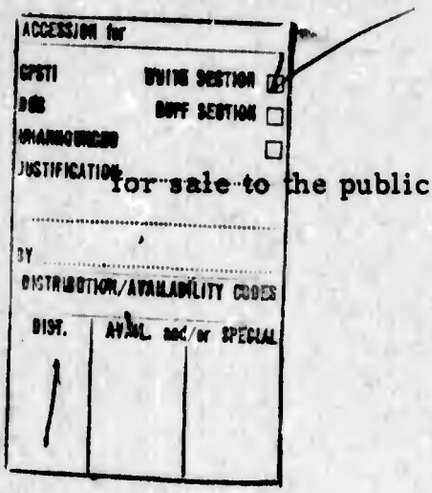

Copies of ARL Technical Documentary Reports should not be returned to Aerospace Research Laboratories unless return is required by security considerations, contractual obligations or notices on a specified document.

400 - April 1968 - CO455 - 30-635

1) AD-668 510 1439 2) 20/9, 20/13, 20/3
4) $3.00/$0.65
5) Minnesota Univ., Minneapolis. Heat Transfer Lab.
6) EXPERIMENTAL STUDY OF A TRANSPIRATION-COOLED, CONSTRICTED ARC. (8) 1 (9) Interim rept. Apr 65-Jun 67,
10) by G. G. Gruber, E. Pfender, and E. R. G. Eckert.
11) Feb 68, (12) 114p (14) -
15) Contract AF 33(657)-7380, F33615-67-C-1353 (16) Proj. AF-7063 (17) -
18) ARL (19) 68-0023
21) -
22) -

avk/5-13-68

MC's

DO NOT PUNCH

Added Entry

68-12

Release Date

Check List for Fields

	DC	SA
1		
2		
4		
5		
6		
8		
9		
10		
11		
12		
14		
15		
16		
17		
18		
19		
21		
22		
23		
25		
27		
29		
30		
33		
34		
35		K

23) Descriptors

(*Plasma generators, Cooling),
(*Electric arcs, Plasma generators),
Evapotranspiration,
Heat flux,
Porous materials,
Mathematical models,
Pressure,
Distribution,
Argon,
Ceramic materials,
Performance (Engineering),
Plasma jets.

25) Identifiers

*Transpiration-cooled arcs,
Pressure distribution.

CG

27) Abstract: See reverse ( ) Page (s) - DD 1473

29) Inventory 19

30) Annotated Title

—

33) Dist. Code 1

34) Serial -

35) Code 165 400

FORM NBS-803 (10-68)

U.S. DEPARTMENT OF COMMERCE
NATIONAL BUREAU OF STANDARDS

DOCUMENT PROCESSING WORKSHEET

USCOMM-DC 35168-P68

ARL 68-0023

EXPERIMENTAL STUDY OF A TRANSPIRATION-COOLED, CONSTRICTED ARC

G. G. GRUBER
E. PFENDER
E. R. G. ECKERT

UNIVERSITY OF MINNESOTA
MINNEAPOLIS, MINNESOTA

FEBRUARY 1968

Contract No. AF 33(657)-7380 and F 33 615-67-C-1353
Project No. 7063

AEROSPACE RESEARCH LABORATORIES
OFFICE OF AEROSPACE RESEARCH
UNITED STATES AIR FORCE
WRIGHT-PATTERSON AIR FORCE BASE, OHIO

FOREWORD

This interim technical report has been prepared by the Heat Transfer Laboratory of the Department of Mechanical Engineering, University of Minnesota, Minneapolis, Minnesota, under Contract No. AF33 (657)-7380 and F33 615-67-C-1353 for the Aerospace Research Laboratories, Office of Aerospace Research, United States Air Force, Wright-Patterson Air Force Base, Ohio. The work reported herein covers the period from April, 1965, to June, 1967 and has been accomplished on Task 706303, "Research on Heat Transfer in Plasma Streams" of Project 7063, "Mechanics of Flight" under the technical cognizance of Mr. Erich E. Soehngen, Director of the Thermomechanics Research Laboratory of ARL.

The authors gratefully acknowledge many helpful discussions with Dr. J. E. Anderson and the assistance of Mr. W. Becker, W. Hagen, J. Heberlein, G. Knowles and R. Willgohs during the experimental phase of these investigations.

Thanks are also expressed to Mr. E. Soehngen and his coworkers for several informative discussions.

ABSTRACT

In this report, experimental work with a transpiration-cooled arc is described. An apparatus has been developed which verifies the analytical prediction that an electric arc can be confined and constricted by an entirely transpiration-cooled wall. The arc has been operated in argon atmosphere with currents ranging from 35 to 160 A. A porous ceramic (ALSIMAG 447) tube has been used as constrictor material. The investigations encompass basic trends of the arc, the constrictor performance, and the flow behavior with their mutual interactions. By introducing some simplifying assumptions, a number of formulae, containing observable quantities, have been derived which are useful for the representation of experimental results and which facilitate their comparison with analytical studies. Three different types of arc characteristics are plotted and used for a description of the transpiration-cooled arc. Results of spectrometric temperature measurements in the arc jet using the 5 mm ID constrictor tube are also included.

Details of an improved transpiration-cooled arc arrangement based on previous experience, are described and some preliminary results obtained with this apparatus are reported.

TABLE OF CONTENTS

LIST OF ILLUSTRATIONS

NOMENCLATURE

A	area
A_1, A_2, A_3	constants def. by Eqs(21), (22), (23)
B	constant def. by Eq(24)
B_T	parameter def. by Eq(40)
c	speed of sound
c_p	specific heat at constant pressure
C	integration constant
D	diameter
E	electric field strength
h	specific enthalpy
h_s	stagnation enthalpy
I	arc current
k_D	specific permeability of porous material
k_g	thermal conductivity of argon
k_w	thermal conductivity of wall material
k_1	integration constant
K^*	parameter def. by Eq(27)
L	length of constrictor tube
$\dot{m}$	mass flow rate
$\dot{m}_0$	cathode flow rate
$\dot{m}_T$	transpirant flow rate
n	parameter def. by Eq(14)
p	pressure

p_s	standard atmospheric pressure
p_R	plenum chamber pressure
p_i	static pressure in flow duct
p_1	p_i at $z/L = 1$
P_r	radiative power per unit volume
P_T	total radiative power per unit arc length
$\dot{q}_w$	heat flux per unit length at $r = r_0$
r	radial coordinate
r_0	inside radius of constrictor
R_z	outside radius of constrictor
R_1	R_z at $z/L = 1$
R	individual gas constant of argon
Re_{De}	Reynolds number for axial flow
Re_{WR}	Reynolds number for transpirant flow
T	temperature
T_0	temperature of inner constrictor wall surface
T_R	temperature of outer constrictor wall surface
T_w	temperature of transpirant at outer constrictor surface
T_∞	gas supply temperature
T_u	turbulence intensity
U	voltage
U_0	overall arc voltage
v	gas velocity
v_r	radial velocity
v_z	axial velocity

$\dot{w}$	mass flow density
$\dot{w}_1$	$\dot{w}$ at z/L = 1
W	parameter def. by Eq(39)
x	mass flow rate per unit length
z	axial coordinate
z_e	axial distance from anode orifice exit
Δp_{wall}	pressure drop across constrictor wall
α	flow parameter, inverse of k_D
β	flow parameter
ζ	normalized axial coordinate
κ	ratio of specific heats
μ	dynamic viscosity
μ_0	susceptibility (in Eq(3) only); temperature independent coefficient of μ
μ_1	temperature dependent coefficient of μ
ρ	mass density
σ	electrical conductivity
σ^*	rms deviation from uniform permeability

Subscripts

c	property of "cold" gas
h	property of "hot" gas

1. INTRODUCTION

Arc-generated plasmas have attracted widespread interest during the past decade in view of possible applications in space flight and reentry simulation, in arc plasma torches for welding, cutting and spraying of refractory materials and plastics, and as useful tools for determining thermodynamic and transport properties at high temperatures. One of the most favored devices for the generation of high-temperature, high-density arc plasmas has been the wall-stabilized, cascaded arc which was first described by Maecker (1). The maximum temperature attainable in an arc column constricted by a water-cooled wall is limited, however, by the highest permissible heat flux to the constrictor, which is about 15 kW/cm^2.

In order to overcome this limitation, transpiration cooling of the constrictor has been suggested. By replacing the water-cooled wall with a porous transpiration-cooled constrictor, the entire heat flux to the wall may be intercepted by the radially orientated gas flow through the porous wall, and this heat is then carried back into the main gas stream. The temperature gradient at the wall is drastically reduced by this cooling mechanism and, therefore, appreciably higher power inputs per unit length of the arc and correspondingly higher axis temperatures are feasible.

From theoretical considerations Anderson and Eckert (2, 3) found that axis temperatures up to about 60,000°K in hydrogen at atmospheric pressure should be attainable. In other gases, such as argon and nitrogen, the possible peak temperatures will be lower due to the high volumetric radiation of these gases at high temperature levels. As long as heat transfer from the hot plasma to the wall of the porous constrictor is mainly caused by conduction and convection,

transpiration-cooling is a very efficient cooling mechanism. If radiation becomes predominant, additional cooling mechanisms for the porous wall (for example, radiation cooling) have to be provided.

Another theoretical study for nitrogen at atmospheric pressure reported by Druxes et al. (4) is in agreement with present theoretical work in this laboratory. A detailed comparison study of a water-cooled and a transpiration-cooled arc based on the same exit mass flow rates has been reported by Watson (5). By comparing peak and average enthalpies of the two arcs, he concluded that there is no advantage in transpiration cooling. The peak enthalpy in the water-cooled arc, however, appears in the entrance section close to the cathode. An arc heater especially designed for a maximum center enthalpy will, therefore, be very short, which invalidates the assumption of a rotationally symmetric arc column and a negligible axial heat flux.

It is felt that a fully-developed transpiration-cooled arc will provide higher peak but probably even lower average enthalpies in the emanating gas. Furthermore, transpiration-cooled arc devices will have higher efficiencies as gas heaters than comparable water-cooled arc devices.

The idea of transpiration-cooled arcs was originally proposed by Mr. E. E. Soehngen of the Aerospace Research Laboratories, WPAFB, and some initial experimental work has been done in his laboratory (6, 7, 8). In his experiments a stack of electrically isolated porous graphite washers mounted in water-cooled holders were used as a transpiration-cooled constrictor tube. To the authors' knowledge there has been no other experimental work reported dealing with an entirely transpiration-cooled arc column.

Due to the promising aspects of transpiration cooling, theoretical as well as experimental work in this field has

been pursued in this laboratory during the past years. The purpose of this technical note is to summarize the experimental work and to compare experimental results with basic trends established by theoretical considerations. The difficulties which are encountered in a desirable comparison of experimental and theoretical results are threefold. First, the theoretical predictions contain a relatively large uncertainty factor due to the uncertainty of thermodynamic and transport properties of most gases at high temperatures. Secondly, the entire plasma column, in the analytical treatment, is assumed to be in a state of local thermodynamic equilibrium. This assumption is, at least in the arc fringes, very questionable. Finally, the flow in the porous tube, which is assumed to be laminar for the analysis, may have various degrees of turbulence, which increases the heat transfer to the wall. Because of these problems a quantitative comparison of analytical and experimental results seems presently impossible. Therefore, comparisons will be undertaken mainly to demonstrate agreement of basic trends.

In the first part of this report the basic equations and assumptions used in the analytical treatment are briefly reviewed. For more details the reader is referred to the literature (2, 3). The experimental studies are preceded by some basic considerations necessary for an interpretation of experimental results. The following section gives a detailed description of the test apparatus along with its instrumentation. Because of the extent to which the properties of the porous material affect the performance of a transpiration-cooled arc, a separate paragraph is devoted to the discussion of these properties. Next, the experimental procedure for acquiring data and a summary and discussion of the results obtained is given. Finally, the conclusions of this investigation are summarized, and

recommendations for continuation of this work are made.

2. THE THEORETICAL MODEL OF A TRANSPIRATION-COOLED ARC

In Fig. 1 a schematic drawing of a transpiration-cooled constricted arc is shown. The arc is confined by a porous cylinder through which the working gas is injected. The arc is termed thermally fully-developed in the transpiration-cooled constrictor when the temperature profile stays axially constant and all of the electric energy dissipated per unit length of the column is used to heat the gas injected per unit length through the porous wall to the mass average enthalpy of the axial flow. The velocity field also becomes developed in the sense that the velocity profiles at various cross-sections are similar to each other.

For the formulation of the governing equations, a fully-developed state of the arc is assumed; the existence of complete LTE (local thermodynamic equilibrium), of rotationally symmetric, laminar flow, and of negligible energy dissipation by internal friction is also postulated. The radial heat flux towards the wall shall be entirely intercepted by the radial inward flow of the transpiring gas and redirected into the main gas stream. The gas properties required for an analysis are assumed to be functions of temperature only (LTE), which implies that the pressure differences in the flow field are moderate. The following equations describe, under these assumptions, conservation of mass, of momentum in axial and in radial direction, and of the energy.

$$\frac{1}{r} \frac{\partial}{\partial r} (r\rho v_r) + \rho \frac{\partial v_z}{\partial z} = 0 \qquad (1)$$

$$\rho v_z \frac{\partial v_z}{\partial z} + \rho v_r \frac{\partial v_z}{\partial r} + \frac{\partial p}{\partial z} = \frac{\partial}{r\partial r}\left(r\mu \frac{\partial v_z}{\partial r}\right) \tag{2}$$

$$\frac{\partial p}{\partial r} = -\rho v_r \frac{\partial v_r}{\partial r} + \frac{2}{3}\frac{\partial}{\partial r}\left[\mu\left(2\frac{\partial v_r}{\partial r} - \frac{v_r}{r} - \frac{\partial v_r}{\partial z}\right)\right]$$

$$+ \mu \frac{\partial}{\partial r}\left(\frac{\partial v_z}{\partial z}\right) + \frac{2\mu}{r}\left(\frac{\partial v_r}{\partial r} - \frac{v_r}{r}\right) - \frac{\mu_o E\sigma}{2\pi}\frac{I(r)}{r} \tag{3}$$

$$\frac{1}{r}\frac{\partial}{\partial r}\left(rk_g \frac{\partial T}{\partial r}\right) + \sigma E^2 - P_r = \rho v_r \frac{\partial h}{\partial r} \tag{4}$$

The coordinate system is indicated in Fig. 1 and the symbols are explained in the Nomenclature. It is found that the radial pressure variation determined by Eq(3) is small in the cases which are of interest.

From an energy balance in the fully-developed region of the arc it is found (2, 3) that the maximum mass-averaged stagnation enthalpy can be expressed by

$$\langle h_s \rangle_{max} = \frac{EI - P_T}{\dot{m}/L} \tag{5}$$

where P_T is the total radiation power emitted per unit length of the fully developed arc column. This equation, which may be considered as a definition of the thermally fully-developed state in a transpiration-cooled arc, states that the power $(EI - P_T)$ available for increasing the gas enthalpy is entirely invested for raising the enthalpy of the cold transpiring gas to the already existing level at any cross section of the constrictor.

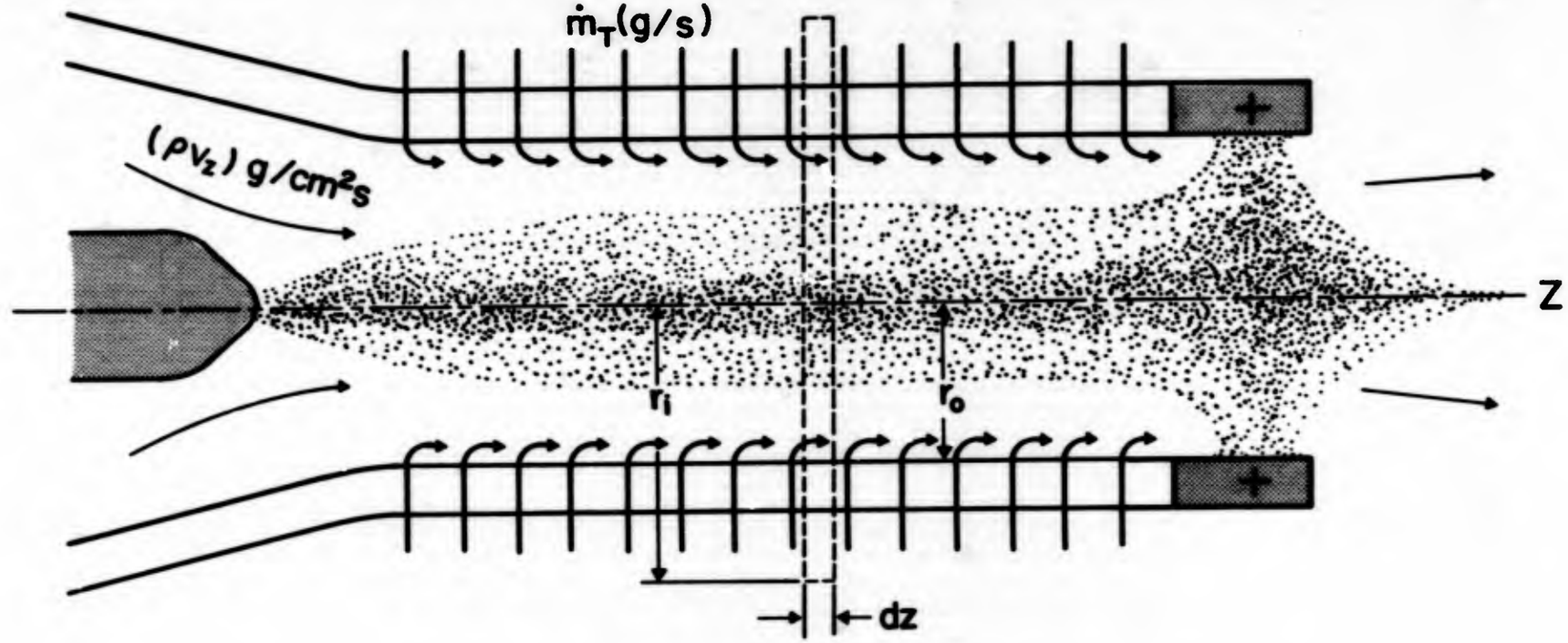

FIG. 1 SCHEMATIC OF A TRANSPIRATION—COOLED CONSTRICTED—ARC

As mentioned before, solutions of these equations have been obtained for hydrogen (2, 3). Presently attempts are being made to extend these calculations to argon and nitrogen. Because of the uncertainty of the transport properties (especially for argon) and the strong influence of the radiation term in the energy equation, convergence problems have been encountered in the numerical solutions. By neglecting the radiation term, numerical results for argon have been obtained. These results are of qualitative interest only and will, therefore, not be further discussed in this report.

3. EXPERIMENTAL STUDIES

3.1 Basic Considerations

3.1.1 Analytical Assumptions

In order to establish a basis for comparison between the analytical predictions and the experimental findings, the assumptions and boundary conditions chosen for the theoretical model must be most realistic yet analytically treatable. This requires, in turn, that experimental evidence be produced, no matter whether or how well the assumptions and boundary conditions are matched to provide this basis for a comparison of analytical and experimental results.

First, it has to be established that transpiration cooling really is the predominant cooling mechanism of the porous tube. Transpiration cooling is defined as a process by which a heat flux towards a porous surface is intercepted by a continuous counterflow of coolant through this surface (9). Heat losses from the outer surface of the porous constrictor tube by radiation, convection, or conduction to otherwise cooled components of the device should be negligible. Film cooling due to coolant leaking into the flow duct, e.g. between the constrictor ends and other components as for example the anode, should also be as small as possible. No current should pass

through any part of the constrictor to cause additional heating. The coolant injection rate should be uniform over the entire constrictor surface, and the existence of a thermally fully-developed region is postulated where the inner wall surface temperature also remains uniform. The axial flow within the duct is supposed to be laminar and far below sonic velocities maintained by moderate pressure gradients. A vortex motion may or may not be superimposed to the axial flow, which is considered to be fully developed in the sense that the velocity profiles are similar in different cross sections of the constrictor tube.

3.1.2 Radial Pressure Distribution

The comparison between experiment and analytical predictions for the thermally fully developed region of the arc will be based on data such as electrical field strength, arc current, radial blowing rate, inner wall surface temperature, wall heat load, and plasma axis temperature. Since it is virtually impossible to take simultaneous local temperature measurements on the inner wall surface while the arc is in operation, formulae must be developed by which the quantities measurable during actual arc operation can be reduced to local quantities of interest in evaluation of the performance of the constrictor. Relatively easily and reliably determinable are the plenum chamber pressure, the integral transpirant flow rate, the gas supply temperature in the plenum chamber, the axial pressure drop in the flow duct and--with less accuracy--the local outside wall temperatures of the constrictor. It is found that the pressure drop necessary to force a certain amount of coolant through the tube wall is very sensitive to the wall temperature. Therefore, an equation for this pressure drop as a function of the mass flow rate is used to correlate the data mentioned above.

The simplest relationship given in the literature (10) is Darcy's law,

$$-\text{grad } p = \frac{1}{k_D} \mu \vec{v} \tag{6}$$

This equation states that knowledge of one property of the material, its specific permeability, k_D, is sufficient to calculate the pressure drop experienced by a fluid of known viscosity as a function of its velocity. A measurement using argon gas in the range of velocities needed for the present experiment has revealed, however, that knowledge of this single property is not sufficient to correlate the data accurately (unless the permeability is taken as a function of the gas velocity). For a more accurate description of the flow, suggestions in the literature (10, 11) offer the choice between raising the velocity to a power different from unity or adding another term to Darcy's law which is proportional to the square of the velocity. The latter yields the so-called Forchheimer equation:

$$-\text{grad } p = \alpha \mu \vec{v} + \beta \rho v^2 \frac{\vec{v}}{v} \tag{7}$$

The first term in this equation represents the viscous forces, the second term the inertia forces. The ratio of these two forces yields a Reynolds number which, according to (12), has proven to be an effective way to correlate data of flow phenomena even in porous media. The characteristic length is given by $\frac{\beta}{\alpha}$, which is an "artificial" length because it equals neither the particle size nor the pore size even in a homogeneous bed. However, it seems to represent an average effective pore diameter. Because of these features, Eq(7) is

chosen as basis for data correlation and found to be accurate enough, although the values of α and β seem to vary slightly from tube to tube of the same specification. If one-dimensional concentric compressible flow is assumed and all external volume forces are neglected, Eq(7) combined with the continuity equation

$$\frac{d}{dr}\ (r\rho v) = \frac{1}{L}\ \mathrm{div}\ \dot{m}_T = o \tag{8}$$

and the perfect gas law

$$p = \rho\ RT \tag{9}$$

R = individual gas constant

yields the following equation:

$$\int_{p_i}^{p_R} 2p\ dp = \alpha\frac{R}{\pi}\ \int_{r_o}^{R_z} \mu(T)\ T\ (r)\ \frac{d\dot{m}_T}{dz}\ \frac{dr}{r} + \\ + \beta\frac{R}{2\pi^2}\ \int_{r_o}^{R_z} T(r)\ \left(\frac{d\dot{m}_T}{dz}\right)^2\ \frac{dr}{r^2} \tag{10}$$

Eq(10) implies perfect circumferential symmetry. Integration over the radius can be executed provided that the functions $\mu(T)$ and $T(r)$ are known.

The function $\mu(T)$ is obtained from the literature (3):

$$\mu = \mu_0 + \mu_1 T + \cdots\cdots$$

with $\mu_0 = 5.6092 \times 10^{-6}$ (μ in $\frac{kg}{ms}$, T in ^oK)

$\mu_1 = 5.4646 \times 10^{-8}$

Higher terms in this expansion may be neglected for the following calculations.

3.1.3 Radial Temperature Distribution

The radial temperature profile T(r) in the porous wall can be calculated, under the simplifying assumption that the gas temperature at the wall is equal to the local temperature of the constrictor, from the energy and mass conservation equations as shown in detail in Appendix A. The task becomes more complicated if, as in the case of porous ceramics, the thermal conductivity of the material depends upon temperature. An equation describing this dependence (14) is of the general form

$$k_w = k_o + \frac{k_1}{T} + k_2 T^3 + \cdots \qquad (11)$$

For the present investigation, as a first approximation k_w is taken to be a constant effective value because, at the present time, the experimental methods are not accurate enough to determine either k_1 or k_2; an approximate value for k_w in the range $300^oK < T < 600^oK$ is furnished by the manufacturer of the constrictor material.

The differential equation governing the temperature profile is obtained from an energy balance (see Appendix A)

$$\frac{d}{dr}\left[2\pi r\, dz\, k_w \frac{dT}{dr} + c_p T \dot{m}_T\right] = 0 \qquad (12)$$

Integration of Eq(12) yields

$$k_w \frac{dT}{T-K_1} = -\frac{c_p}{2\pi} \frac{\dot{m}_T}{dz} \frac{dr}{r} \qquad (13)$$

Using

$$n = \frac{c_p}{2\pi k_w} \tag{14}$$

and

$$x = \frac{d\dot{m}_T}{dz} \tag{15}$$

and integrating Eq(13) from r to R_z and T to T_R, one obtains

$$\frac{T - K_1}{T_R - K_1} = \left(\frac{R_z}{r}\right)^{nx} \tag{16}$$

To determine the integration constant K_1, one boundary condition must be known. Because it is found experimentally that practically no heat loss out of the plenum chamber occurs --in agreement with the assumption--one has the following boundary condition for the outside wall:

$$k_w \left.\frac{dT}{dr}\right|_{r=R_z} = -\frac{c_p}{2\pi R_z} \times (T_R - T_w) + k_g \left.\frac{dT}{dr}\right|_{r=R_z} \tag{17}$$

The differential equation governing the temperature profile of the gas in the plenum chamber is identical to Eqs(12) and (13), if k_w is replaced by k_g, which is assumed to be independent of temperature for the temperature range under consideration. Thus, the radial gas temperature distribution becomes

$$\frac{T - T_\infty}{T_w - T_\infty} = \left(\frac{R_z}{r}\right)^{\frac{c_p x}{2\pi k_g}} \quad , \quad R_z < r < \infty \tag{18}$$

Eq(18) satisfies the boundary condition which requires that for $r \to \infty$, i.e. $r >> R_z$, the temperature in the plenum chamber approaches the gas supply temperature T_∞ with sufficient accuracy. Due to the blowing against the radial heat flux, the gas temperature, T_w, at the outer constrictor wall surface will always be somewhat lower than the temperature, T_R, of the surface material, but from a certain point $R_z - \delta$ on, the gas temperature and the porous wall temperature will be essentially equal. Estimates of the boundary layer thickness δ indicate that it is very small compared to the wall thickness and, therefore, δ is considered to be zero; i.e., a jump in gas temperature equal to $T_R - T_W$ is assumed to occur at $r = R_z$.

If Eqs(16) and (18) are introduced into Eq(17), the constant K_1 turns out to be equal to T_∞. Eq(16) which describes the temperature distribution in the porous material now assumes the form

$$T = T_\infty + (T_R - T_\infty)\left(\frac{R_z}{r}\right)^{nx} \quad , \quad r_o \leq r \leq R_z \tag{19}$$

3.1.4 Data Reduction Formula

Eq(19) introduced into Eq(10) yields, after integration over the radial coordinate,

$$A_1 \ln\left(\frac{R_z}{r_o}\right) x + A_2 (T_R - T_\infty) \left[\left(\frac{R_z}{r_o}\right)^{nx} - 1\right] +$$

$$A_3 (T_R - T_\infty)^2 \left[\left(\frac{R_z}{r_o}\right)^{2nx} - 1\right] + B \frac{T_\infty}{R_z} \left(\frac{R_z}{r_o} - 1\right) x^2 +$$

$$B \frac{T_R - T_\infty}{R_z} \left[\left(\frac{R_z}{r_o}\right)^{nx+1} - 1\right] \frac{x^2}{nx+1} - \frac{p_R^2 - p_i^2}{p_s^2} = 0 \qquad (20)$$

$$A_1 = \alpha \frac{R}{\pi p_s^2} \mu_o T_\infty \left(1 + \frac{\mu_1}{\mu_o} T_\infty\right) \qquad (21)$$

$$A_2 = \alpha \frac{R}{\pi p_s^2} \frac{\mu_o}{n} \left(1 + 2\frac{\mu_1}{\mu_o} T_\infty\right) \qquad (22)$$

$$A_3 = \alpha \frac{R}{\pi p_s^2} \frac{\mu_o}{n} \frac{\mu_1}{2\mu_o} \qquad (23)$$

$$B = \beta \frac{R}{2\pi^2 p_s^2} \qquad (24)$$

To make Eq(20) dimensionless every term in this equation has been divided by the square of the standard atmospheric pressure, p_s.

Eqs(19) and (20) describe the flow through the porous constrictor at a particular axial location z. If the boundary values p_i, p_R, r_o and R_z are constant with respect to z, the quantities T_R and x are also constant over the whole constrictor

length, L, provided the arc column is fully developed over this entire length. In this case $x = \frac{m_T}{L}$, and Eq(20) contains only quantities which are known or measurable during actual arc operation. Thus, if it is once experimentally checked for its validity it can be used to determine the consistency of the data.

3.1.5 Derivation of Tube Shape

Because r_o is chosen to be independent of z to form a constant area flow duct for the plasma column, there exists necessarily an axial pressure gradient, $\frac{dp_i}{dz}$, which is not always negligible. If the gradient is big enough x will become a function of z unless it is compensated for by axial variation of either p_R or R_z. A variation of p_R would require segmentation of the plenum chamber and, consequently, of the constrictor. This, however, would in turn cause a discontinuity in x which should be avoided. Therefore, it has been decided to provide for a proper axial variation of R_z. R_z as a function of z can be found from Eq(20) after elimination of T_R using Eq(19) in the form

$$T_R = T_\infty + (T_o - T_\infty) \left(\frac{r_o}{R_z} \right)^{nx} \tag{25}$$

As shown in Appendix B, all terms which are independent of z can be combined into a single parameter K* which depends upon T_o and m_T only. The tube shape is then given by

$$R_z(z) = R_1 \exp \left(K^* \frac{p_1^2 - p_i^2(z)}{p_s^2} \right) \tag{26}$$

(R_1 is the outside tube radius at the downstream end, the maximum value which $R_z(z)$ can assume; p_1 is the minimum value for $p_i(z)$ at the same location). Fortunately, K* contains terms only which are either independent of or depend linearly on T_o, as one can see from Eq(27). An order-of-magnitude analysis reveals that for most of the parameter values of interest, the first term, $A_1 x$, predominates and can, therefore, be used for an approximate evaluation of Eq(26).

$$K^* = x \left\{ A_1 + B \frac{T_\infty}{R_1} x + (T_o - T_\infty) \left(\frac{r_o}{R_1} \right)^{nx} \left[A_2 n + A_3 (T_o - T_\infty) 2n \frac{r_o}{R_1} \right]^{nx} + B \frac{x}{R_1} \right\} \qquad (27)$$

As can be seen from Eqs(26) and (27), the tube shape is exactly correct only for one given transpirant mass flow rate, $\dot{m}_T$, one corresponding pressure distribution, $p_i(z)$, and, strictly, for only one value of T_o. However, as long as the pressure drop across the wall is large compared to the axial pressure gradient in the flow duct, there exists a wide range of flow rates and pressure distributions for which the deviation from a uniform transpirant mass flow distributions can be neglected.

3.1.6 Axial Pressure Distribution

In order to obtain the general shape of the pressure profile and some approximate data, one-dimensional frictionless compressible flow and absence of volume forces is assumed. From Bernoulli's Equation in the form

$$\rho v \frac{dv}{dz} + \frac{dp}{dz} = 0 \tag{28}$$

(v = flow velocity in axial direction) and the perfect gas law, Eq(9), one obtains

$$\left[\left(\frac{\dot{w}}{p}\right)^2 - \frac{1}{RT}\right] \frac{d(p^2)}{dz} = \frac{d(\dot{w}^2)}{dz} + 2\dot{w}^2 \frac{d(\ln RT)}{dz} \tag{29}$$

In the case of thermally fully developed flow,

$$\frac{d(\ln RT)}{dz} = 0,$$

and integration of Eq(29) yields

$$\dot{w}^2 RT = p^2 \ln \frac{C}{p^2} \tag{30}$$

By introducing the downstream boundary conditions $p = p_1$ and $w = w_1$ one can determine the integration constant C, as shown in Appendix C. Eq(30) takes the form

$$\frac{p_1 \dot{w}}{p \dot{w}_1}^2 = 1 + \frac{2}{RT} \left(\frac{p_1}{\dot{w}_1}\right)^2 \ln \frac{p_1}{p} \tag{31}$$

This equation will be used in the following section.

3.1.7 Two Channel Arc Model

As long as the temperature profile, T(r), in an arc column is not known, T and R are unknown functions of the radius, r. For an approximate analysis the following model (15) is proposed (see Fig. 2): the radial temperature distribution is assumed

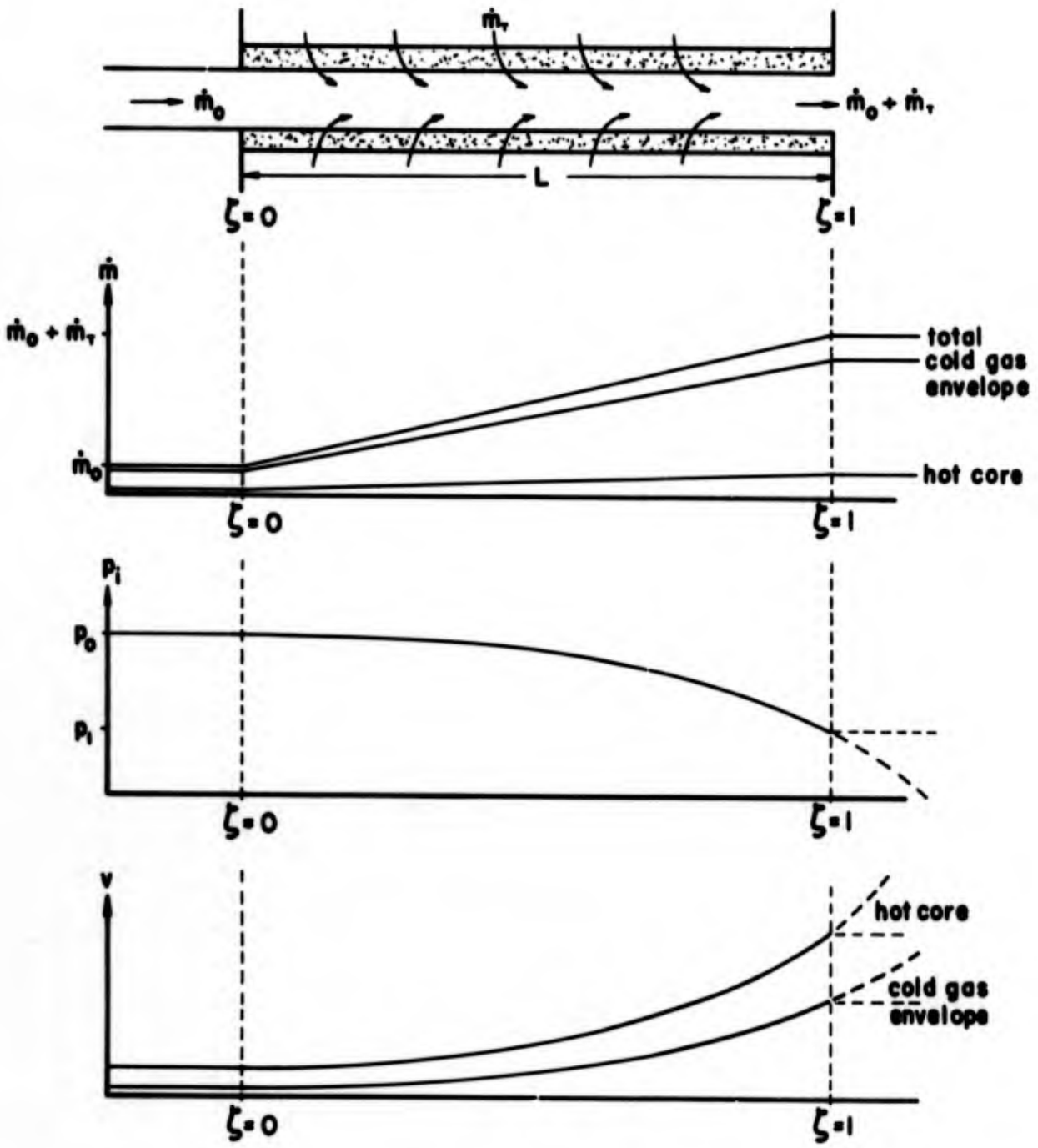

Temperature and radius of the hot gas core as well as the cold gas envelope are constant over the total length.

FIG. 2 Two Channel Arc Model (Qualitative Illustration)

as a step function, where the hot core shall be at a constant temperature T_h and the "cold" gas envelope at a constant temperature T_c. The pressure is taken to be indepenuent of the radial coordinate. Thus, there are two simultaneous equations in the form of Eq(31), one each for the hot core and for the cold envelope. As the actual temperature profile in the thermally fully developed region--which, for this calculation, is postulated to cover the whole porous constrictor length, L,--does not change axially, the respective flow areas of the hot and the cold gas can be assumed to be constant:

$$A = A_h + A_c \tag{32}$$

($A = \pi r^2$ = flow area) The total mass flow then is

$$\dot{m} = \dot{w}_c A_c + \dot{w}_h A_h = \dot{m}_o + \dot{m}_T \tag{33}$$

The condition of a fully developed arc requires that the electric energy dissipated per unit length is absorbed by the gas introduced per unit length reaching the mass average enthalpy. If the radiative power P_T in Eq(5) is neglected one obtains

$$EIL = \dot{m}_T \langle h \rangle \tag{34}$$

$$\langle h \rangle = \frac{\dot{w}_c A_c h_c + \dot{w}_h A_h h_h}{\dot{m}} \tag{35}$$

The arc current is obviously carried in the hot core; thus

$$I = \sigma E A_h \tag{36}$$

As shown in Appendix C, Eqs(28) through (36) yield the following relations:

$$\frac{AE}{I} = \frac{1}{\sigma}\left[1 + \sqrt{\frac{R_c T_c}{R_h T_h}}\left(\frac{h_h - h_c}{\langle h\rangle - h_c} - 1\right)\right] \tag{37}$$

$$\frac{\dot{m}(z)}{\dot{m}_o + \dot{m}_T} = \frac{p(z)}{p_1}\left[1 - W \ln\left(\frac{p(z)}{p_1}\right)\right]^{\frac{1}{2}} \tag{38}$$

Where

$$W = 2B_T\left(\frac{Ap_1}{\dot{m}_o + \dot{m}_T}\right)^2 \tag{39}$$

and

$$B_T = \left[\frac{\langle h\rangle - h_c}{h_h - h_c}\left(\sqrt{R_h T_h} - \sqrt{R_c T_c}\right) + \sqrt{R_c T_c}\right]^{-2} \tag{40}$$

Eq(37) can be used to determine the hot core temperature, T_h, from measurements of E, I, and $\dot{m}_T$, if the temperature, T_c, of the cold envelope is known. If T_c has to be estimated, the inner wall surface temperature is obviously the lower limit for such an estimate. The upper limit is given by $\langle T\rangle = \frac{EIL}{\dot{m}_T c_p}$, which is an average temperature obtained from the mass average enthalpy. Equation (40) is needed as an intermediate step to calculate the parameter W defined by Eq(39). Numerical values of Eq(38), then, shown in Fig. 3, describe the axial pressure distribution in the flow duct. The general shape of the curves in Fig. 3 is independent of the radial temperature profile as long as the arc is thermally fully developed.

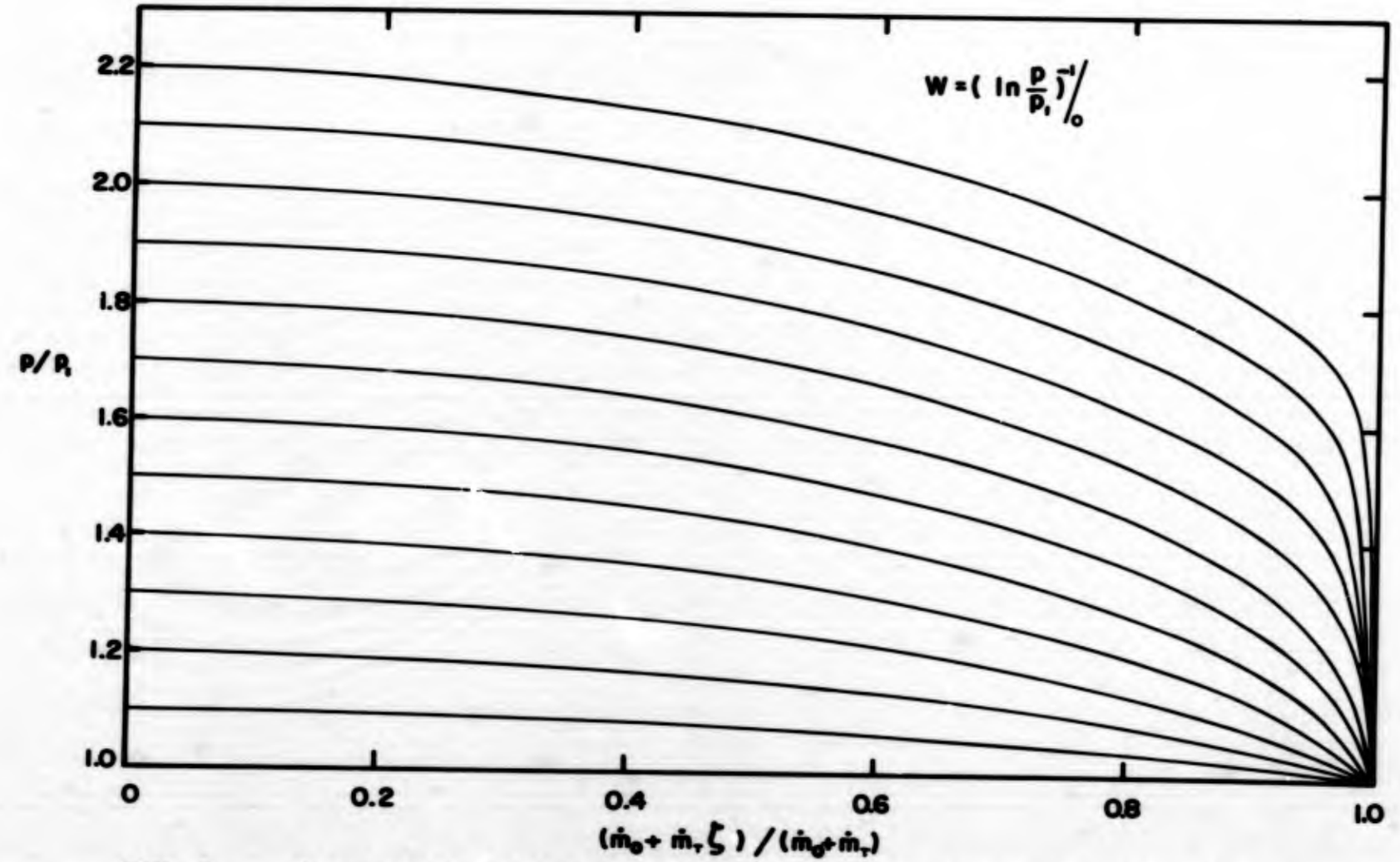

FIG. 3 Normalized Axial Pressure Distribution (Computed Curves), Argon

3.1.8 Limiting Flow Conditions

Equation (38) is also valid for cold gas flow only, i.e., without operating an arc; the parameter, B_T, is then equal to $R_c T_c$ (which still implies that there is a heat source which keeps T_c axially constant). This offers the opportunity to calculate the conditions under which a choked flow situation will be reached. With the arc in operation the cold gas envelope carries a much higher fraction of the total mass flow than the hot core. Sound velocity at the downstream end of the constrictor tube is reached, when

$$\frac{\dot{m}_c}{A_c} = \frac{\dot{m}_o + \dot{m}_T}{A} = \rho_c c_c = \frac{p_1}{R_c T_c} c_c \qquad (41)$$

Since

$$c_c = \sqrt{\kappa_c R_c T_c} \qquad (42)$$

and for

$$\frac{\dot{m}_o + \dot{m}_T \zeta}{\dot{m}_o + \dot{m}_T} \approx 0$$

which, for $\dot{m}_T >> \dot{m}_o$, corresponds nearly to the upstream end of the porous constrictor, one obtains

$$\ln \frac{p^*}{p_1} = \frac{\kappa_c}{2} \qquad (43)$$

For $\kappa_c = 1.65$ the critical pressure ratio is

$$\frac{p^*}{p} = 2.28$$

This means that the gas will be streaming at sonic velocity in the downstream cross-section of the constrictor if the stagnation pressure in the upstream end of the constrictor reaches p^* given by Eq(43). Raising the upstream pressure further causes p_1 to increase proportionally, leaving the gas velocity constant but increasing its density. Using Eq(43) one can now calculate values for the parameter B_T from the relation

$$B_T = \frac{1}{\kappa} \frac{\dot{m}_o + \dot{m}_T}{A p_1}^2 \qquad (44)$$

In this way the influence of the electrical arc parameters and of the flow rates on the flow conditions with respect to the choked flow situation can be determined.

3.2 Test Apparatus and Instrumentation

3.2.1 Test Apparatus

The test apparatus used to take most of the measurements described in this report is shown schematically in Fig. 4. It incorporates a commercial F-40 plasma torch used as a starting device and as a cathode section. The constrictor and anode section, placed on top of the torch, is designed and built to allow various types of measurements with as little modification as possible. It also provides for unobstructed viewing of the entire porous constrictor tube, which proved to be extremely useful in detecting glowing of the outer constrictor surface, leaks, detached probes etc. This section has the shape of a flat cylinder consisting of the constrictor tube and a coaxial plexiglas tube as outside

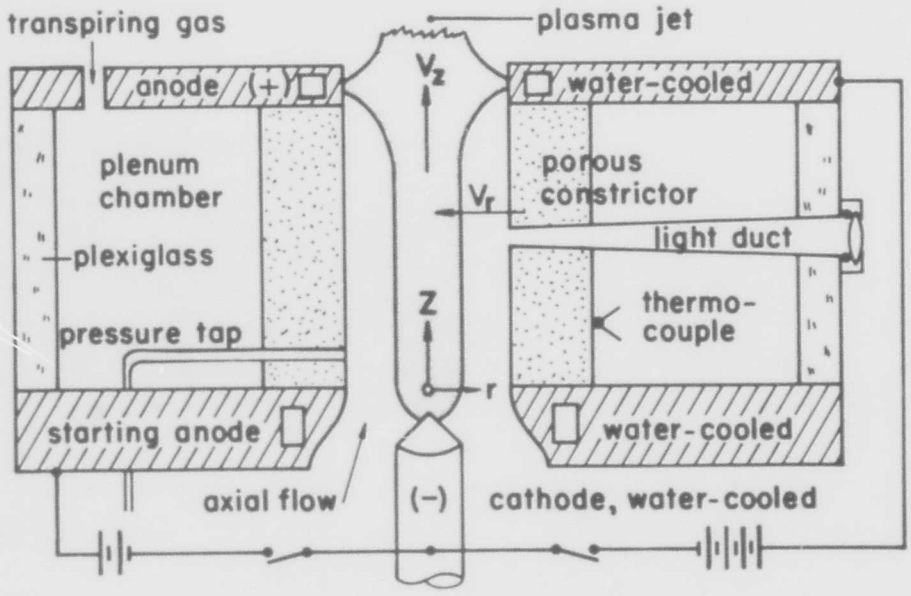

FIG. 4 Schematic of Transpiration-Cooled Arc Apparatus

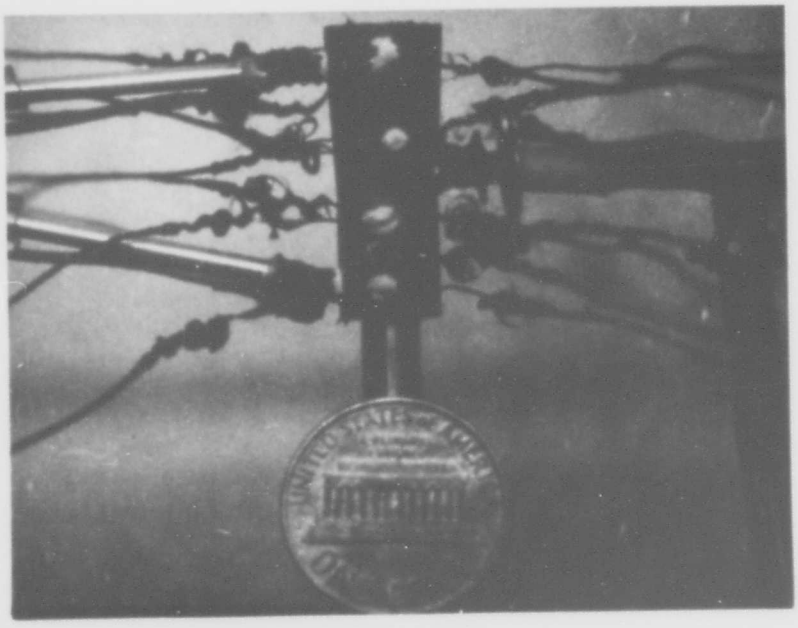

FIG.5 MATCHED CONSTRICTOR TUBE WITH PROBES ATTACHED

wall of the plenum chamber sealed between a base and a top plate. The inner bore of the constrictor tube is aligned with the anode opening of the plasma torch to form a straight flow channel for the arc column, which extends from the cathode in the torch up to the main anode. The latter is incorporated in the top plate of the device. The space between the outer constrictor wall and the plexiglas tube, the so-called plenum chamber, is big enough to house pressure and electric potential connections as well as thermocouples which are attached to the constrictor tube. The bottom plate is fitted with a large number of feed-throughs in order to conduct pressures and electrical signals to the outside instrumentation. The important dimensions of the apparatus are:

flow duct diameter	5 mm
cathode section length (cathode tip to auxiliary anode top)	17 mm
porous constrictor length	25 mm
main anode thickness	6 mm
constrictor OD	10 mm
plenum chamber diameter	115 mm

Numerous technological problems are encountered with this apparatus. The seals required on the porous tubes at the end faces and around the holes through the constrictor wall cause particular difficulties. In both cases a gas-tight seal covering the whole wall thickness is required. The wall temperature variation lies between room temperature and 1600^{o}K on the inside, with a steep radial temperature gradient in the wall of the order of several hundred ^{o}K/mm. For the end faces, a seal consisting of an elastomer, which allows for thermal expansion of the constrictor tube, must be used. Experimentation with different sealants has revealed that a thin film of spreadable self-vulcanizing GE-RTV-106 silicone rubber yields an almost perfect seal against the

water-cooled surfaces of the torch and the top anode. In this case the tube ends and the anode surfaces had to be machined within close tolerances. For the attachments of thermocouples, potential taps, etc. to the constrictor wall, a special high temperature cement, called Astroceram, which withstands temperatures up to 2500°C is found to be suitable.

3.2.2 Probes Attached to Constrictor Tubes

An example of a porous constrictor, fitted with some probes is shown in Fig. 5 (the shaft serves as holder). The two stainless steel tubes on the left-hand side of the picture are pressure and electric potential probes. They are flush with the inside wall of the constrictor and at this point have an OD of 1 mm. Outside the constrictor tube, the ID and OD of the probes are about three times larger, and plastic tubes are connected to the very end of the probes, leaving a large area of metal in contact with the surrounding gas for cooling. The holes through the porous constrictor wall are of the smallest size which can be sandblasted with the equipment available. Drilling of these holes with solid carbide drills is a more accurate but also a much more time-consuming method. The right-hand side of Fig. 4 and 5 shows the light duct for the photoelectric temperature measurement of the inner constrictor wall surface. The slightly conical outer part, which incorporates a pressure tap, is fitted with a teflon sleeve to the finned 2 mm-ID stainless steel part, which is cemented into the porous wall. Eight chromel-constantan thermocouples are attached to the outside wall of the tube, four of which can be seen in the photograph; the other four are on the back side. Tubes without light ducts but with as many as nine pressure and potential probes are also used. The light duct at times also serves as a leak-proof connection to the porous tube, which permits insertion of a movable

tungsten wire probe through the constrictor wall. A traversing mechanism mounted outside of the plenum chamber allows moving of the probe radially into the flow channel and, thereby, closer to the plasma column. For measuring the gas temperature in the outer regions of the plenum chamber, a thermocouple, soldered to a piece of copper foil, is located close to the plexiglas wall.

3.2.3 Electrical Circuit

The arc power is supplied by a 40 kW Miller saturable reactor rectifier followed by a ripple filter. A commercial RF-starting unit is used to start the arc between the cathode and the auxiliary anode in the F-40 torch. The circuit necessary to transfer the arc from the auxiliary anode to the main anode (as described in section 3.4) consists of three knife switches and a one-Ohm water-cooled resistor. A 100 A Weston shunt is modified for coaxial pick-up of the voltage signal to measure the amount of ripple in the arc current, which is found to be less than 1% rms. It has been established that the electrical circuit is mainly inductive.

3.2.4 Other Instrumentation

The main parameters, arc current, total voltage, mass flow rate and plenum chamber pressure are measured using a shunt with a millivoltmeter, a regular moving coil voltmeter, a rotameter-type flow meter, and a Bourdon tube pressure gauge, respectively. The gas inlet pressure to the flowmeters is also measured and kept constant by a pressure regulator. The cooling water for the cathode, the auxiliary, and the main anode is circulated by a rotary pump at a pressure of 120 psi. The axial pressure distribution in the plasma channel is measured using a special manifold panel which provides for

a variety of differential measurements by means of a 50-cm water and 50-cm mercury manometer and precision 60 psi Bourdon tube pressure gauge. Accurate temperature readings from the various thermocouples are obtained by using either a hand-balanced potentiometer or a Dymec multichannel digital voltmeter. The latter instrument, which has an input impedance of 10^7 Ohm, is also used for the potential measurements. For the determination of a possible current dependence of these potential measurements, a series circuit of variable resistors ranging from 0 to 100 Ohms up to values from 0 to 10^6 Ohms is connected in parallel to the Dymec voltmeter to control the electron current drawn to the probes.

The instrumentation required for the photoelectric temperature measurement of the inner wall surface is shown in Figs. 6 and 7. The light duct inside the plenum chamber, shown in the schematic of the optical system is the one actually photographed in Fig. 5. The converging lens focuses the light beam on the entrance diaphragm of the photomultiplier housing. The diverging lens spreads the light out over most of the photocathode in order to decrease the light and, therefore, the photo current density. The filter limits the wavelengths received to the yellow region of the spectrum. The electric triggering circuit, shown in Fig. 7, works as follows. With switch S_B closed, relay B is energized and the arc can be struck. After proper adjustment of the operating parameters, the manual shutter S_1 in the multiplier housing is opened, simultaneously closing switch S_s. Relay A is energized and turns the recorder on. It also causes relay B to fall off after a delay time of about 100 ms, determined by its own resistance and the capacitor C_1. As relay B falls off, the arc current is interrupted and the solenoid operated shutter S_2 is opened after a delay time of 15 ms determined by the

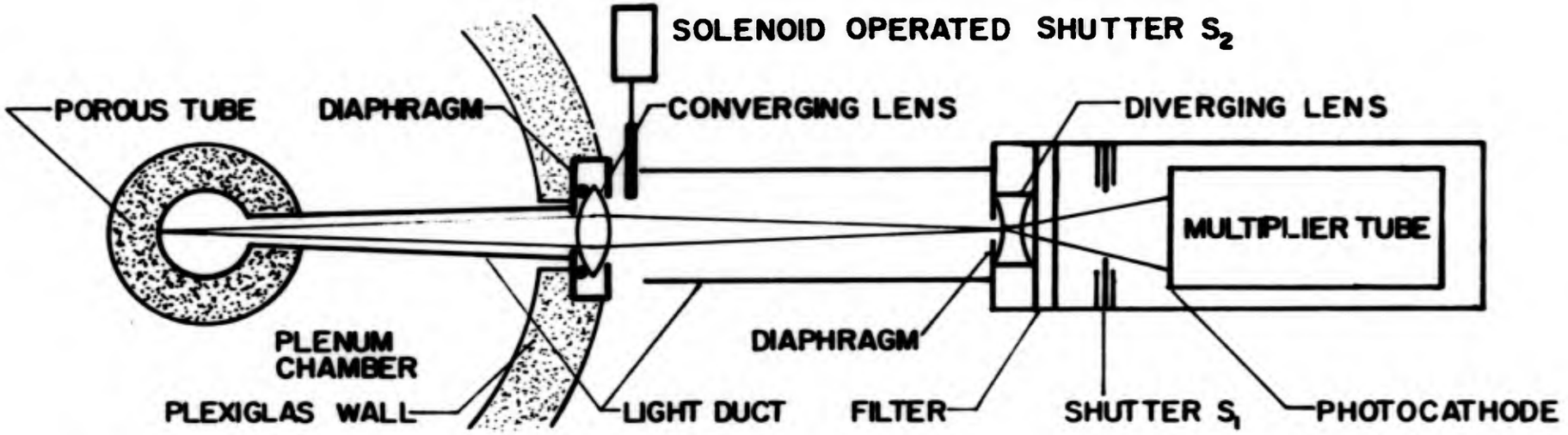

FIG. 6 SCHEMATIC OF OPTICAL SYSTEM FOR PHOTOELECTRIC TEMPERATURE MEASUREMENT

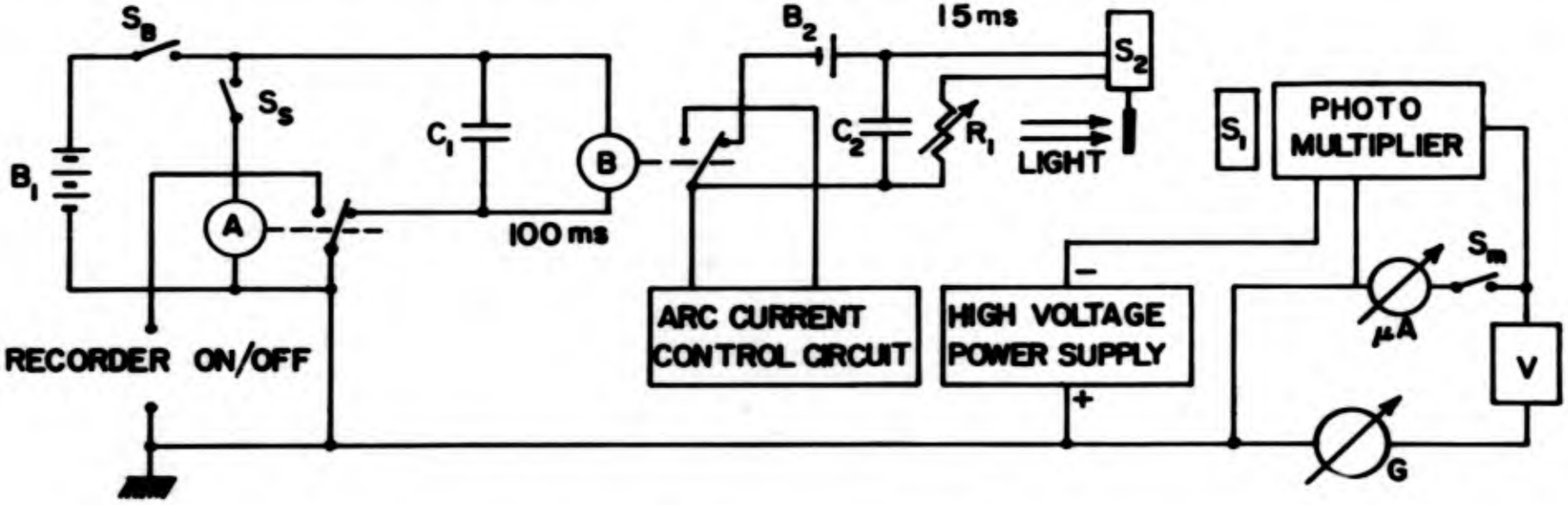

FIG. 7 CIRCUIT DIAGRAM FOR PHOTOELECTRIC TEMPERATURE MEASUREMENT

the capacitor C_2 and the variable resistor R_1. The multiplier (DuMont Type 6292, blue sensitive) now transforms the light signal into an electrical current signal which is amplified by the solid state amplifier V and measured by the galvanometer G in the recorder (Honeywell 1508 Visicorder). The delay time of 100 ms is needed for the recording paper to reach its speed of 2 m/s; the delay time of 15 ms elapses from the moment the arc current control unit receives the signal to shut off until the arc has decayed. The amplifier V serves also as a current-limiting device to protect the galvanometer if the shutter S_2 opens too early, in which case the immense light intensity from the plasma column could cause damaging currents in the photomultiplier. In order to calibrate the recorded photomultiplier signals for the appropriate temperature range, the porous tube is simply replaced by a tungsten ribbon lamp as shown in Fig. 6 (secondary standard). When the switch S_m is closed, the photomultiplier output can be measured directly by the microammeter, and the high voltage supplied to the tube is adjusted according to the manufacturer's recommendations. Provision is made to place a rotating segmented disc in the light path close to the same plane in which the shutter S_2 is located to check the reliability of the output signal.

3.2.5 Modified Test Apparatus

The design of this test apparatus is based on the experience gained with the previous one and represents a definite improvement in many ways. It is shown schematically in Fig. 8. In the new design the length of the transpiration-cooled column and the inner radius of the constrictor walls are exactly twice those of the old design. This increase in scale facilitates the installation of pressure and potential probes and

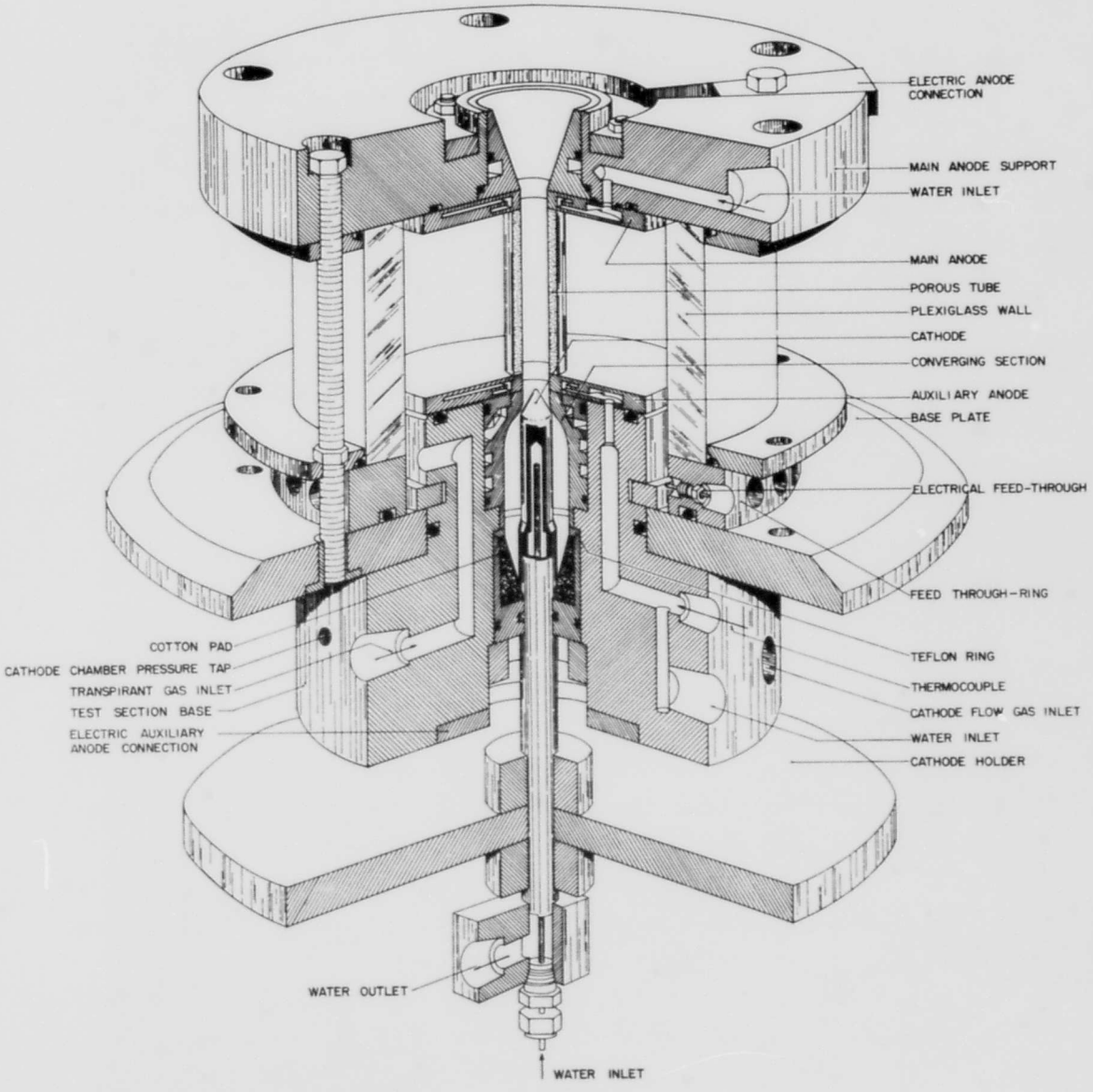

FIG. 8 SCHEMATIC OF TRANSPIRATION-COOLED ARC APPARATUS

yields more truly "local" measurements.

In the old apparatus, the F-40 torch incorporates a number of components: auxiliary anode, cathode, inlet section for supplying gas with a swirl component, and the necessary cooling water supplies. Thus, to replace the torch a rather complicated base (see Fig. 8) is required. The base is made from the finest-grade linen phenolic material with a high electrical resistance, a low thermal conductivity, and high mechanical strength.

Because the gas inlet section is an integral part of the apparatus, separate from the base, inlet sections with varying degrees of swirl components may be used to determine their effect on the stability of the arc column. The mounting of the cathode provides easy exchange of cathodes without disassembling the plenum chamber and porous tube seals. Independent water supplies to the auxiliary anode, cathode and converging section, equipped with thermocouples for heat balances, are provided.

To reduce the length of the water-cooled part of the arc column, both the main and the auxiliary anodes are made as thin as possible. This provision is especially important for the main anode since spectroscopically determined temperature profiles of the plasma jet, emanating from this anode, reflect the characteristic distribution of a transpiration-cooled arc only if the influence of the water-cooled anode portion on these profiles is kept sufficiently small. The disc-shaped anode is designed to accomplish this while providing efficient heat transfer in the region in which the arc attaches (see Fig. 9). The anode is only 4 mm thick so that the arc column is transpiration-cooled over more than 80% of its length.

To obtain a sufficiently high water flow rate through the anode, the flow passages are maximized within the given limits of the anode size. The annular flow passage at the

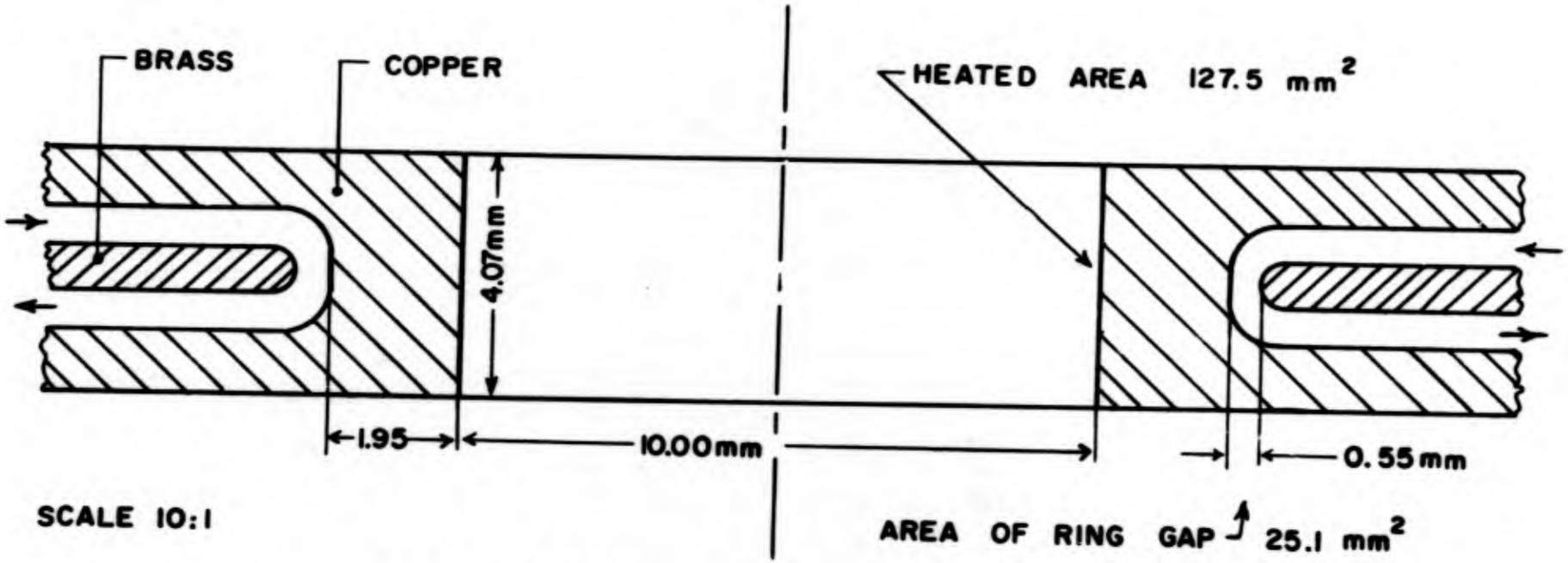

FOR A WATER FLOW RATE OF 0.1 $\frac{kg}{s}$

FLOW VELOCITY IN RING GAP IS 4.0 $\frac{m}{s}$

REYNOLDS NUMBER THERE IS 2.25×10^4

COOLING CAPACITY IS 3.35×10^3 $\frac{kw}{m^2 \cdot K}$

FIG. 9 NEW ANODE DESIGN

center of the anode matches with the size of the other flow passages in the anode. The maximum flow rate is determined by the water pressure level which the thin copper walls of the anode can withstand without deforming.

The Reynolds number in the porous constrictor tube is determined primarily by the arc current and the flow rate of gas required for cooling. Since these parameters cannot be arbitrarily adjusted, efforts to reduce the turbulence level are confined to removing turbulence from the gas blown axially past the cathode. To accomplish this a tight cotton pad, held in place by a conus of copper wire mesh as shown in Fig. 10, is used. The flow above the pad has no swirl component. The flow area as plotted in the lower part of Fig. 10 is monotonically decreasing towards the cathode tip to reduce remaining fluctuations in the flow to a minimum. The shape of the converging section near the cathode has been determined using the charts of Rouse and Hassan (16) with the location of the inflection point chosen to minimize the wake behind the cathode.

The main anode support is designed so that a water-cooled disc can be mounted directly beneath the anode without modifying the apparatus. This is desirable in order to determine the effect of a water-cooled section on the heat transfer to the anode and on the temperature profiles in the arc jet. The necessity of minimizing the amount of time required to change porous tubes is reflected in the design of the apparatus. A separate feed-through ring is used so that all solder connections of the potential probes and thermocouples in the porous tube can be made before the apparatus is assembled. O-ring seals are used throughout the apparatus for safe sealing and fast assembly.

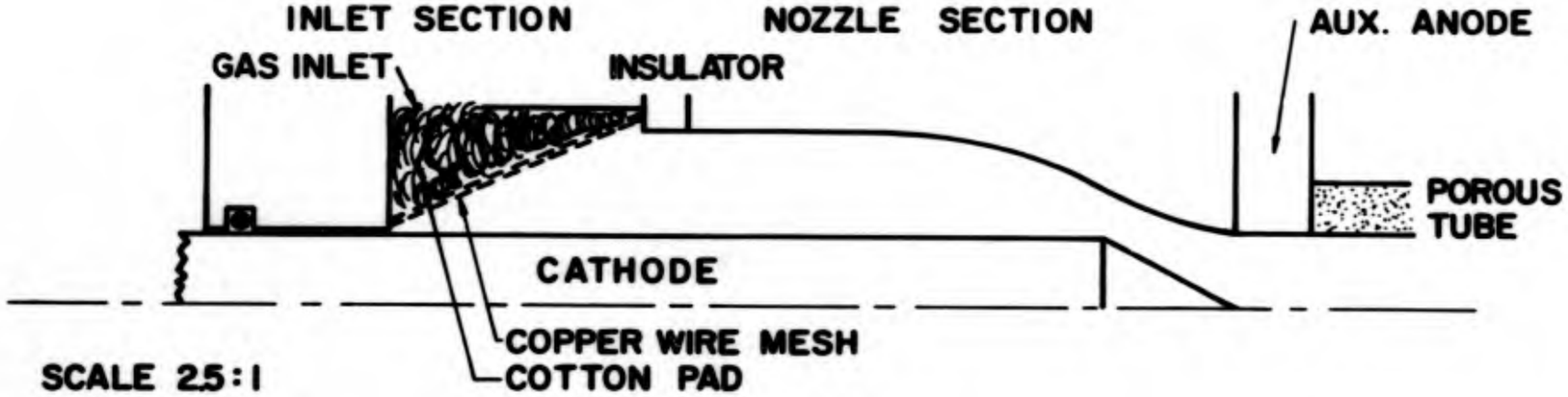

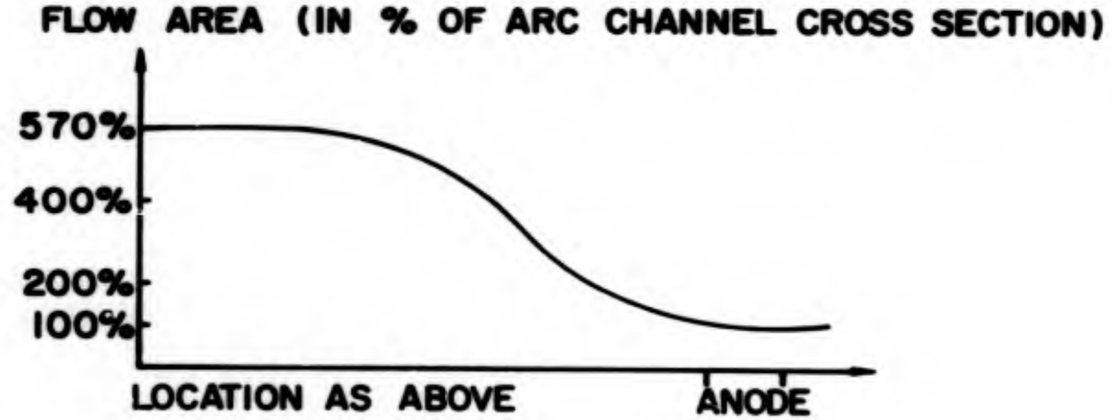

FIG. 10 CATHODE FLOW CHANNEL

3.2.6 Instrumentation of Modified Test Apparatus

The instrumentation of the new apparatus is functionally identical with the one described in sections 3.2.2 and 3.2.4. For the measurements reported here a porous tube is used which is 5 cm long, 10 mm I.D., 16 mm O.D., and has the following attachments (see Fig. 11): 9 tungsten wires of ½ mm O.D. (as potential taps), each 5 mm apart from the next and staggered in angles of 180^{o} around the tube; 6 thermocouples peened into the outer wall surface, grouped in opposing pairs in the upstream, center, and downstream portions of the constrictor.

The electrical power for these experiments is obtained from a 200 kW Rectifier filtered to a ripple level of about 1%. Due to the steep voltage-current characteristic of this power supply the current range of stable arc operation is appreciably larger than that obtained with the other unit.

A closed-loop distilled-water circuit is employed for those components of the apparatus which must be water-cooled, and its working pressure is about 200 psi. The instrument panel shown in Fig. 12 is used to control and measure the water (right-hand side) and gas (left-hand side) flow rates; the center portion is the manifold panel mentioned in 3.2.4. Most of the electrical connections and switches are housed in the left-hand side of the panel.

A hot-wire anemometer is temporarily used in connection with this apparatus.

3.3 Constrictor Material and Its Properties

3.3.1 Selection Criteria for Material

The selection of the material for porous constrictors is based on four criteria:

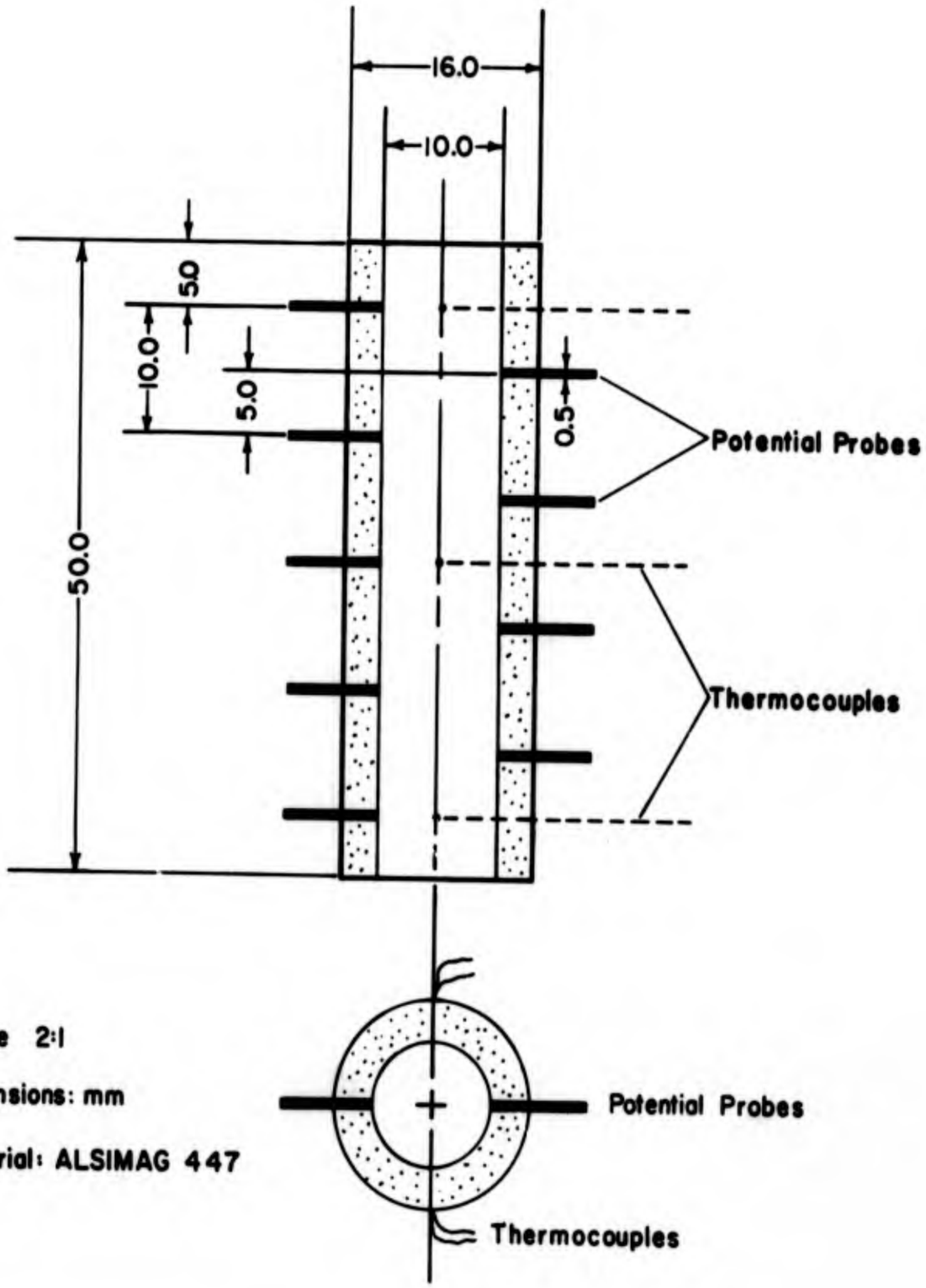

FIG. 11 Probe Location on Constrictor Tube

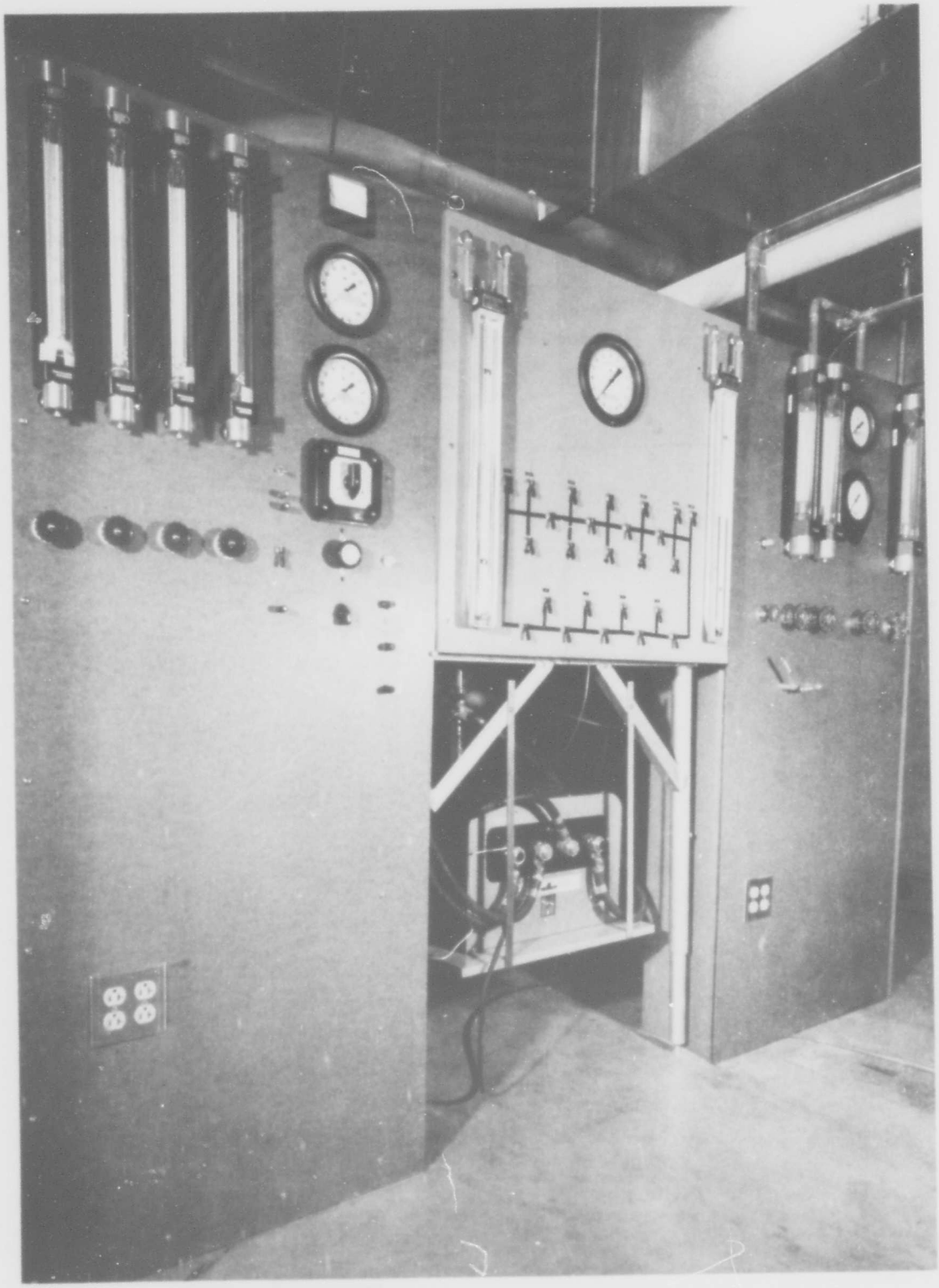

FIG. 12 INSTRUMENTATION

1) high electric resistivity
2) high safe operating temperature
3) high thermal shock resistance
4) permeability range

An electrical non-conductor is chosen to eliminate the need for segmentation of the constrictor because of the unsolved technological difficulties involved in segmentation. The problem lies in maintaining a tight seal between conducting segments and separating insulating sealants at high temperatures and simultaneous high heat loads.

A high but still safe operating temperature is required for the constrictor material to keep the transpirant flow rates within reasonable limits. Although there are a number of ceramic materials with very high melting points, only a few can be made porous and are commercially available.

High resistance to thermal shocks includes a qualitative relationship between the properties of thermal conductivity, thermal expansion coefficient, and tensile or compressive strength. In the case of a cylindrical tube, sudden heating of the inner wall surface or sudden cooling of the outer wall surface will cause a radial temperature gradient in the tube wall; according to the thermal expansion coefficient the inner portions of the wall will tend to expand or the outer portions will tend to contract. In either case the inner portion then experiences a circumferential compressive force and the outer a corresponding circumferential tensile stress. As the thermal conductivity and the compressive and tensile strength increase and the thermal expansion decreases, the material's resistance to thermal shock improves.

With transpiration-cooled arc constrictors a shock heating or cooling situation occurs when the arc is struck or extinguished, respectively. To minimize this effect, a starting procedure has been developed as outlined in 3.4.1.

A similar situation to shock heating can prevail even under steady-state conditions for a transpiration-cooled tube, because the radial temperature gradient becomes steeper with increasing steady heat load on the inner surface. This effect could possibly restrict the applicability of nonconducting constrictor materials to lower arc power levels.

The permeability of the constrictor--for a given wall thickness--should be in a range such that the radial pressure drop across the wall during arc operation is several times larger than the axial pressure drop in the flow duct. The reason for this is discussed under 3.1.5. The material actually chosen is ALSIMAG 447, a product of American Lava Corporation. It has, according to the manufacturer, a very high specific electrical resistivity, a safe operating temperature of 1250°C, a linear thermal expansion coefficient of 6×10^{-7} per °K (at room temperature), a thermal conductivity of 1.25 $\frac{W}{m\,^{o}K}$, a compressive strength of 18,500 psi, a tensile strength of 2,500 psi, and 14 to 17% of interconnected void space (porosity); its chemical composition is given as $2\ MgO \cdot 2\ Al_2O_3 \cdot 5\ SiO_2$.

3.3.2 Permeability and Pore Size Measurement

The experimental setup for permeability measurements is shown in Fig. 13 schematically. In this arrangement the flow direction is inverted, i.e., the gas is supplied to the inside of the porous tube and escapes into the open atmosphere, which does not influence the measurements, since the pressure drop across the wall does not depend on the flow direction. Thus, Eq(10) can be applied to describe the pressure drop across the tube wall as a function of the mass flow rate using the gas temperature as a parameter. In this case the wall and the gas temperature are equal, uniform, and known.

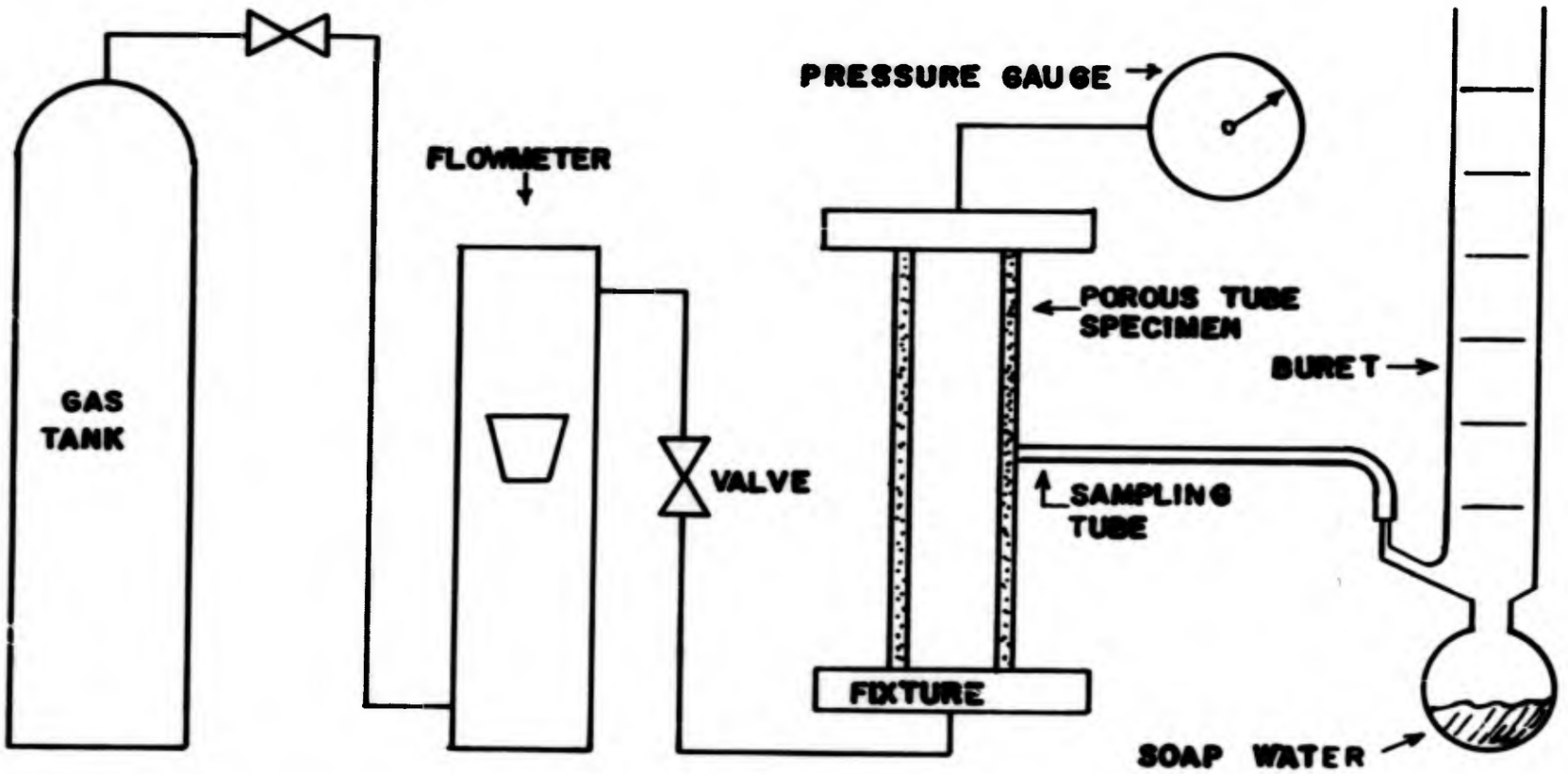

FIG. 13 SET-UP FOR PERMEABILITY DISTRIBUTION MEASUREMENT

Therefore, the radial integration is greatly simplified. If a porous tube with constant O.D. is used, the local mass flow rates are uniform as long as the axial pressure drop inside the tube stays negligibly small, as is the case for the range of flow rates of interest. Thus, the terms $\frac{d\dot{m}_T}{dz}$ in Eq(10) can be replaced by $\frac{\dot{m}_T}{L}$, and one obtains

$$p_R^2 - p_i^2 = \alpha \frac{\mu R T \dot{m}_T}{\pi L} \ln\left(\frac{R_z}{r_o}\right) + \beta \frac{RT}{2} \left(\frac{\dot{m}_T}{\pi L}\right)^2 \frac{R_z - r_o}{R_z r_o} \qquad (45)$$

This equation is used to determine the coefficients α and β by comparing experimentally determined curves $\dot{m}_T$ vs. $(p_R - p_i)$ with Eq(45). A curve for an individual tube is shown in Fig. 32. Two different tubes have been tested, a small one with 5.0 mm I.D. and a larger with 10.0 mm I.D. The results are shown in Table I. The specific permeability k_D is equal to the inverse of the flow parameter α and describes the pressure drop in case of very low flow rates according to Eq(6). The average effective pore diameter is obtained from β/α as explained under 3.1.2. The porosity of the tube material, based on the water absorption is assumed to be 15% (manufacturer specifies the range 14% to 17%). Based on this value one can calculate from β/α the average distance from pore edge to pore edge as well as the average number of pores per mm^2 (see Table I). The latter values are believed to be reliable within a factor of 2.

Another method of measuring the pore size is the so-called bubble pressure test; it is based on a theory by M. Cantor (17) which has been checked experimentally by various investigators (18). For this test the tube is held in

TABLE I

	Small Tube	Big Tube
inside diameter	5.0 mm	10.0 mm
outside diameter	10.0 mm	16.0 mm
length	25.0 mm	50.0 mm
flow parameter α	$4.56 \times 10^{6} \frac{1}{mm^2}$	$5.86 \times 10^{5} \frac{1}{mm^2}$
flow parameter β	$6.23 \times 10^{4} \frac{1}{mm}$	$6.20 \times 10^{3} \frac{1}{mm}$
specific permeability k_D	$2.19 \times 10^{-7} mm^2$	$1.71 \times 10^{-6} mm$
av. eff. pore diam. $\frac{\beta}{\alpha}$	$13.6 \times 10^{-3} mm$	$10.6 \times 10^{-3} mm$
av. distance from pore edge to pore edge	$25.5 \times 10^{-3} mm$	$20.2 \times 10^{-3} mm$
number of pores per mm^2	1.03×10^{3}	1.7×10^{3}
largest eff. pore diameter	$18.0 \times 10^{-3} mm$	$38.0 \times 10^{-3} mm$
av. eff. pore diameter	$10.8 \times 10^{-3} mm$	$18.8 \times 10^{-3} mm$
largest pore opening	$28.8 \times 10^{-3} mm$	$67.5 \times 10^{-3} mm$

a fixture, submerged in water and allowed to saturate with water. Then the gas pressure inside the tube is raised very slowly (several minutes) and measured on a mercury manometer. The pressure at which the first bubble leaves the tube wall is noted; it gives a value for the effective size of the largest pore. Then the pressure is increased again until bubbles appear uniformly over the entire tube surface; this pressure reading gives a value which is close to the average effective pore size. When the pressure is slowly reduced, the pressure at which the last bubble disappears gives the largest actual pore opening at the surface. The equation to correlate these pressures to pore diameters is

$$D = \frac{30\gamma}{p} \tag{46}$$

(D = pore diameter in 10^{-3} mm; γ = surface tension of water [72 dynes/cm at room temperature]; p = pressure in mm Hg). The error limit of these measurements is also given by a factor of about 2. The results are presented in Table I.

The photomicrograph in Fig. 14 shows the tube material approximately 100 times enlarged. The dark spots of varying size are the pores as they show up in light impinging under a 30^{o} angle. The pore diameters appear to range from 5×10^{-3} mm to 50×10^{-3}mm. Averaging over the distance from the outer to the inner wall surface it is conceivable that the average effective pore diameter is between 10^{-2} mm and 2×10^{-3} mm as shown in Table I. The distribution of the pores does not seem as homogeneous as is desirable. However, the most important quantity, the uniformity of the permeability, cannot be judged from this photograph alone.

Obviously, the permeability of a porous material is extremely nonuniform if one considers an area the size of a pore. As

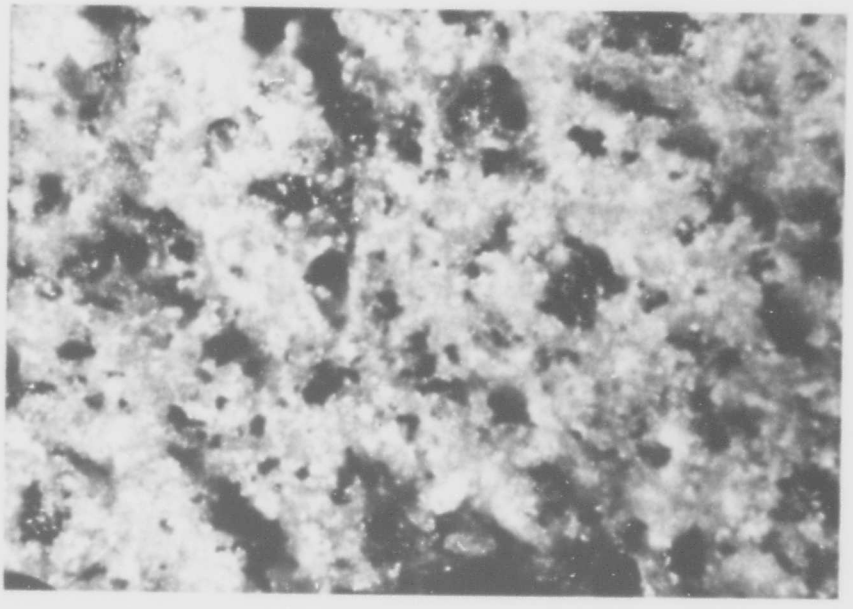

FIG. 14 PHOTOMICROGRAPH OF ALSIMAG 447
(100 TIMES ENLARGED)

the area considered increases and covers more and more pores, a uniform permeability is approached. The big tube with the dimensions given in Table I has been tested for the uniformity of its permeability as shown schematically in Fig. 13. Five different sizes of sampling tubes are used with probe areas ranging form 0.8 to 35.5 mm^2. As an extremely sensitive flow meter serves a soap bubble in a side-filling buret. The time required for a soap bubble to pass through a certain volume is proportional to the gas flow rate. By randomly sampling the whole tube surface one obtains a large number of measurements, the arithmetic mean of which corresponds to the bulk flow rate diminished by the ratio of the sampling area over the sampled surface area. With basic statistical formulae one can calculate the rms-deviation σ and normalized distribution curves as shown in Fig. 15. The curve labeled $\sigma = 4.08\%$ states, for instance, that a deviation of plus or minus 8% from uniformity will be encountered in just 1% of all measurements if the surface is randomly sampled. The sampling area corresponding to this σ-value can be found from Fig. 16. The starred σ in this graph indicates that the random experimental error inherent to all these measurements was subtracted. An approximate equation for the area dependence of the deviation from uniform permeability, as described by σ^* and given on the graph, is

$$\sigma^* = \frac{0.0708}{\text{probe area}} = \frac{120}{\text{number of pores covered}} \qquad (47)$$

The maximum value which σ^* can assume is 100%, which corresponds to "perfect" nonuniformity. Eq(47) indicates that this situation is reached when the probe area is decreased to 0.0708 mm^2, which on the average covers about 120 pores. A probe of this size is likely to hit a spot which is completely

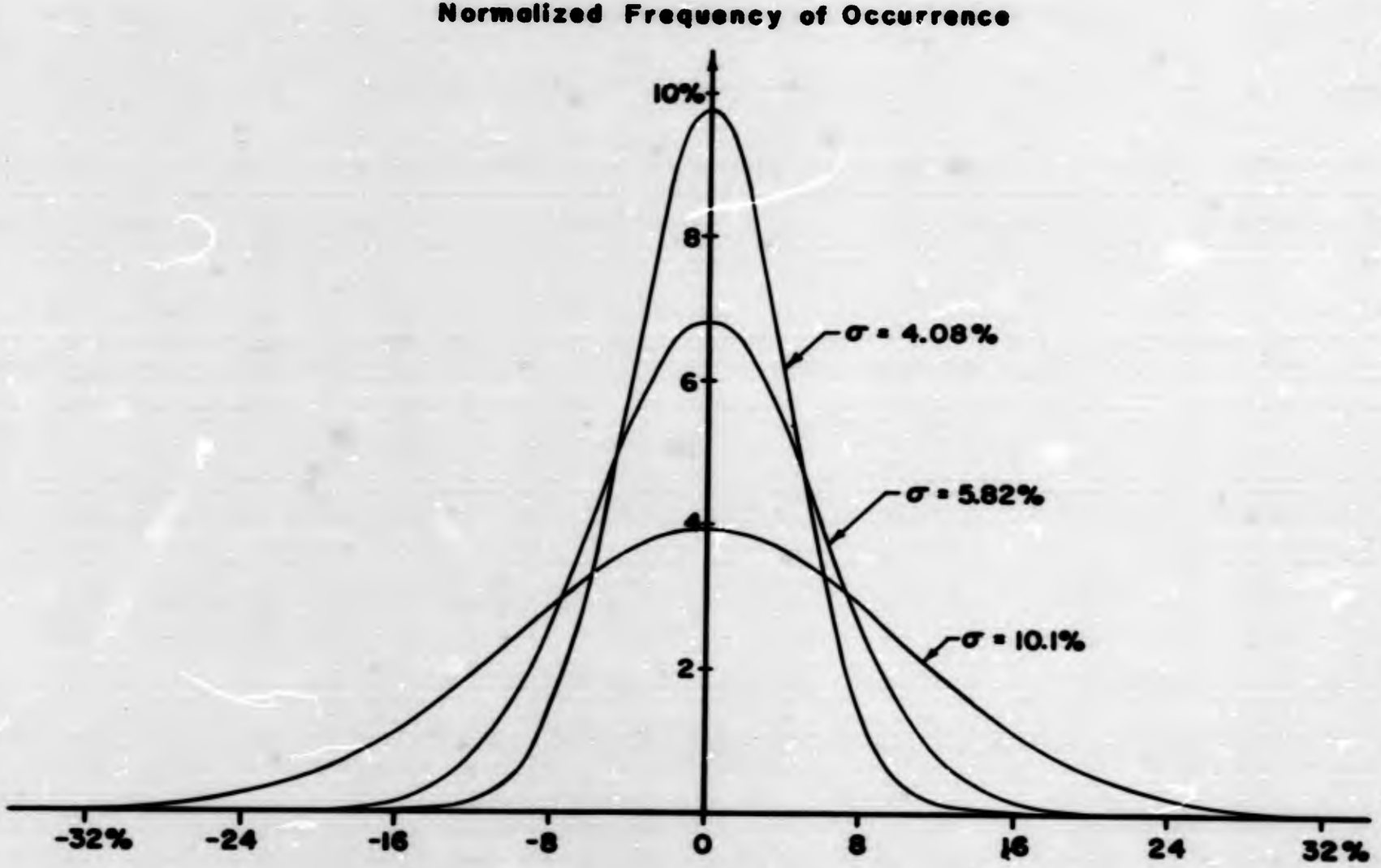
Normalized Frequency of Occurrence
10%
8
6
4
2
σ = 4.08%
σ = 5.82%
σ = 10.1%
-32%
-24
-16
-8
0
8
16
24
32%
Deviation from Uniform Permeability

FIG. 15

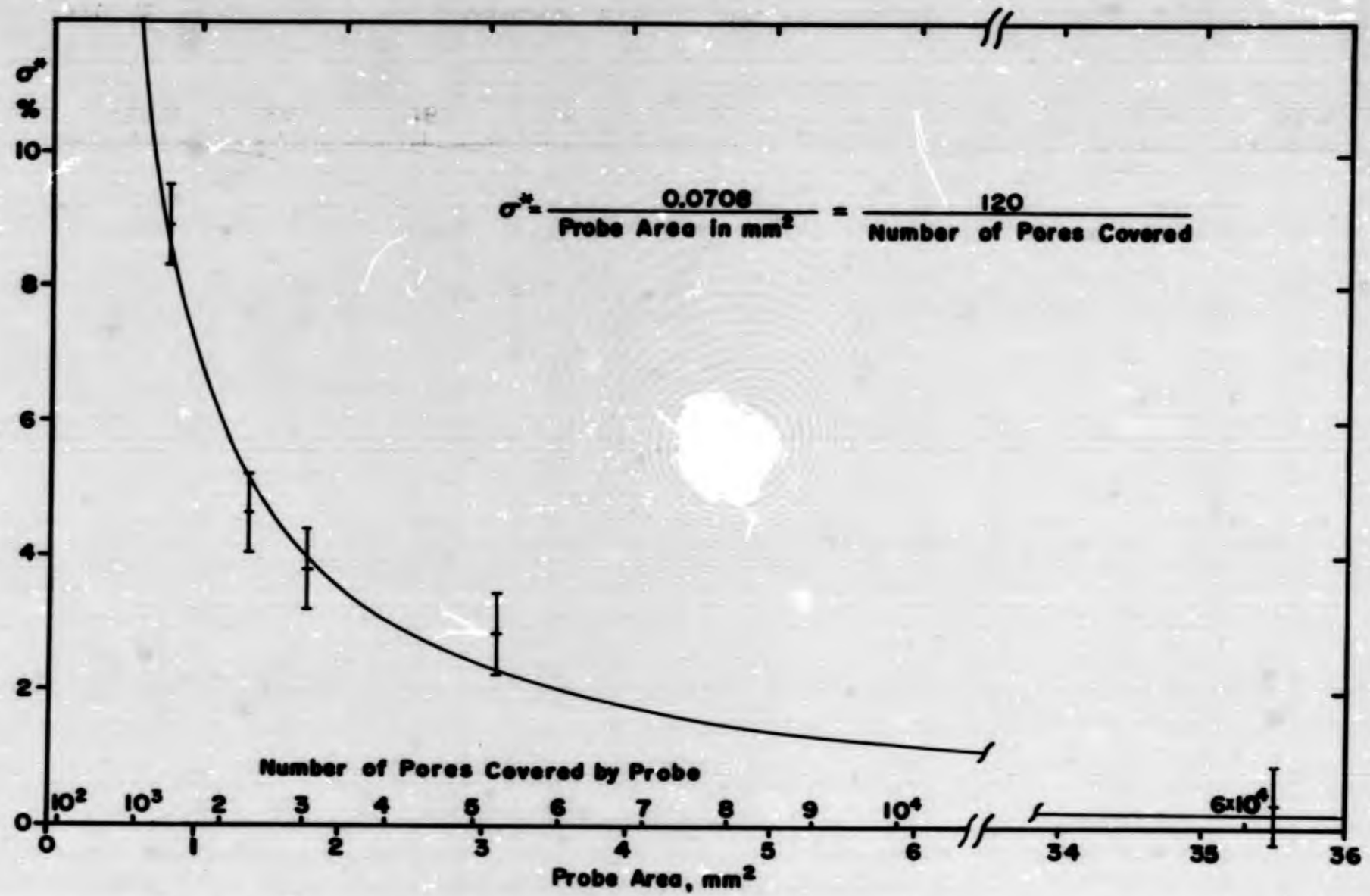

FIG. 16 Area Dependence of Deviation from Uniform Permeability

impermeable and--if circular--has a diameter equal to 30 average effective pore diameters. Because this figure is obtained by extrapolation, its accuracy is probably within ±50%, with the lower limit being most reasonable (see Fig. 14).

3.3.3 Local Temperature Distribution

It is obvious that the tube will no longer fulfill its function when the hottest point on the inner wall surface reaches the melting temperature, although other points may be relatively cold. To prevent such a failure the transpirant mass flow rate must be kept at sufficiently high values. This flow rate, on the other hand, must be limited in order to avoid high levels of turbulence and choked flow conditions. Therefore, the local temperature distribution on the inner wall surface is of great interest. The areas, that can assume a temperature different from the average, range from the size of a single pore to a major portion of the constrictor tube. A relatively large area may become hotter or colder than the average, in the thermally fully-developed region, if the arc axis is not identical with the axis of the apparatus or if a nonuniform transpirant mass flow distribution caused by mismatched wall thickness and pressure drop across the wall exists. Very small areas (in the order of the pore size) deviate in temperature for other reasons: nonuniform permeability distribution and/or the fact that the energy radiated to the tube wall and absorbed by the solid material can only be transferred to the transpiring gas if there is a finite temperature gradient. The latter problem is discussed in a paper by J.E. Anderson (19), and the results published permit an estimate of the highest temperature gradient to be expected in case of perfectly uniform permeability. Using experimental values given in later sections of this report one obtains the following limits: if less than 85% of the heat load received by the wall is transferred

by radiation, the temperature of the solid and the gas on the inner wall surface are not distinguishable; however, if 100% of the heat is transferred by radiation, the temperature difference is

$$\Delta T = 0.18\ (T_w - T_\infty) \tag{48}$$

Estimates for a nonuniform permeability distribution are more difficult. If one bases an estimate on the deviation from uniformity as given by Eq(47), one obtains an effective porosity of about 0.6% in the worst case. Provided the analysis (19) still holds in this porosity range, one obtains by extrapolation that $\Delta T = 0$ again if less than about 85% of the heat is transferred by radiation. An extrapolation for the case of 100% radiative heat transfer is not possible.

If attention is focused on areas as large as several thousand cross-sections of pores, a change in the local temperature due to a change in the local flow rate can be estimated from the consideration that the local heat flux per unit length to the wall, $\dot{q}_w$, is approximately equal to the average value defined by

$$\dot{q}_w \approx \langle \dot{q}_w \rangle = \frac{\dot{m}_T}{L}\ c_p\ (T_o - T_\infty) \tag{49}$$

From Eq(49) one finds that

$$\Delta T_o = \frac{\Delta \dot{m}_T}{\dot{m}_T}\ (T_o - T_\infty) \tag{50}$$

The upper limit for $(T_o - T_\infty)$ is about 1300°C, and a local change in mass flow rate of 10% would correspond to a change in local inner wall surface temperature of 130°C.

If the transpirant mass flow distribution deviates from uniformity in large portions of the porous tube, its effects on the wall temperature are covered by the general theory of the transpiration-cooled arc (as long as the arc is concentric with the tube).

3.3.4 Determination of Tube Shape

Tubes of two different shapes are employed: a cylindrical tube with constant O.D., and a somewhat conical one with an analytically determined O.D. increasing in axial direction. The cylindrical tube is used for experiments in the low current regime where only moderate flow rates are required and, therefore, the axial pressure gradients in the flow duct are also moderate. In this range the transpirant mass flow distribution deviates only slightly from uniformity as far as variations caused by the pressure gradient are concerned. In the higher current and, thus, flow rate ranges, however, this uniformity must be improved by shaping the outside wall of the porous constrictor as discussed in Section 3.1.5. Eq(26) is used to calculate the tube shape (see Appendix B). The pressure distribution $p_i(z)$ is taken from measurements reported in Section 3.4.3. Although these results have been obtained using a cylindrical tube, they are accurate enough for a first approximation for reasons outlined in Section 3.1.5. The analytically determined tube shape and the actual shape of the tube are shown in Fig. 17. Experimental evidence shows that the accuracy achieved is sufficient for the range of flow rates for which the tube was designed (see Section 3.5.2).

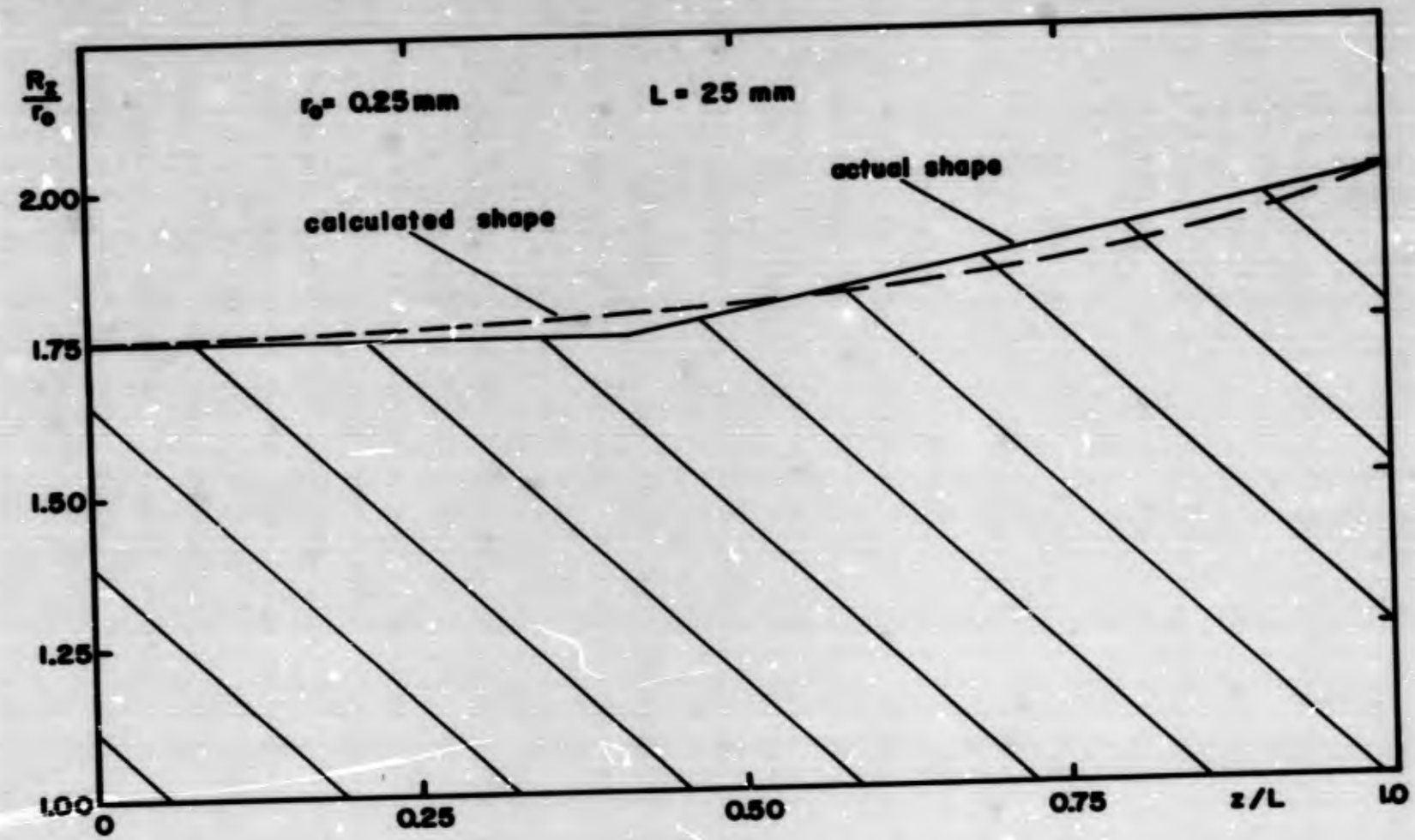

FIG. 17 Matched Tube Shape

3.4 Experimental Procedure and Results

3.4.1 Starting of the Arc

With both test apparatus an auxiliary arc is struck between the cathode and the auxiliary anode preionizing this gap by means of a high-frequency discharge. As soon as the porous constrictor is preheated, the arc is transferred to the main anode and the auxiliary anode is electrically disconnected.

3.4.2 Measurement of Main Parameters

Main parameters of the arc are the overall voltage, the arc current, the transpirant mass flow rate, the cathode mass flow rate, the plenum chamber pressure, and the total axial pressure drop in the flow duct. These parameters are integral quantities which are relatively easily and accurately measurable. If they assume identical values for any two arcs, the arcs are considered to be identical. Typically, the arc current is used as the independent parameter; the gas flow rates are adjusted to ensure stable operation of the arc and integrity of the constrictor, and the overall voltage and the pressures assume their respective values accordingly.

Table II gives the range of parameters for the experiments evaluated in this report. For the small apparatus the full range of capability is covered, whereas for the big apparatus it is only the lower portion of the range, as indicated by the values for the axial pressure drop. Data for individual experiments are given in the following section.

3.4.3 Pressure Distribution

The axial pressure distribution in the flow duct is measured during actual arc operation using a constrictor tube equipped with pressure probes as described in Section 3.2.2. All probes are connected to individual toggle valves which are

TABLE II

	5.0 mm ID apparatus	10.0 mm ID apparatus
current	35 - 100 A	60 - 160 A
overall voltage	80 - 120 V	55 - 100 V
cathode flow rate	generally 0.5 g/s	generally 0.25 g/s
transpirant flow rate	0.4 - 2.5 g/s	1.0 - 7.5 g/s
plenum chamber pressure	25 - 90 psi	6 - 30 psi
axial pressure drop	1.5 - 12 psi	0.2 - 5.2 psi

opened consecutively and thereby connected to the manometers on the manifold panel mentioned in Section 3.2.4. Two pressure distribution curves measured with the 5 mm I.D. apparatus are shown in Fig. 18. Curves obtained from cold gas flow tests (i.e., without striking the arc) have general shapes which agree with the theoretically determined shape as exhibited in Fig. 3. Because there is no way of measuring the pressure within the anode bore, the section of the curve from 2 mm below the anode to the anode top surface is somewhat uncertain. (in the theory the existence of an anode is disregarded). The true pressure distribution might be somewhere between that of Fig. 3 and that of Fig. 18. The modified test apparatus incorporates a pressure probe in the inlet section close to the cathode tip. Therefore, the total pressure drop across the whole arc column can be measured continuously and under any conditions. If the pressure distribution is needed it can be obtained from the theoretical curves since the area of the flow passage, the mass flow rates, and the total pressure drop are easily measurable quantities.

3.4.5 Electric Field Strength

Constrictor tubes prepared to allow the measurement of the electric potential distribution are described in Sections 3.2.2 and 3.2.6. An example of individual test results for either apparatus is given in Figs. 19 and 20. In both cases small electron currents, primarily determined by the internal impedance of the instrument, are drawn to the probes, and perfect circumferential symmetry is found.

Generally, the potential measured depends upon the sign and the amount of the current drawn to the probe in a manner similar to the dynamic characteristic of a Langmuir probe. Fig. 21 demonstrates the change of the probe potential ΔU

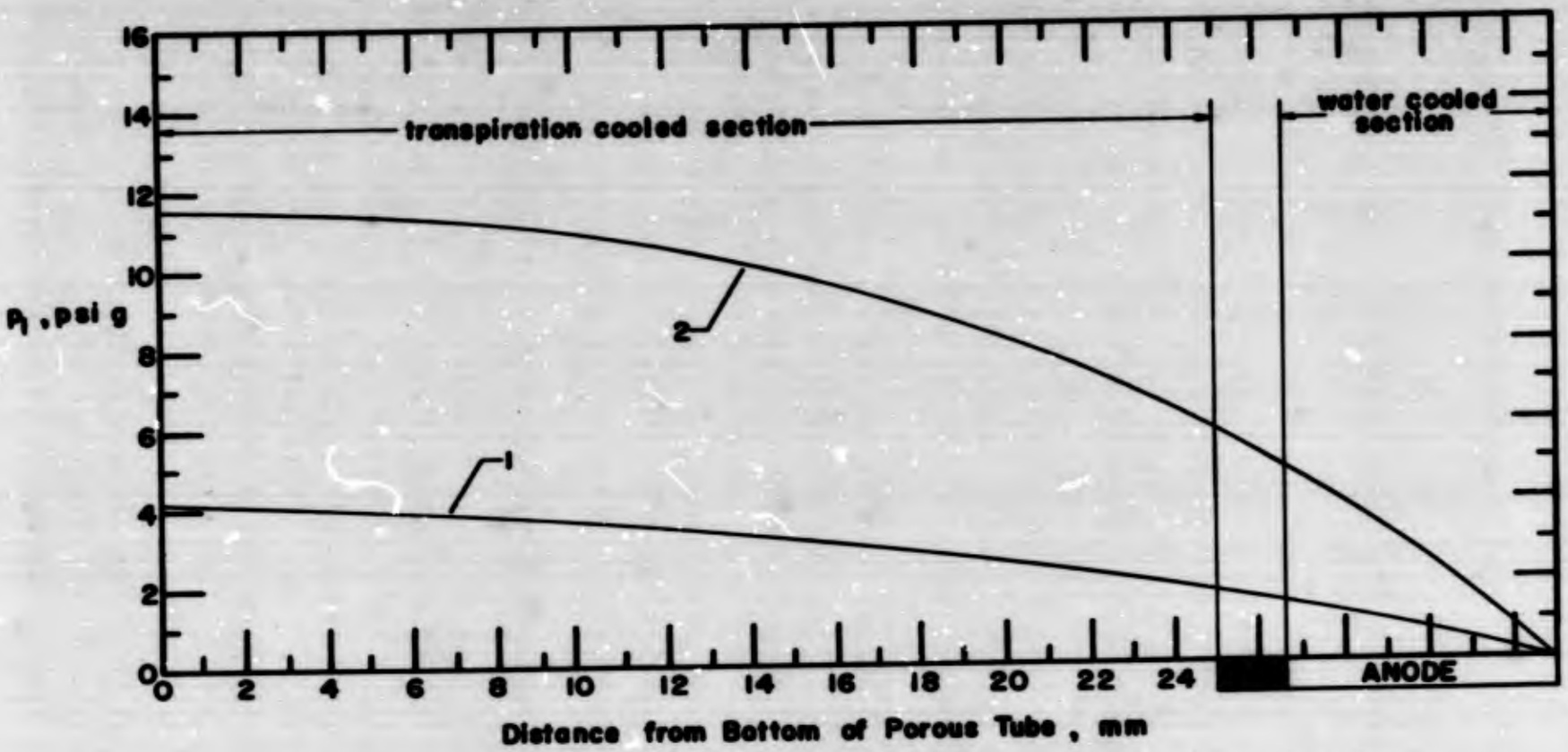

1: Transpirant flow 1.3 g/s, total flow 2.4 g/s, arc power 3.2 kW

2: Transpirant flow 1.5 g/s, total flow 2.0 g/s, arc power 5.9 kW

FIG. 18 Axial Pressure Distribution (5 mm I.D. Apparatus), Argon

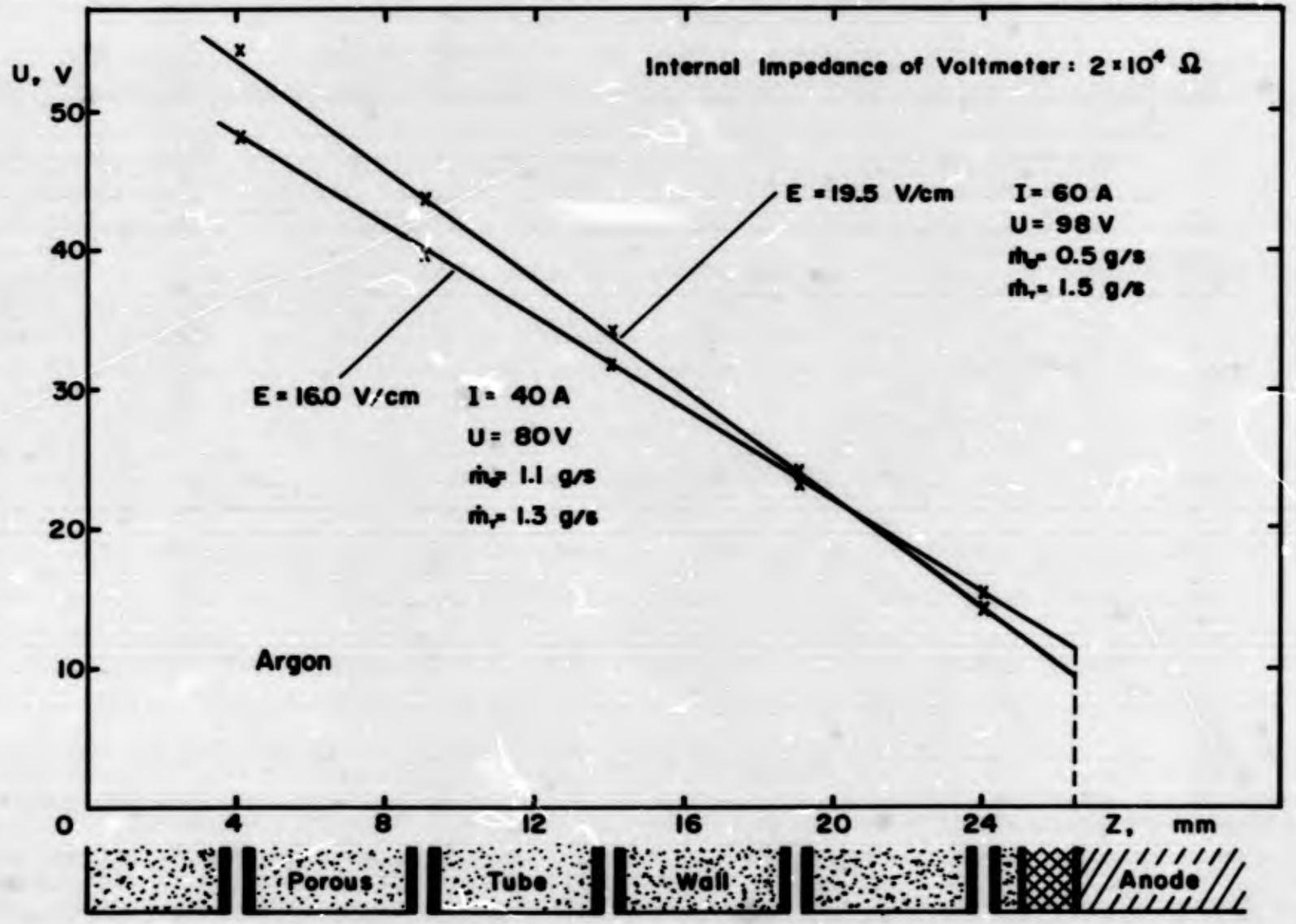

FIG. 19 Potential Distribution (5 mm I.D. Apparatus)

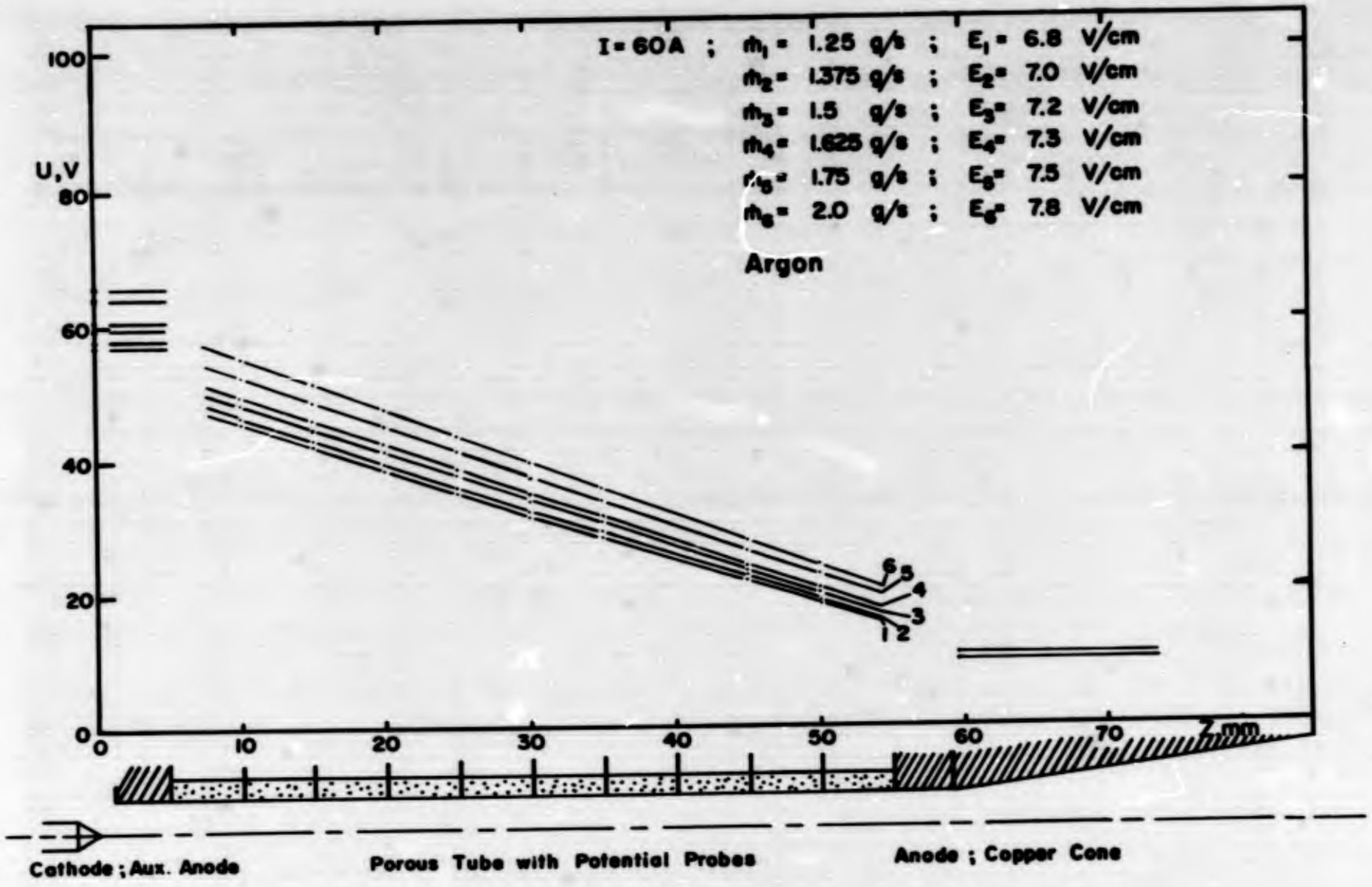

FIG. 20 Potential Distribution at Different Mass Flow Rates (10 mm I.D. Apparatus)

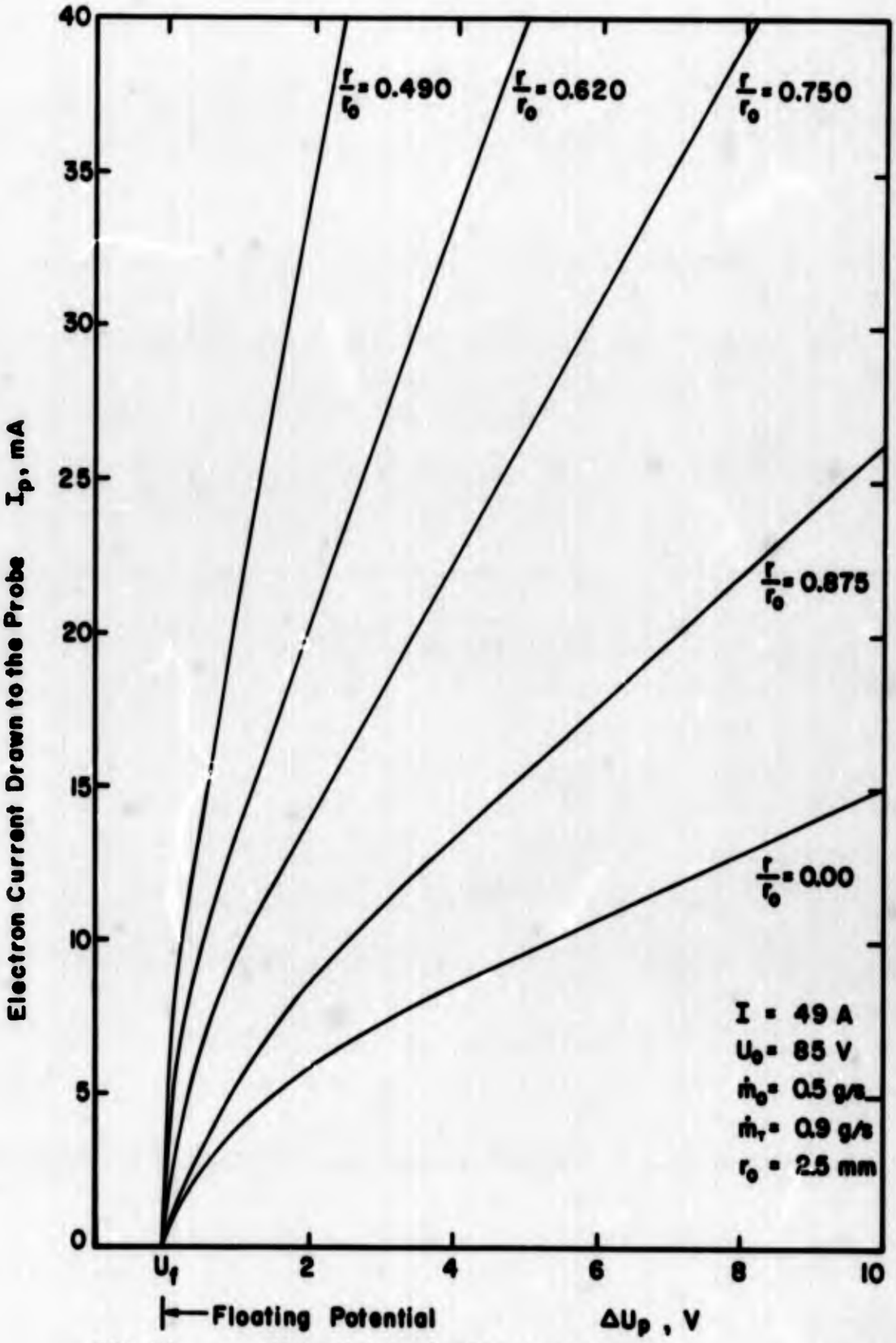

FIG. 21 Potential Probe Characteristics

with respect to the floating potential U_f as a function of the electron current drawn to the probe. The probe which is described in Section 3.2.2, is moved radially towards the plasma column. To every position of the probe tip, designated by the normalized coordinate $\frac{r}{r_o}$, belongs one of the probe characteristics shown. This experiment indicates that as the probe is moved closer to the plasma column, the probe potential is influenced less by the current drawn. However, the probe disturbs the flow to an unknown extent. Thus, the most reliable way to determine the field strength of the arc column is to measure the floating potentials of the probe whereby the true plasma potential remains unknown. In the case of Fig. 19 the electron current never exceeded 3 mA; in the case of Fig. 20 it was below 0.01 mA.

The two potential distribution curves allow an important conclusion to be drawn: the development length of the transpiration-cooled arc seems to be short enough so that the electric field strength is almost constant over the entire constrictor length.

3.4.6 Inner and Outer Wall Surface Temperatures

Outer wall surface temperatures are determined using thermocouples cemented onto this surface or peened into it. The EMF's with respect to a reference junction at $0^{o}C$ are measured with a hand-balanced potentiometer or a digital voltmeter. Temperature readings from thermocouples at different locations on the wall show a certain scatter for a given set of parameters. One or more of the following reasons may explain this scatter: nonuniform inner wall surface temperature due to nonuniform mass flow distribution caused by the axial pressure gradient or nonuniform permeability; nonuniform permeability of the outer wall surface caused in part by the cement, or varying quality of the thermal contact between the

surface and the thermocouple junction.

The inner wall surface temperature is measured by means of the instrumentation described in Section 3.2.4. The following experimental procedure is used. The arc is struck and the parameters are adjusted to the desired setting. After the temperature in the tube wall reaches its equilibrium distribution the arc is shut off using the electrical circuit shown in Fig. 7. A few milliseconds after the arc is fully extinguished the temperature decay of the inner wall surface is recorded without turning off the transpirant gas flow. The temperature during arc operation is obtained by extrapolating back to the moment of arc shut-off. The extrapolation covers a temperature range of about 20°C. The reliability of the light signal is checked by a rotating segmented disc which interrupts the light beam periodically and simultaneously causes the recorded trace to go to zero. Fig. 22 shows an example of such a recording. The system is calibrated with a tungsten ribbon lamp for black body temperatures taking into account the emissivity of tungsten over the wave-length band covered and assuming that the radiation in the center of the constrictor tube with $\frac{L}{D} = 5$ is close enough to black body radiation. More details about such temperature measurements are reported in a M.S. thesis (20). Results of the present measurements are contained in Table III. Unfortunately, very little is yet known about the uniformity of the inner and outer wall surface temperatures. Therefore, it is not yet possible to pinpoint the reason for the scatter of the measured and the calculated inner wall surface temperatures. The measurable range of inner wall surface temperatures is from 800°C up to 1000°C.

An attempt to check the relationship between the inner and outer wall surface temperature as given by Eq(25) and shown in Fig. 23 confirmed the general shape of the curve. Fig. 23 also

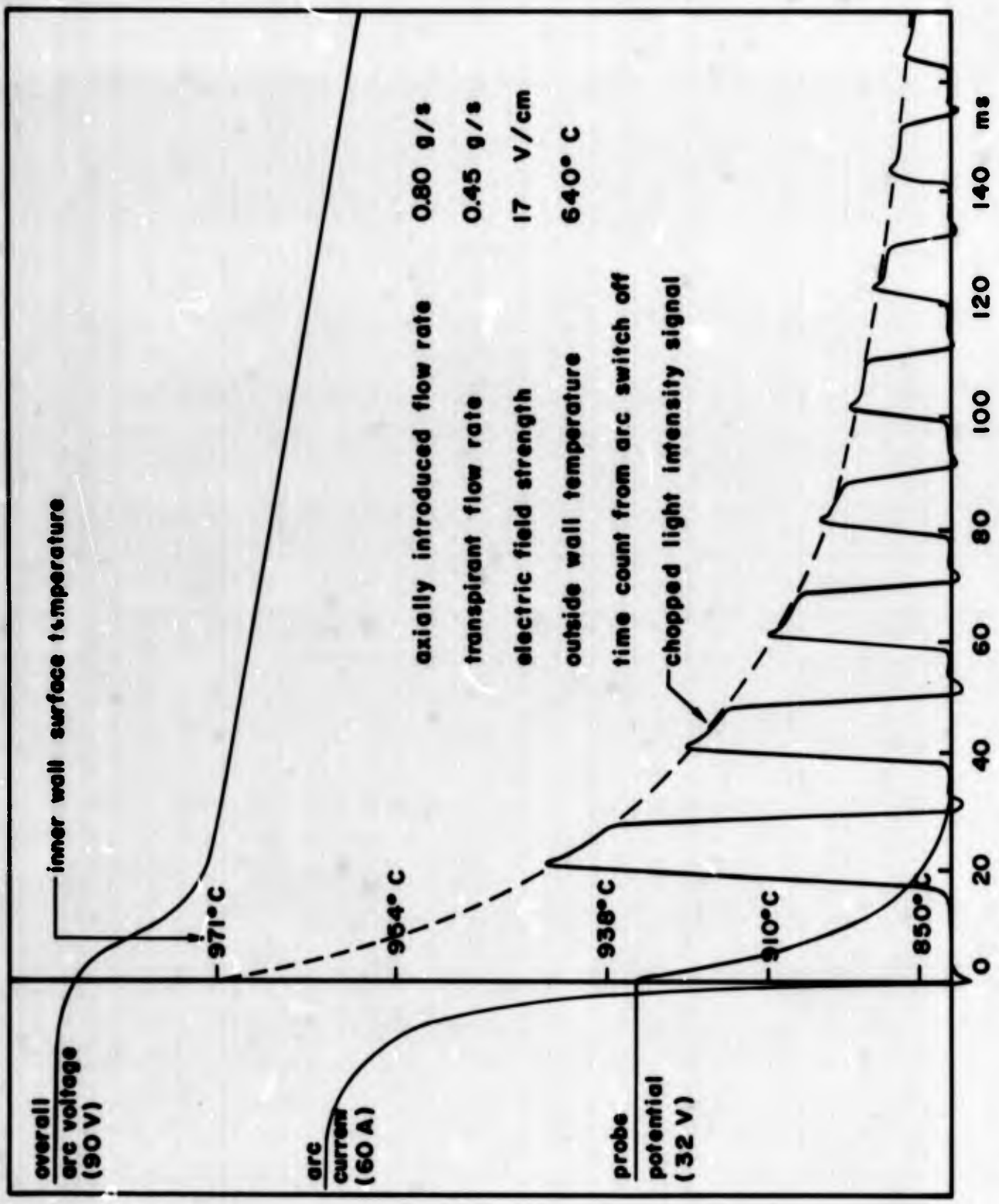

FIG. 22 Example of Recorder Output for Inner Wall Surface Temperature Measurement

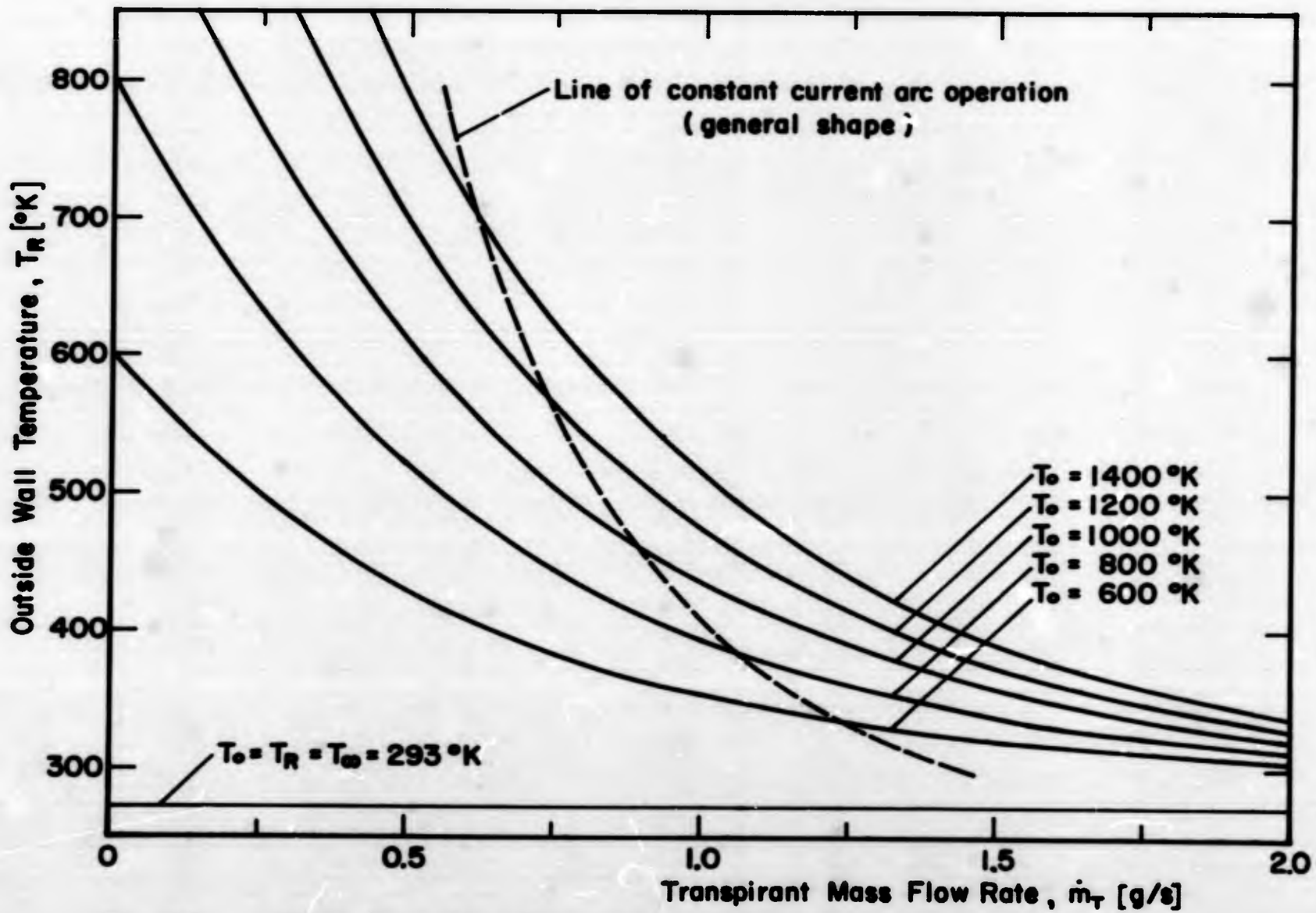

Fig. 23 Mass Flow Rate Dependence of Outer Wall Surface Temperature (Computed Curves for 5 mm I.D. Apparatus)

contains a typical experimental curve which is obtained if the transpirant mass flow rate is decreased for a fixed current setting. In Table III measured as well as calculated parameters are listed. From measured values of the average outside wall temperatures, T_R, and the corresponding measured transpirant mass flow rates, $\dot{m}_T$, an average value of the inside wall temperture, T_o, can be calculated, using Eq(25). These calculated values of T_o are used as parameter in Figs. 27, 29, and 31 in conjunction with measured values of current, field strength and mass flow rates. The heat flow per unit length, $\dot{q}_w$, which flows towards the inside wall and is intercepted by the transpiring gas flow is also listed in Table III. These values have been calculated from Eq(49). Since the transpirant mass flow rate, $\dot{m}_T$, the plenum chamber pressure, p_R, the pressure drop along the constrictor tube, and the outside wall temperature, T_R, are interrelated according to Eq(20), one of these parameters may be calculated if the remaining parameters are known. Therefore, Eq(20) may be used to check the reliability of the measured parameters. As an example measured and calculated values of the transpirant mass flow rate are listed in Table III.

3.4.7 Flow Behavior

Unfortunately, very little is known about criteria which allow decision as to whether or not a plasma flow is in the turbulent regime, and especially whether turbulence exists over the whole duct cross-section or in portions of the flow only (for instance the cold gas envelope). The present investigation follows mainly an experimental procedure reported by Runstadler (21). First, the time-resolved arc current signal is examined on the oscilloscope. For either apparatus and any current setting a ripple of ±1% peak to peak is found which stems from 60 cycle AC power supplied to the rectifier

TABLE III

I	E	$\dot{m}_T$	$\dot{m}_T$ *	p_R	$T_{R\ av}$	$T_{o\ av}$ *	$\dot{q}_w$ *	Δp_{wall}	T_o
A	V/cm	g/s	g/s	psig	^oK	^oK	W/cm	psi	^oC
39.0	16.3	0.30	0.34	26.1	513	652	25.4	24.2	
43.9		0.39	0.41	31.8	527	713	35.5	30.5	
44.7	19.1	0.72	0.80	43.6	388	594	50.2	40.4	
46.2	15.4	0.36	0.43	34.5	538	746	40.2	32.3	
48.3	14.0	0.42	0.47	37.6	535	767	46.2	35.0	
48.7	18.4	0.81	0.87	49.2	395	649	64.6	45.3	
50.7	17.1	0.90	0.83	48.8	411	679	66.3	45.2	
52.5	14.0	0.66	0.55	45.4	548	852	63.5	41.6	
53.9	13.8	0.63	0.60	47.5	528	850	69.5	44.9	890
54.4	14.9	0.51	0.61	48.0	528	853	70.3	44.8	
54.7	16.9	0.90	0.85	51.3	418	713	73.8	47.3	
54.8	16.1	0.96	0.93	56.3	413	745	86.8	51.4	
54.9	15.3	0.90	0.82	52.3	438	759	78.9	48.8	
58.6	12.1	0.72	0.72	52.7	493	852	83.1	49.8	>950
59.0	14.3	1.02	0.91	60.5	443	840	102.7	55.2	
59.8	12.7	0.84	0.73	56.3	508	938	92.4	51.8	
64.5	12.4		0.80	64.3	518	999	117.0	58.5	
64.7	16.6		1.33	79.5	380	874	159.9	68.7	
66.7			1.26	74.0	383	838	142.1	65.6	
69.7	18.0		1.36	87.5	395	997	197.0	73.6	
71.2	14.1		0.99	77.5	485	1085	162.4	68.4	
74.3			0.91	72.0	501	1060	144.9	65.5	980
75.4	16.0		1.15	86.0	455	1123	196.5	73.4	
76.5	17.7		1.25	91.0	430	1114	212.9	72.9	
79.4	17.2		1.16	95.2	480	1266	232.3	76.8	
80.8			1.04	79.0	471	1079	168.9	68.7	>980

* calculated quantities

unit and which is suppressed to this percentage by the filter. This is the only ripple in the current signal that can be detected; thus, if there is any fluctuation in the arc, it has to show up in the voltage trace. Fig. 24 shows photographs of traces produced by a dual beam oscilloscope for various arc parameter settings obtained with the small apparatus. The upper beam records the overall arc voltage fluctuations. Frequency as well as amplitude of these fluctuations increase with higher mass flow rates. The lower trace represents the intensity fluctuations of the emitted light viewed through the center of the arc column. The light signal is observed by the same photomultiplier and transformed to an electrical signal as in the case of the inner wall surface temperature measurements, except that the voltage supplied to the multiplier tube is reduced.

In none of the four tests does the light intensity trace show enough similarity to the voltage trace to suggest that fluctuations in the arc voltage are the cause of the light fluctuations. Because the arc current must pass through the cold gas envelope in the vicinity of the anode in order to reach the anode, it is conceivable that the "cold" gas flow has a significant effect on the arc voltage. If turbulence were the main cause of the fluctuations observed one would expect that turbulence phenomena in the cold gas would manifest themselves on the voltage trace, whereas such phenomena in the hot plasma core would influence the intensity of the light radiated from the plasma. Furthermore, as the plasma has a higher viscosity than the cold gas, one would expect generally higher fluctuation frequencies in the cold gas envelope and, thus, on the voltage trace, than in the plasma column. The results shown in Fig. 24 exhibit all these features believed to be characteristic for a turbulent flow. Fig. 25 further corroborates these findings. The two series of photographs

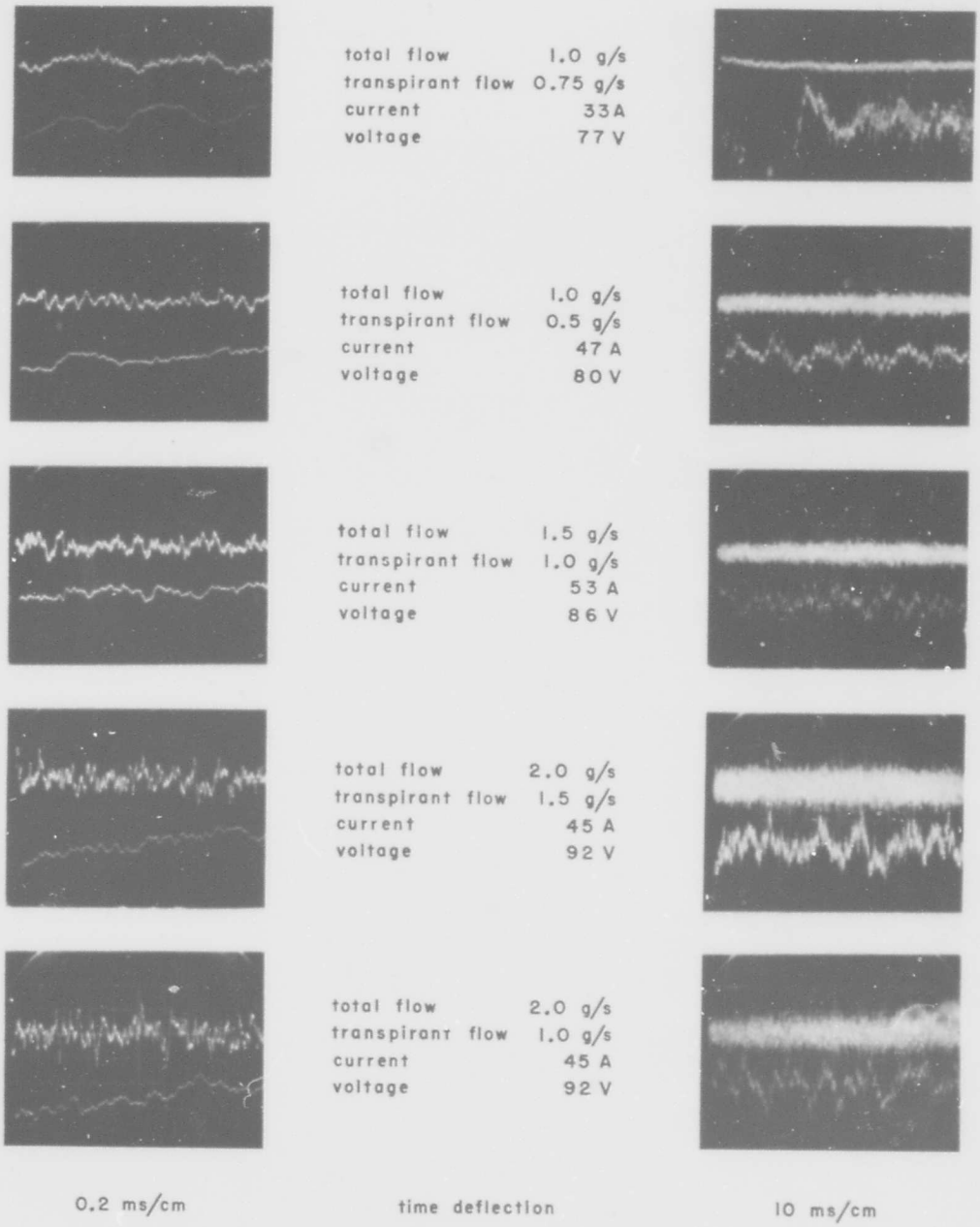

upper beam: overall voltage, 2 V/cm, AC-signal
lower beam: light intensity, arbitrary units, AC-signal

Argon

FIGURE 24 FLUCTUATION of the ARC VOLTAGE and the LIGHT RADIATED from the CENTER of the TRANSPIRATION-COOLED ARC COLUMN

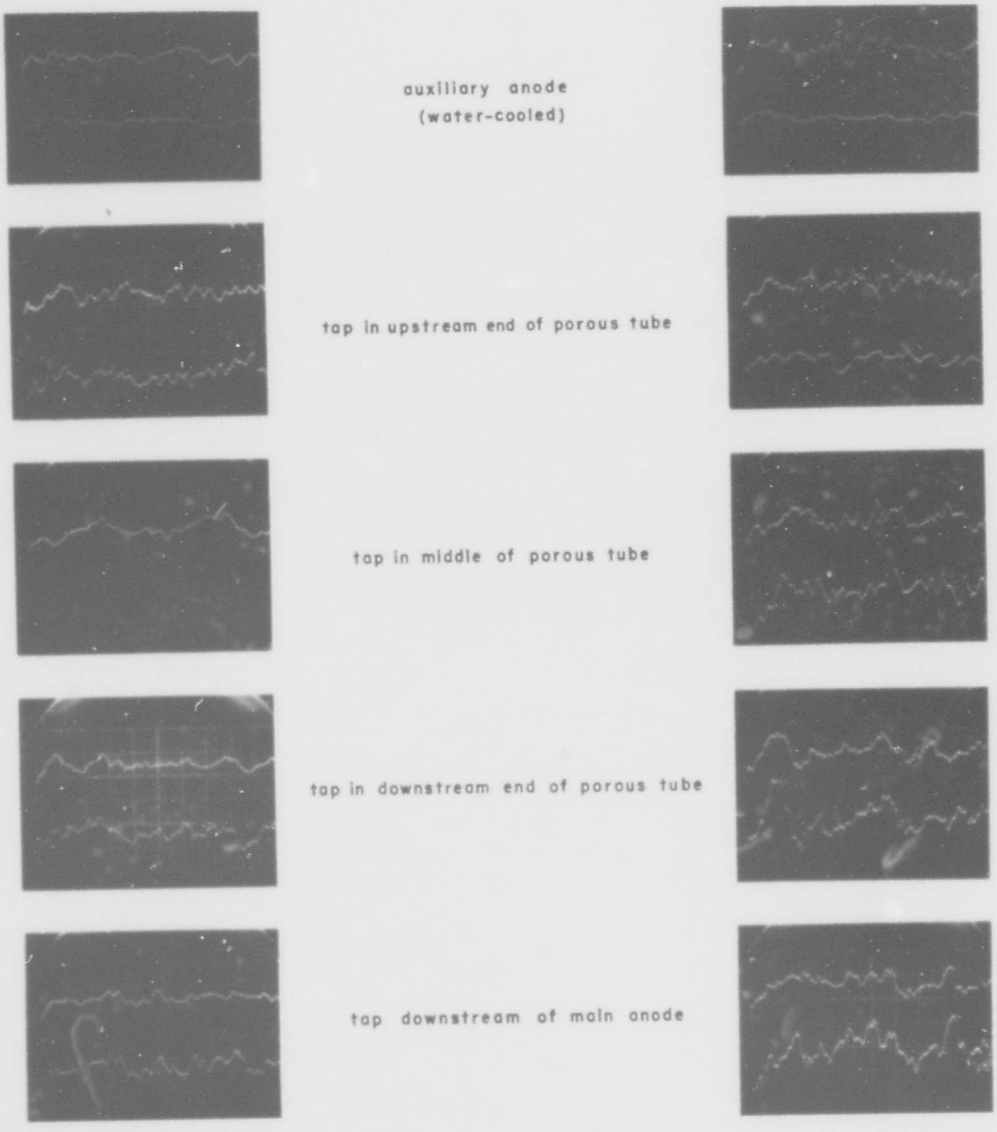

FIGURE 25 POTENTIAL FLUCTUATIONS AT VARIOUS LOCATIONS OF THE ARC COLUMN

show potential fluctuations at various axial positions along the arc column. They clearly demonstrate that the phenomena causing fluctuations of the overall voltage occur in the anode region. One can see again that frequency and amplitude of the fluctuations increase in downstream direction, i.e., with increasing mass flow rate, just as the degree of turbulence is expected to behave. These results strongly suggest that the flow in the small apparatus is turbulent, probably in the arc column proper as well as in the cold gas envelope. A deviation from this behavior is not observed for other parameter settings.

Because a particular feature of the modified 10 mm I.D. apparatus is the turbulence-suppressing inlet section, some measurements of the remaining degree of turbulence in the argon flow at room temperature are made with a hot wire anemometer located in the bore of the top anode. The result is shown in Fig. 26, in which the turbulence intensity T_u is plotted vs. the exit mass flow $\dot{m}_e = \dot{m}_o + \dot{m}_T$, the exit velocity v_e, and the exit Reynolds number Re_{De} which is based on the tube diameter. Because the exit mass flow consists of the axially introduced cathode flow $\dot{m}_o$ and the radially introduced transpirant flow $\dot{m}_T$, an additional parameter to Re_{De} is needed to describe the flow behavior in the exit cross-section; therefore, the transpirant Reynolds number

$$Re_{WR} = \frac{\dot{m}_T \, r_o}{A_o \mu}$$

based on the inside tube radius r_o ($A_o = 2\pi r_o L$, L = tube length, μ = dynamic viscosity) is used and given as function of Re_{De} in Fig. 26.

From this figure two different conclusions may be drawn. First, it can be expected from the relatively low turbulence level up to high Reynolds numbers that the turbulent motion

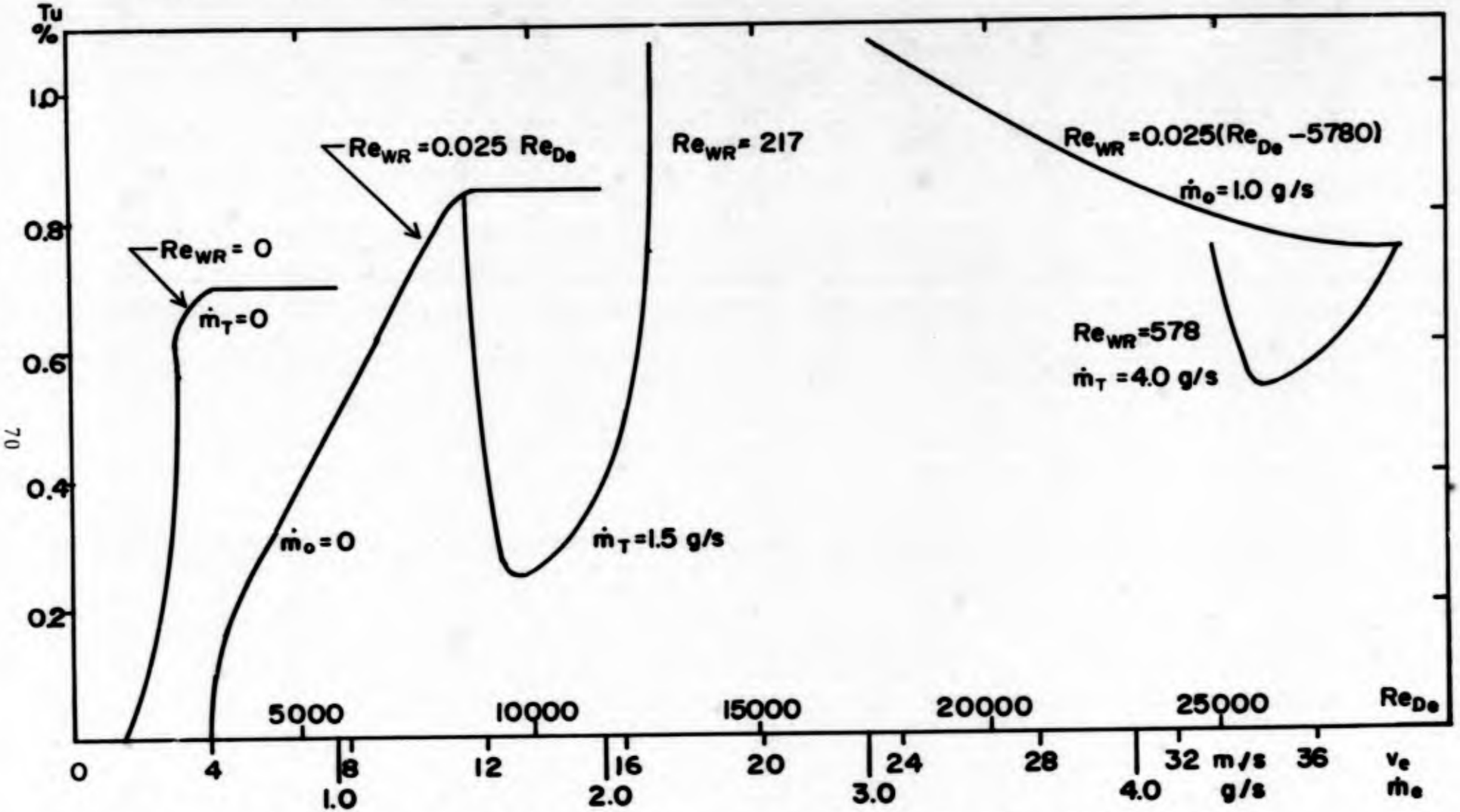

FIG. 26 TURBULENCE INTENSITY OF ARGON FLOW AT ROOM TEMPERATURE (10 mm ID Apparatus)

will contribute only very little to the radial heat transfer. Second, a comparison with a recent study in this laboratory (22) shows that the transition from laminar to turbulent flow (for transpirant flow only, $\dot{m}_o = 0$) occurs at $Re_{WR} \approx 70$. The latter value coincides exactly with that point in Fig. 26 ($v_e = 4$m/s) where a minimum intensity of turbulence becomes measurable under the same condition ($\dot{m}_o = 0$). In order to estimate what the situation might be when a hot plasma is passing through the center of the tube, the following model will be used: the plasma is replaced by a solid rod filling ½ of the original flow cross-section. The characteristic dimension then becomes the hydraulic diameter (radius), which is 0.7 times its original value. Thus, Re_{De} increases by a factor of 1.4 whereas Re_{WR} decreases by a factor of 0.7. The effect of a higher bulk temperature of the gas will decrease either Reynolds number. For this model a bulk temperature would be, for example, 2000°K, for which the Reynolds numbers already reduce to about ¼ of their values at room temperature. Now the rod is replaced by a plasma flow, also filling ½ of the original flow cross-section, which is considered to be independent of the surrounding flow. The Reynolds numbers change with diameter (radius) as they did for the cold flow. In this case, a typical bulk temperature would be 10,000°K or more, thus decreasing the Reynolds numbers more drastically than in the case of cold flow. However, there is an even more significant factor which further reduces the Reynolds number of the hot flow in this model: the plasma typically carries only about 10% of the total mass flow in an actual arc. One can conclude from this consideration that, for a given flow cross-section and a given mass flow rate, the turbulence intensity will be considerably lower with a plasma passing through than for a gas flow at room temperature as shown in Fig. 26.

This estimate is at least partially corroborated by the measurement of voltage fluctuations taken with the modified apparatus in a fashion similar to the ones reported for the smaller apparatus. For the arc parameter setting

$I = 60$ A $\qquad U_o = 55$ V

$\dot{m}_o = 0.25$ g/s $\qquad \dot{m}_T = 1.25$ g/s

one finds only very small and slow fluctuations on the arc voltage trace. For the setting

$I = 140$ A $\qquad U_o = 100$ V

$\dot{m}_o = 0.25$ g/s $\qquad \dot{m}_T = 6.75$ g/s

the arc voltage traces look exactly like those shown in Fig. 24 and Fig. 25. The transition from small to larger fluctuations seems to be continuous.

3.5 Summary and Discussion of Results

3.5.1 Arc Characteristics

The experimental results are summarized in the form of graphs representing arc characteristics. Special emphasis is put on the electric field strength-current characteristic. For a fully developed water-cooled arc of given constrictor radius there is only one such characteristic, as the boundary conditions at the constrictor wall are fixed within close limits. For a transpiration-cooled arc, however, the boundary conditions can vary over a wide range, and, therefore, there

are a number of characteristics depending on more than one parameter. A very important parameter is the inner wall surface temperature, because arc operation is possible only if it stays below the melting point of the wall material for any arc power setting. For some values of this parameter continuous curves are obtained over the entire range of arc current and voltage or field strength covered in the experiments. Unfortunately, there is no simple method with which the inner wall surface temperature can be measured continuously while changing the arc parameters. On the other hand, the parameters which can be more easily measured, such as transpirant mass flow rate or outer wall surface temperature, will not yield continuous curves and, furthermore, they depend upon material properties of the constrictor tube. Other parameters, such as the heat load on the inner wall surface are even more impractical, as there is no way to measure them directly. Thus, field strength-current characteristics are plotted in Fig. 27 using the inner wall surface temperature as parameter, although the accuracy of the temperature values is still in doubt. The absolute error in the temperatures quoted is believed to be less than $\pm 200^{o}C$. The general trend of the curves is not much affected by this error. Figs. 27 and 28 show the E-I-characteristics obtained from the arc in the small and the larger apparatus respectively. Because the scaling law for an arc column with negligible radiation losses holds also for transpiration-cooled arcs, the parameters Er_o and $\frac{I}{r_o}$ should be about the same for both arcs. Comparing the two sets of Er_o values, one finds for any $\frac{I}{r_o}$ that the field strength data obtained for the small apparatus are lower than in the case of the larger apparatus. This finding may be due to the fact that the inner wall surface of the larger tube is kept at rather low temperatures. It is also worth noting that the field strength in a transpiration-cooled

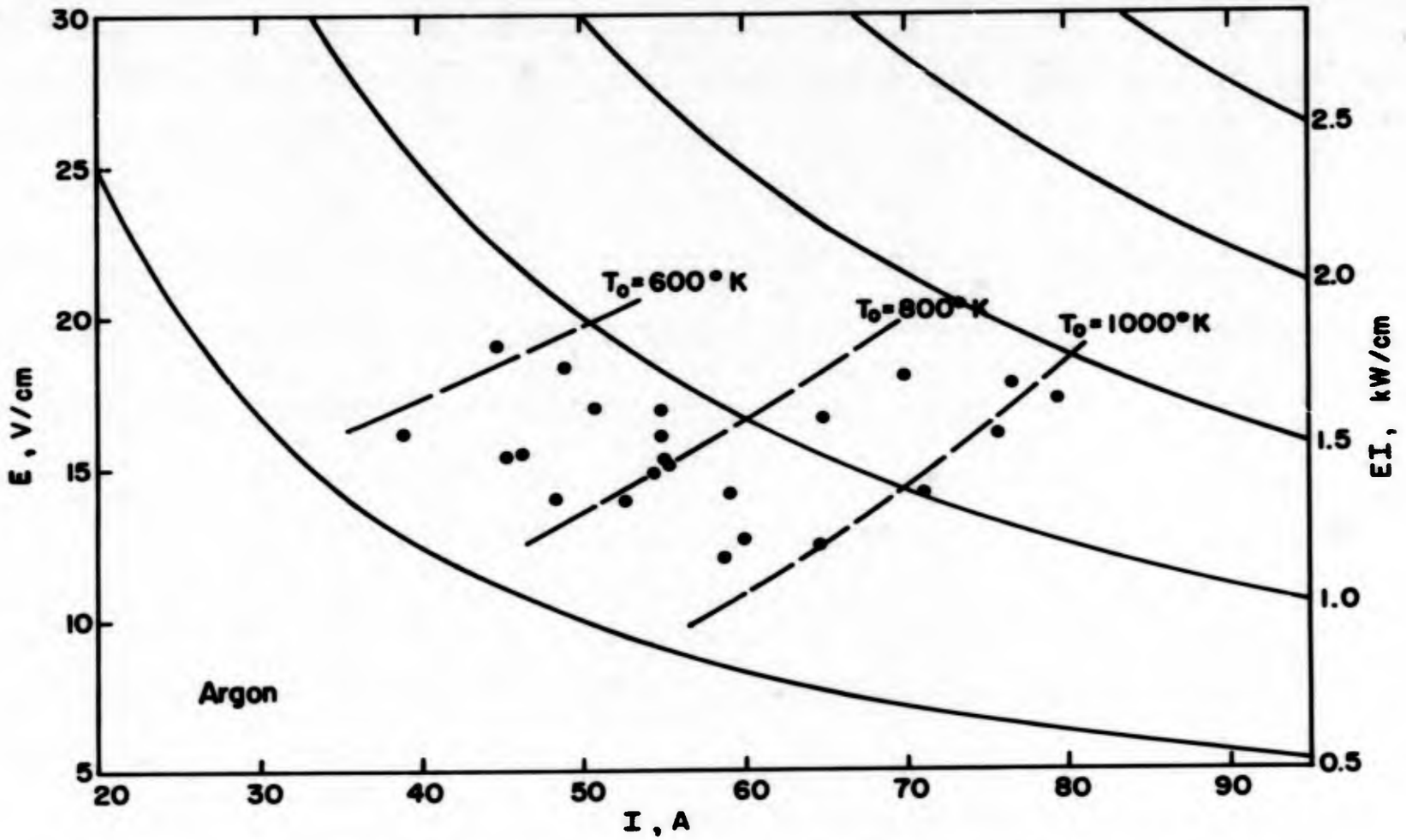

FIG. 27 Electric Field Strength - Arc Current Characteristic (5 mm I.D. Apparatus)

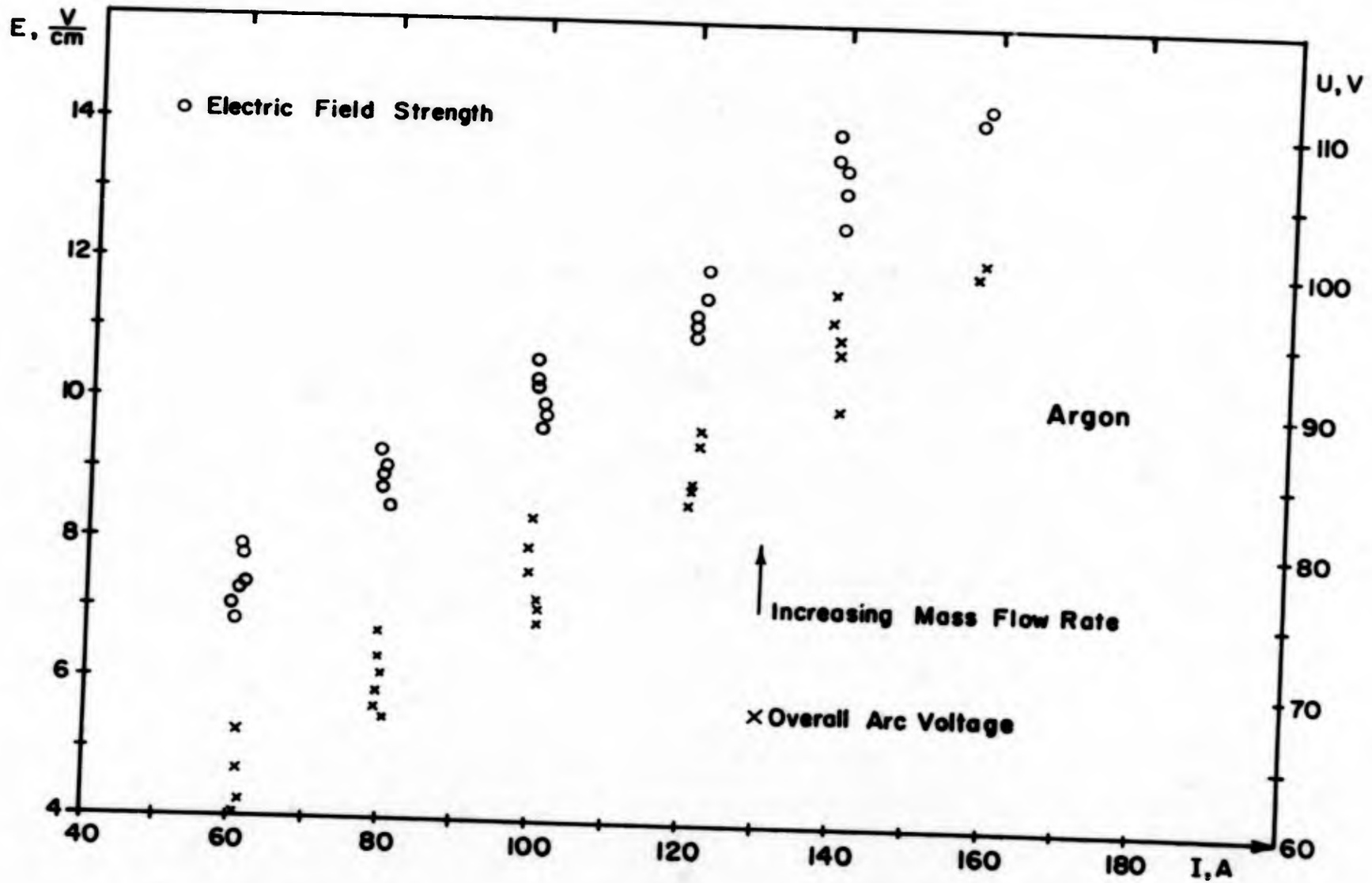

FIG. 28 Current Dependence of Field Strength and Arc Voltage (10 mm ID Apparatus)

arc is higher than in a water-cooled arc of identical diameter (of the duct) for a given current, except for currents of about 60 A in the small apparatus under hot tube wall conditions.

Another type of characteristic which may be established is the field strength-transpirant flow rate characteristic as shown for the small apparatus in Fig. 29 and for the larger one in Fig. 30. The abscissa in Fig. 30 is the square root of the transpirant mass flow rate; by using this scale the field strength mass flow rate characteristic becomes a straight line. This proportionality between the square of the electric field strength and transpirant mass flow rate probably holds only in the ascending portion of the field strength-current characteristic. The curve shown in Fig. 30 corresponds to low inner wall surface temperatures.

A third type of characteristic which may be established for a transpiration-cooled arc is shown in Fig. 31 for the small apparatus. It indicates what percentage of the heat generated electrically per unit arc length is transferred to the porous wall before it is redirected into the gas stream by the transpiring gas. It is anticipated that this characteristic will indicate the influence of the turbulence level in the flow on the arc performance.

3.5.2 Constrictor Performance

The experimental results establish beyond any doubt that an arc can be safely operated in an entirely transpiration-cooled constrictor without employing any other additional cooling method. Although the constrictor material is somewhat inhomogeneous in its permeability distribution as discussed in Section 3.3.2, the tube maintains its integrity even at average inner wall surface temperatures which are close to the melting point of the wall material. One finds that due to the low thermal conductivity of the wall material the outer wall

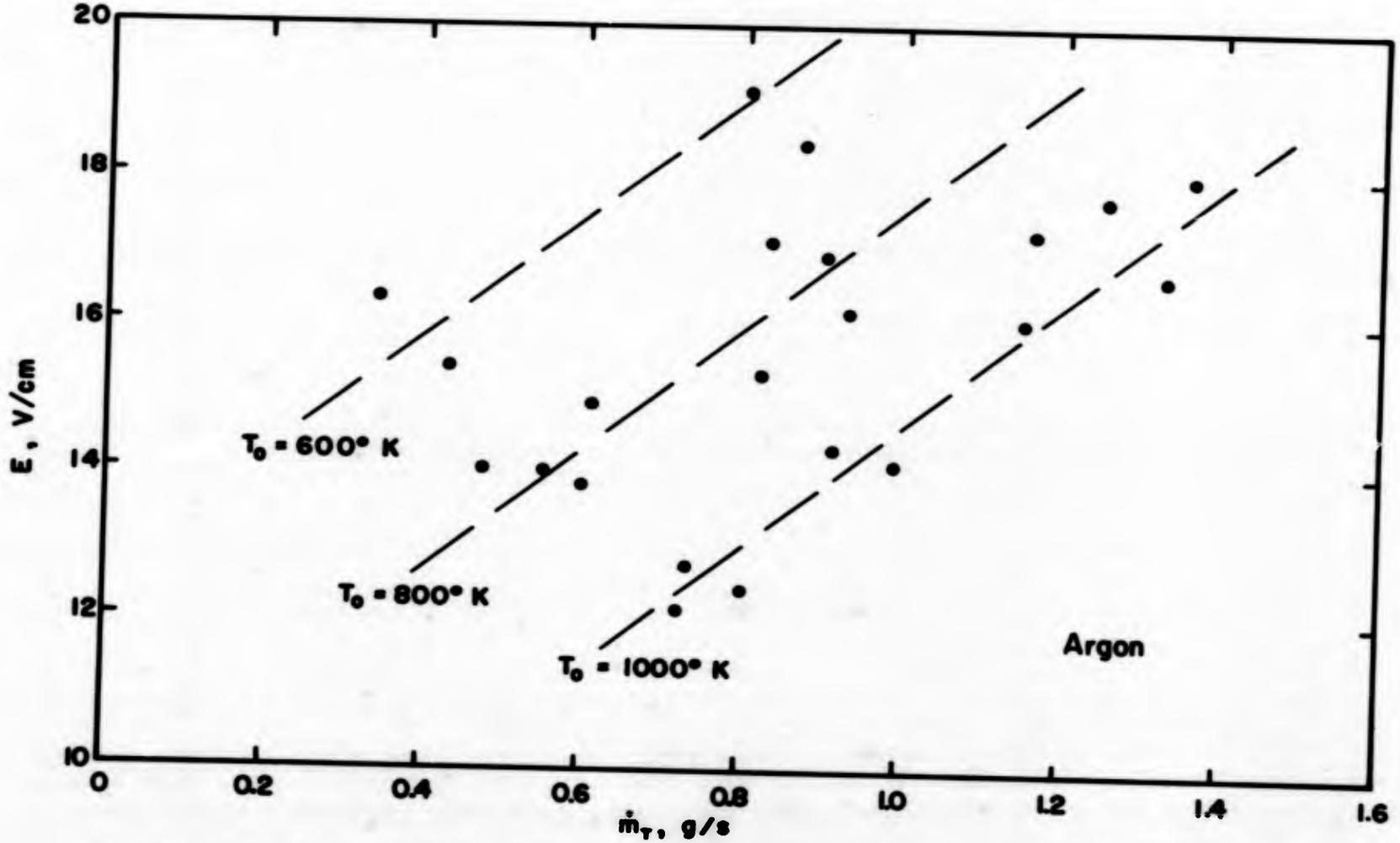

FIG. 29 Electric Field Strength - Mass Flow Characteristic (5 mm I.D. Apparatus)

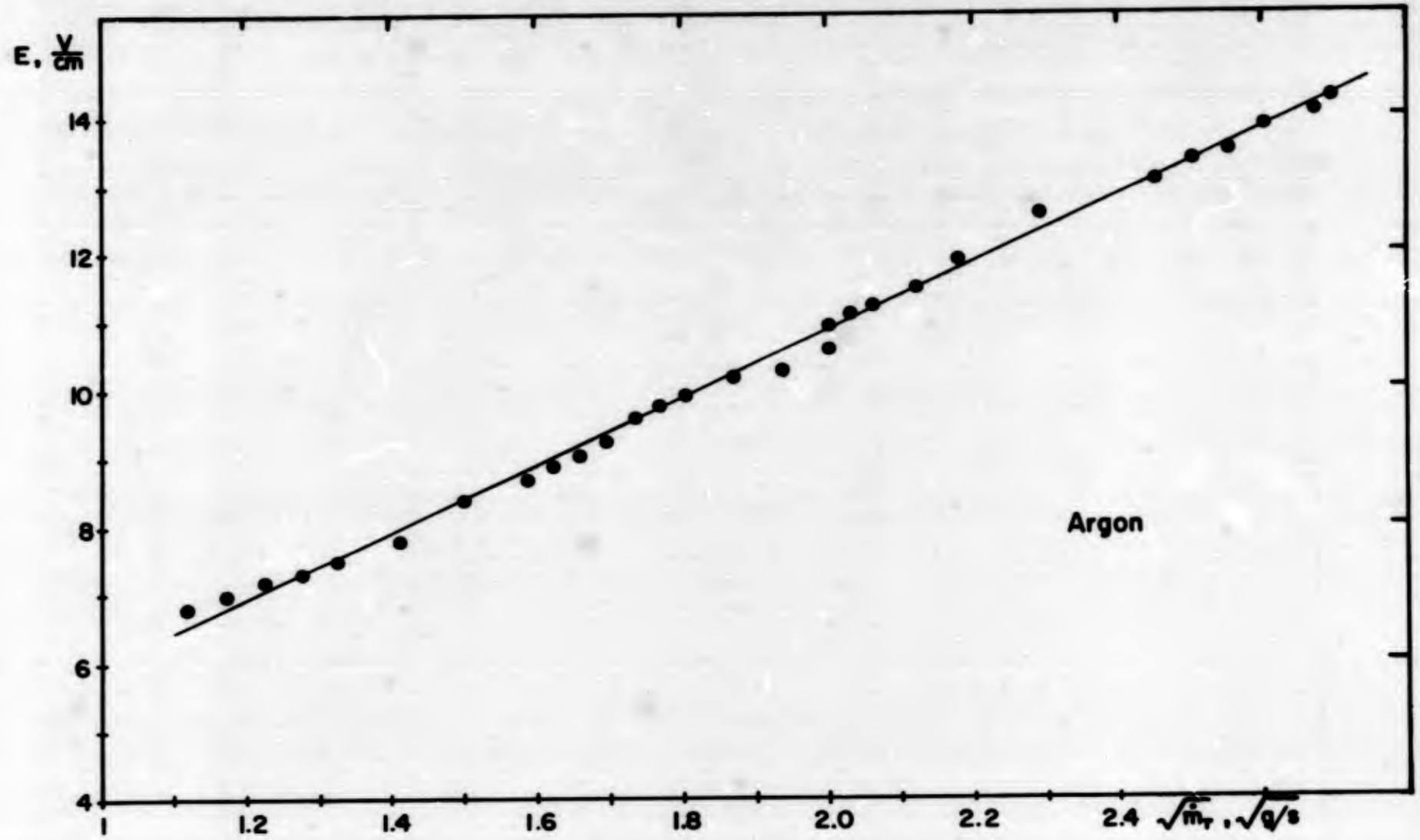

FIG. 30 Mass Flow Dependence of Electric Field Strength (square root scale)
(10 mm ID Apparatus)

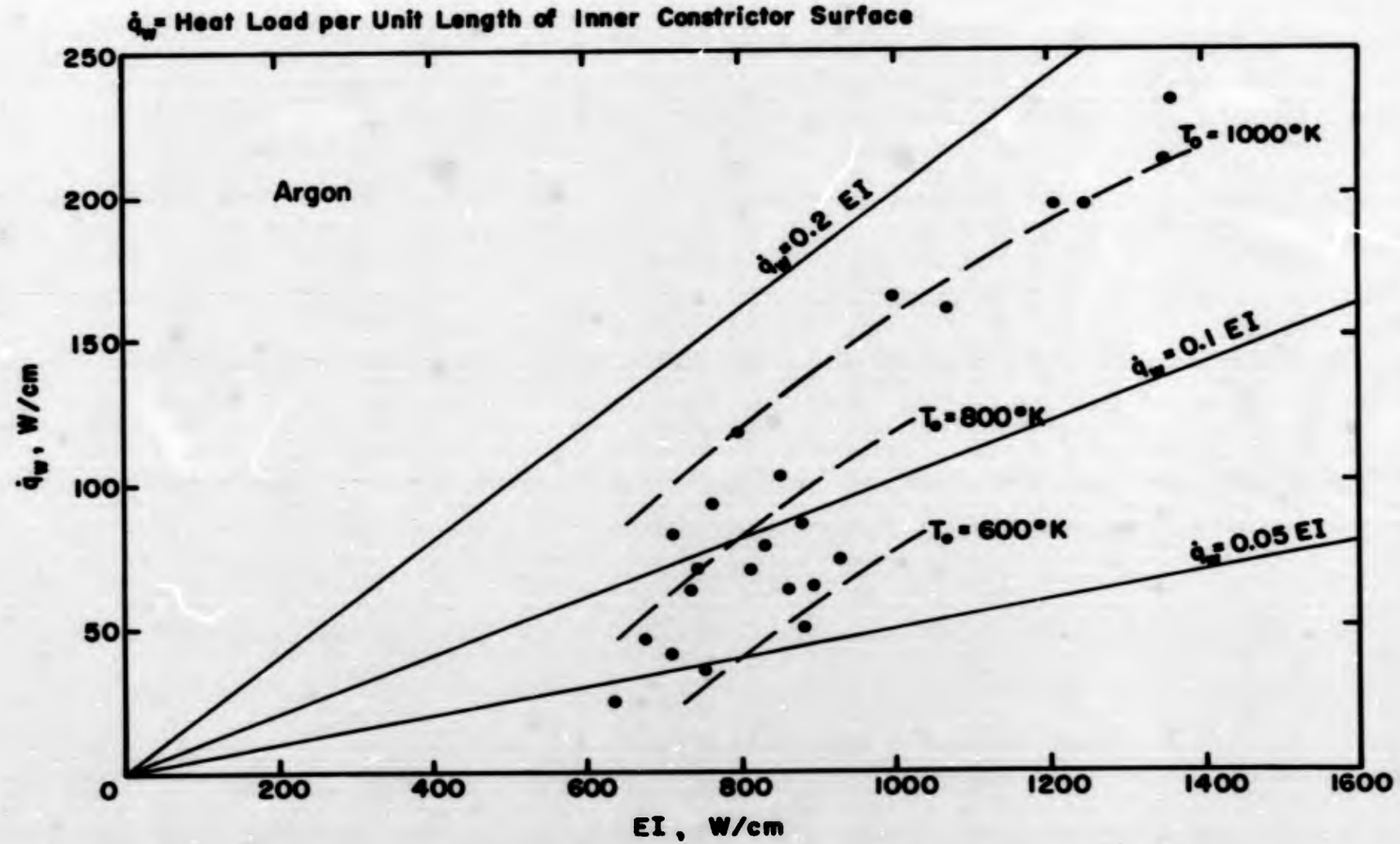

FIG. 31 Heat Transfer Characteristic of Transpiration-Cooled Arc (5 mm I.D. Apparatus)

surface temperatures generally stay below 300°C. Therefore, radiative cooling of this surface can be neglected. Conductive or convective heat transfer from the tube to other boundaries of the plenum chamber is also negligible; a thermocouple located in the plenum chamber close to the plexiglas wall never measured temperatures more than 5°C above room temperature. Thus, there is no net heat loss through the constrictor to the outside. This means that the efficiency with respect to gas heating is 100% within the transpiration-cooled section of the apparatus.

The mass flow rate-pressure drop characteristic obtained with the 5 mm I.D. constrictor is shown in Fig. 32 for different inner wall surface temperatures T_o. The curves are calculated from Eq(20) after the parameter T_R has been replaced by T_o using Eq(25). It is found that the thermal conductivity k_w of the constrictor material, which is not well known, has only very little influence on these characteristics. The mass flow rates in Fig. 32 are obtained partly by direct measurement and partly by using the data reduction formula, Eq(20). The validity of Eq(45) has been checked up to 500°C with uniform wall temperature by supplying argon at this temperature to the porous tube in the test set-up shown in Fig. 13 (without sampling tube). This shows that Eq(7) may be used safely in this temperature range.

The effect of the "matched" tube shape, as derived in Section 3.1.5, on the local mass flow and the local heat load distribution at the inner wall surface is shown in Fig. 33 under conditions close to the ideal ones (see Appendix B). For different arc parameter settings deviations from uniformity are somewhat larger but never exceed ±15% because the pressure drop across the tube wall is several times larger than the axial pressure drop in the flow duct. The limiting factor for the applicability of a certain tube shape is the inner wall

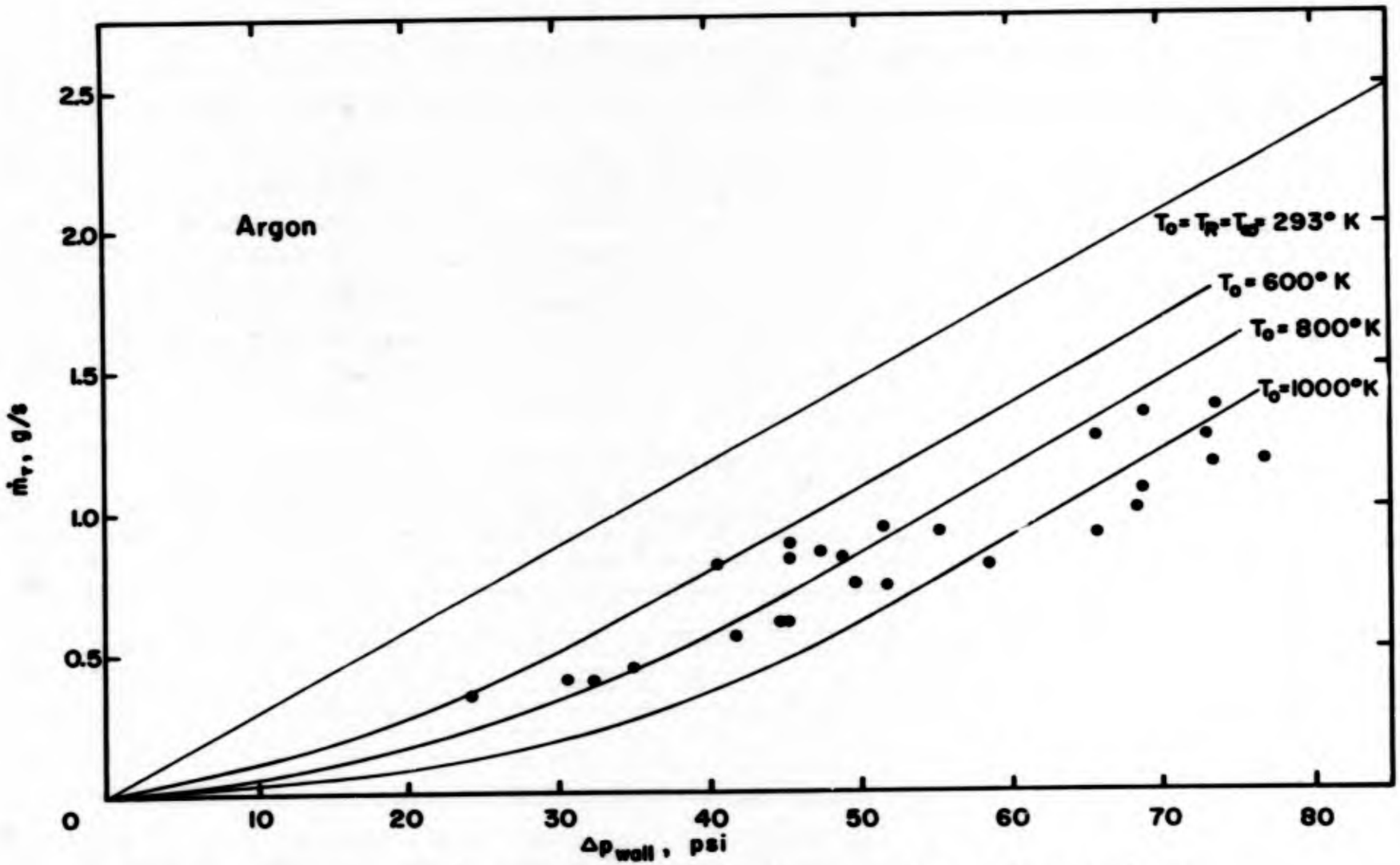

FIG. 32 Mass Flow Rate - Pressure Drop Characteristic of Porous Constrictor (5 mm I.D. Apparatus)

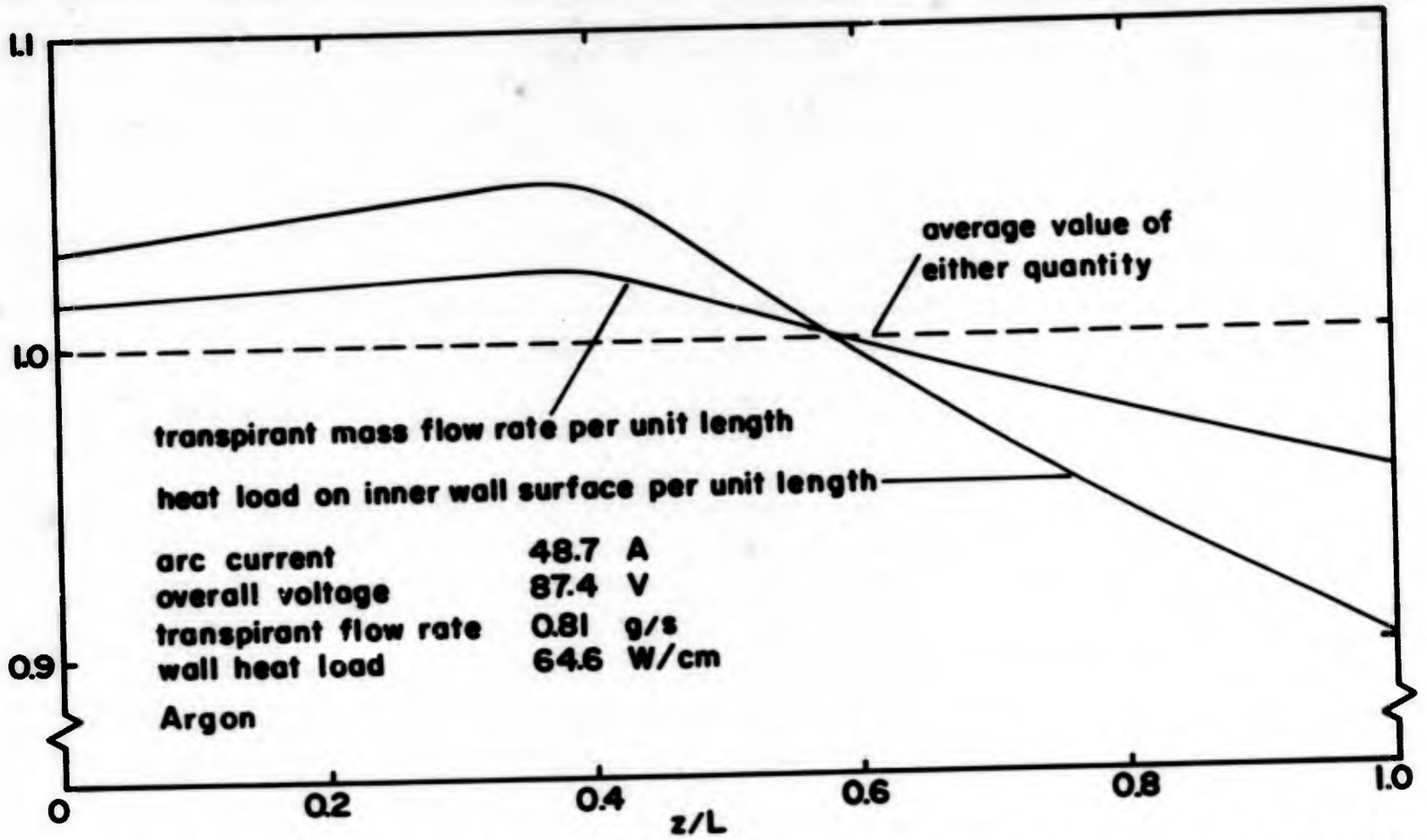

FIG. 33 Normalized Axial Distribution of Transpirant Flow Rate and Wall Heat Load (5 mm I.D. Apparatus)

surface temperature, which varies drastically with the mass flow rate if large portions of the tube are affected.

3.5.3 Plasma Temperature Profile

Presently, there seems to be no possibility of measuring spectroscopically the temperature profile of the arc column proper. The principle of transpiration cooling excludes the possibility of replacing a disc-shaped section of the constrictor tube by a quartz ring, for example. This ring would melt because there is no cooling provided in it. The other possibility, that of using a horizontal slot in the constrictor, creates sealing problems which are technologically insoluble so far. Besides that, the axial flow would be severely disturbed and the arc will bulge out. Thus, the only method left is to measure the temperature profile in the jet emanating from the anode. This method also has its drawbacks in that the temperature profile of the transpiration-cooled arc is somewhat altered by the passage of the arc through a water-cooled section, which is in this case the anode. In order to obtain an approximate idea of the size of this influence on the temperature profile, two anodes of different thickness, 4.0 mm and 10.0 mm, are used with the small apparatus. Furthermore, the axial pressure drop across the anode will cause a lowering of the temperature which has to be taken into account if one wishes to find the temperature within the arc proper. For further details on these measurements the reader is referred to a M.S. thesis on this subject (23). Only a few typical results are briefly discussed here. Fig. 34 shows two temperature profiles of the transpiration-cooled arc jet measured 1 mm downstream of the anode end face in comparison with the one of a water-cooled arc. The axis temperatures in the transpiration-cooled arc prove to be higher than those in the water-cooled arc; this effect becomes more pronounced

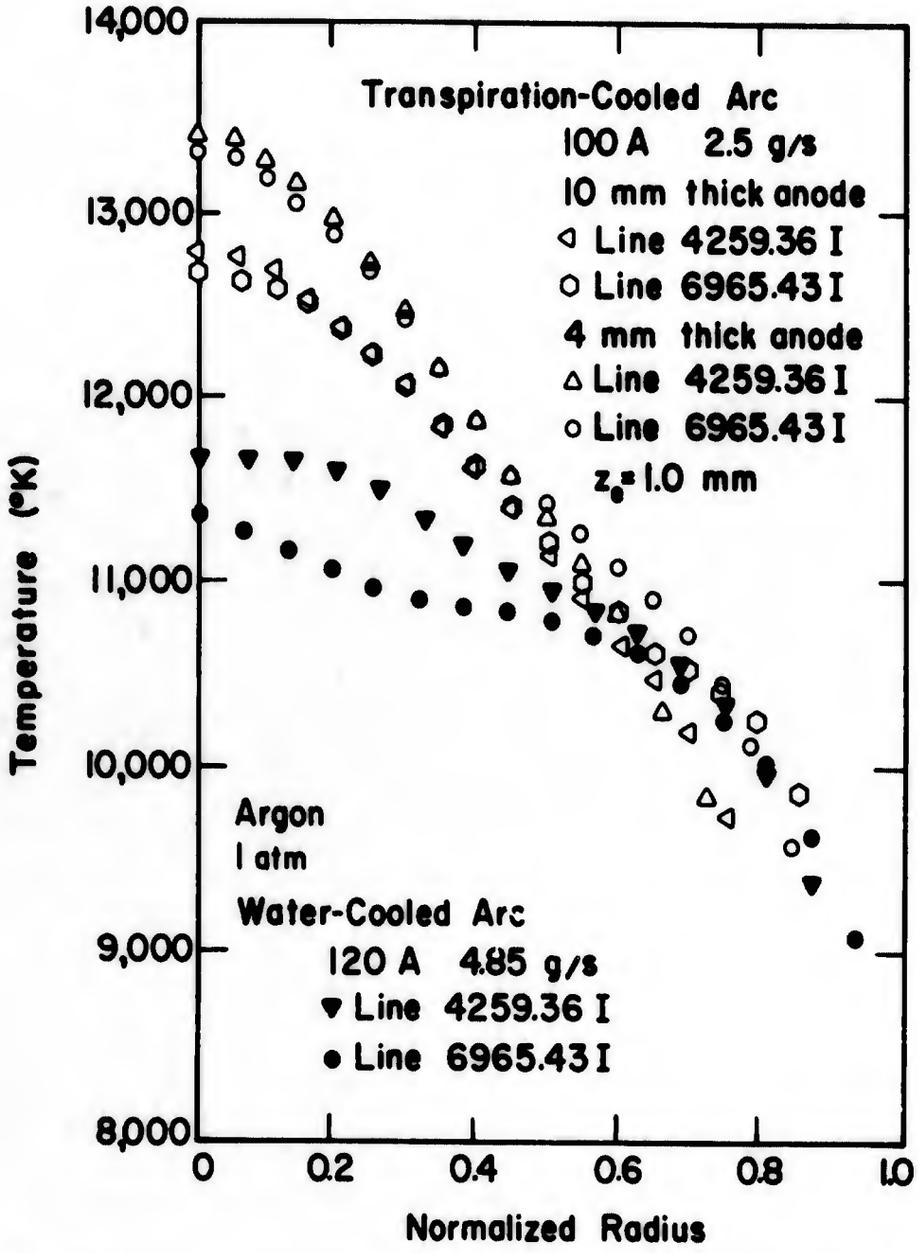

FIG. 34 Comparison of Temperature Profiles of Water-Cooled and Transpiration-Cooled Arcs

as the anode length decreases. The temperature gradient is also much higher in the transpiration-cooled arc, and the arc diameter is smaller. The comparison with the water-cooled cascaded arc should be based on the same current values and the same averaged mass flow density in the anode bore. Because the cascaded arc apparatus has a larger diameter than the transpiration-cooled arc apparatus the comparison parameters are actually $\dot{m}/r_o$, I/r_o and L/r_o. In the cascaded arc all the gas is introduced axially, whereas in the transpiration-cooled arc

$$\dot{m} = \dot{m}_o + \dot{m}_T \qquad\qquad \dot{m}_o = 0.2\ \dot{m}$$

Fig. 35 shows isotherms for the transpiration-cooled arc jets emanating from the 4 mm- and the 10 mm-thick anode. Both jets reach relatively far; this slow decay of the jet temperature may be advantageous in applications where high-temperature jets of considerable length are needed (e.g. cutting, welding, plasma spraying, etc.)

4. CONCLUSIONS AND RECOMMENDATIONS

The experimental results presented herein prove that transpiration cooling is applicable as sole cooling mechanism for arc constrictors. The gas heating in the transpiration-cooled arc section is almost 100% efficient. Peak temperatures tend to be higher and jets to be longer in transpiration-cooled arcs than in comparable water-cooled arcs. The results are also encouraging for a possible development of a completely transpiration-cooled arc plasma generator which could be used without any cooling water.

Two recommendations for improvements of the existing apparatus can be made based on the present experience. The first one is to use a porous material which has a higher

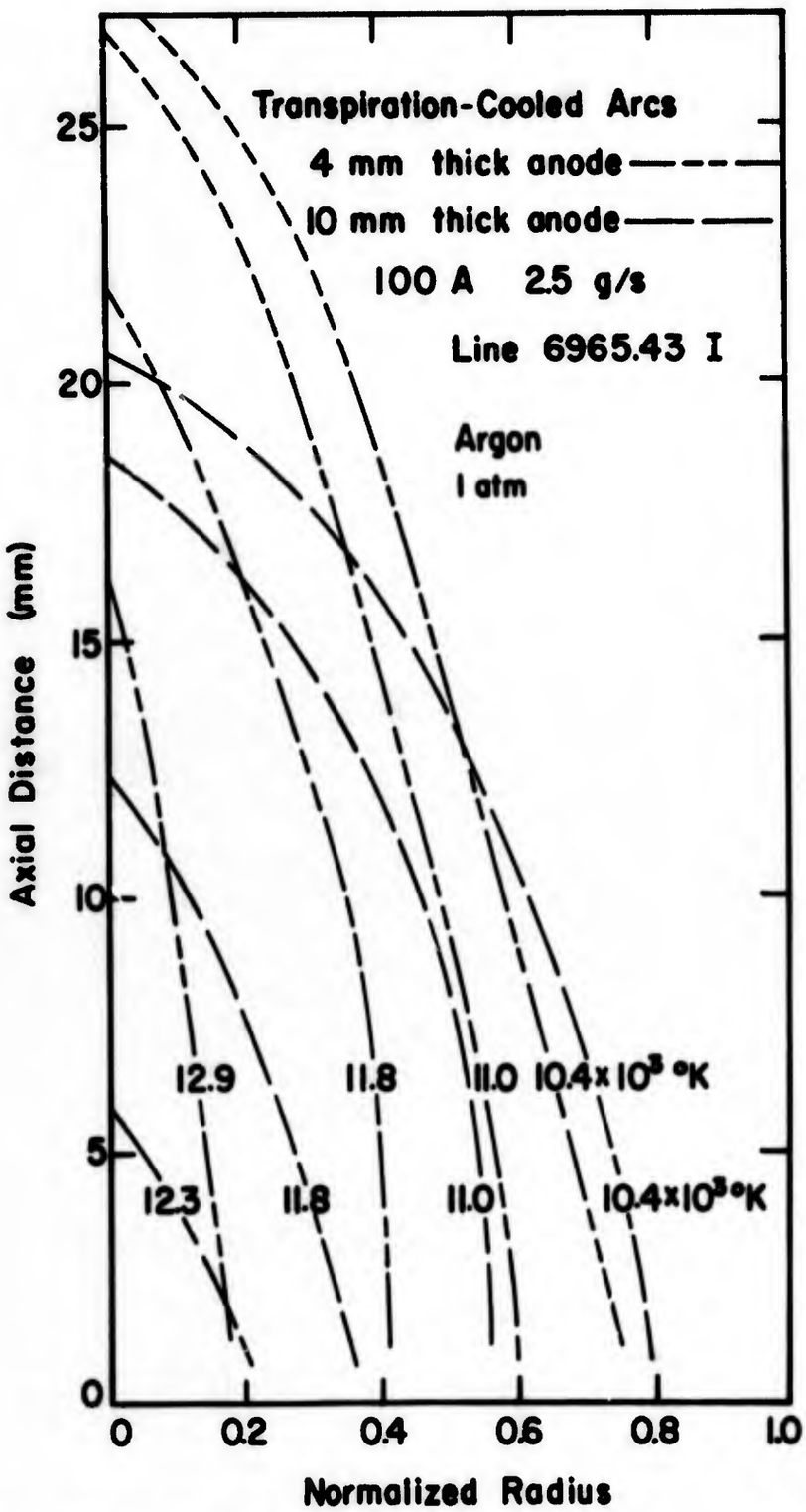

FIG. 35 Isotherms of Transpiration-Cooled Arcs

melting point and a better uniformity in the local permeability distribution. Porous tungsten would be suitable provided the technological difficulties in preparing a segmented tube can be overcome so that the individual segments can be electrically insulated from each other. In this case the plenum chamber would not be segmented, and it might be necessary again to shape the outside tube wall in order to achieve a uniform mass flow distribution in the high flow rate range.

The second recommendation applies only in the case in which high axis temperatures but not maximum efficiency of gas heating is desired. It is to use a material with a high melting point and a high thermal conductivity so that additional radiative cooling of the outer wall surface can be achieved. The application of such an additional cooling mechanism becomes necessary as the radiative heat load on the inner wall surface increases in comparison to the heat load due to conduction. This is so because the predominant cooling effect of the transpirant is to form a protective layer of cool gas on the surface to be cooled; this is frequently called "blanketing". Only a small portion of the enthalpy rise experienced by the transpirant takes place within the porous structure, if no radiative heating is present. Radiation, however, penetrates a non-absorbing protective layer and heats the surface of the porous material so that all the heat exchange with the transpirant must occur within the porous structure. Thus, the mass flow rate required to keep the porous material from melting must be sharply increased which may cause prematurely choked flow conditions. Porous tungsten would probably be a suitable material with which additional radiative cooling of the outer wall surface can be achieved.

REFERENCES

(1) Maecker, H., "Messung und Auswertung von Bogencharakteristiken (Ar, N_2)", Zs. f. Physik, 158, 392 (1960)

(2) Anderson, J.E., Transpiration Cooling of a Constricted Electric-Arc Heater, ARL 66-0517 (August 1966)

(3) Anderson, J.E., Eckert, E.R.G., "Transpiration Cooling of a Constricted Electric-Arc Heater", AIAA J., 5, 699 (April 1967)

(4) Druxes, H., Schmitz, G., Patt, H.J., "Der Einfluss einer radialen Masseneinströmung auf elektrische Lichtbögen", Zs. f. Physik, 203, 192 (1967)

(5) Watson, V.R., "Comparison of Detailed Numerical Solutions with Simplified Theories for the Characteristics of the Constricted-Arc Plasma Generator", Proc. of the 1965 Heat Transfer and Fluid Mechanics Inst., Univ. of Calif., Los Angeles, Calif. (1965)

(6) Tannen, P.D., Experimental Study of a Transpiration-Cooled, Wall Stabilized DC Arc, Air Force Institute of Technology, Wright-Patterson Air Force Base, Ohio, GA/ME/62-6 (August 1962)

(7) Baran, M.F., An Experimental and Theoretical Study of the Wall-Stabilized, Transpiration-Cooled DC Electric Arc, Air Force Institute of Technology, Wright-Patterson Air Force Base, Ohio, Phys/63-2 (August 1963)

(8) Jones, R.N., An Investigation of the Wall-Stabilized, Transpiration-Cooled DC Electric Arc, Air Force Institute of Technology, Wright-Patterson Air Force Base, Ohio, GAW/Mech 64-11 (June 1964)

(9) Eckert, E.R.G., Gross, J.F., "Heat and Mass Transfer", McGraw-Hill Book Company (1963)

(10) Scheidegger, A.E., "The Physics of Flow Through Porous Media", The Macmillan Company, New York (1957)

(11) Bernicker, R.P., "An Investigation of Porous Wall Cooling", ASME Paper 60-WA-233 (1960)

(12) Druzhinen, S.A., "On the Calculation of Internal Heat Exchange During Porous Cooling", Teploenergetika, 9, 73 (September 1961)

(13) Thermophysical Properties Research Center, "Data Book", Vol. 2, Purdue University, Lafayette, Indiana (1964)

(14) Pyron, C.M. Jr., Pears, C.D., "The Mechanisms of Heat Transfer through Porous Materials at Elevated Temperatures", ASME Paper 56-HT-46 (August 1965)

(15) Ahlborn, B., "Zur Bestimmung von Temperatur und Geschwindigkeit der Plasmaströmung aus einen Plasmabrenner", Zs. f. Naturforschg. 20a, 466 (1965)

(16) Rouse, H., Hassan, M.M., "Cavitation-Free Inlets and Contractions", Mech. Eng., Vol. 71, 213 (March 1949)

(17) Cantor, M., Ann. Phys. (N.F.) 47, 399 (1892)

(18) Knöll, H., "Zur Methodik der Bestimmung der maximalen Porenweite von Filtern", Kolloid Zeitschr. 90, [illegible] (1940)

(19) Anderson, J.E., "Local Temperature Variati[illegible]a Transpiration-Cooled Wall due to Radiant Heating", ASME Paper 67-HT-29 (August 1967)

(20) Willgohs, R.H., M.S. Thesis to be published

(21) Runstadler, P.W.,Jr., "The Laminar and Turbulent Flow of an Argon Arc Plasma", AIAA Paper 66-189 (March 1966)

(22) Huesmann, K., Eckert, E.R.G., "Untersuchungen über die laminare Strömung und den Umschlag zur Turbulenz in porösen Rohren mit gleichmässiger Einblasung durch die Rohrwand", to be published

(23) Dutt, M., Spectrometric Measurement of the Temperature Fields in the Jets of Transpiration-and Water-Cooled Argon Arcs, M.S. Thesis, University of Minnesota (1967)

BLANK PAGE

APPENDIX A

RADIAL TEMPERATURE PROFILE WITHIN THE CONSTRICTOR WALL

In order to determine approximately the radial temperature profile in the porous constrictor wall the following assumptions are made:

1) At every point within the wall the temperature of the porous material is equal to the temperature of the transpiring gas.
2) There is no net heat flux through the porous wall; i.e. the heat transferred to the inner wall surface is entirely returned into the main gas stream by the transpirant flow.
3) Within the wall heat conduction of the gas in negligible.
4) The thermal conductivity of the porous material as well as of the transpiring gas are independent of temperature.
5) The problem is strictly one-dimensional.

The equality of wall and gas temperature constitutes a boundary condition at the inner wall surface, provided radiative heating is negligible. For further details on possible deviations from this equality the reader is referred to a recent paper by Anderson (19). At the outer wall surface the gas temperature, T_w, is somewhat lower than the wall temperature, T_R. Within the depth of one or two pores ($\leq$ 1% of the wall thickness) the gas temperature will be practically equal to the wall temperature. Therefore, a jump in the gas temperature equal to $T_R - T_w$ is assumed to occur at the outer wall surface.

From an energy balance over a disc of the height dz and radius $r_o < r < \infty$ Eq(12) in section 3.1.3 is obtained.

Conservation of mass requires that

$$d\dot{m}_T = 2\pi r dz\ \rho \frac{dr}{dt} = \text{const}\ (r) \tag{A1}$$

Using Eq(14) and Eq(15) one obtains

$$\frac{d}{dr}\left(r \frac{dT}{dr} + n \times T\right) = 0 \tag{A2}$$

Integration yields

$$r \frac{dT}{dr} + n \times T = n \times K_1 \tag{A3}$$

Rearranging yields

$$\frac{dT}{T-K_1} = -n \times \frac{dr}{r}$$

and a second integration yields the general equation for the radial temperature profile

$$\ln \frac{T_2 - K_1}{T_1 - K_1} = - n \times \ln \frac{r_2}{r_1}$$

or

$$\frac{T_2 - K_1}{T_1 - K_1} = \left(\frac{r_1}{r_2}\right)^{n \times} \tag{A4}$$

which holds in the plenum chamber ($r > R_z$) as well as within the porous wall ($r_o \leq r \leq R_z$).

In the plenum chamber the following boundary conditions

apply:

$$\text{for } r_2 \to \infty \qquad T_2 \to T_\infty$$

$$\text{for } r_1 = R_z \qquad T_1 = T_w$$

thus, Eq(18) is obtained.

Since the plenum chamber has a finite diameter it is interesting to determine how far away from the outer constrictor surface the heat flux by conduction in the gas decreases to 1% of its original value at that surface. By differentiating Eq(18) with respect to r one obtains

$$\frac{(dT/dr)_r}{(dT/dr)_{R_z}} = \frac{R_z}{r}^{n_g x + 1} \tag{A5}$$

Since for the experiments reported in this paper $n_g x > 1$ the maximum plenum chamber radius necessary for $n_g x = 1$ is 10 R_z which is slightly less than its actual radius.

For the porous wall the following boundary conditions apply to Eq(A4):

$$\text{at } r_2 = R_z \qquad T_2 = T_R$$

$$\text{at } r_1 = r_o \qquad T_1 = T_o$$

thus

$$\frac{T_R - K_1}{T_o - K_1} = \left(\frac{r_o}{R_z}\right)^{n x} \tag{A6}$$

K_1 can be either determined from the condition for $R_z \to \infty$ ($T_R = T_\infty$) or by matching the heat fluxes at the outer wall sur-

face according to Eq(17).

By differentiating Eqs(18) and (A6) with respect to r and substituting the result into Eq(17) one obtains

$$K_1 = T_\infty$$

and thus, Eq(A6) becomes Eq(19).

APPENDIX B

MATCHED TUBE SHAPE

The matched tube shape, that is the outside radius R_z as a function of z, which is necessary to achieve a uniform transpirant mass flow distribution for one given parameter setting of the arc can be calculated from Eq(20) in section 3.1.4.

The constants A_1, A_2, A_3, and B are defined in Eqs (21) through (24), n and x in Eqs(14) and (15). In Eq(20) T_R, R_z, and p_i are functions of z whereas x shall be made a constant with respect to z. The outer wall surface temperature T_R can be eliminated by substituting Eq(25) in Eq(20). Rearranging yields

$$A_1 \, x \ln\left(\frac{R_z}{r_o}\right) + A_2 \, (T_o - T_\infty)\left[1 - \left(\frac{r_o}{R_z}\right)^{n\,x}\right]$$

$$+ A_3 \, (T_o - T_\infty)^2\left[1 - \left(\frac{r_o}{R_z}\right)^{2n\,x}\right] + B\,\frac{T_\infty}{r_o}\left(1 - \frac{r_o}{R_z}\right)x^2 \qquad \text{(B1)}$$

$$+ B \, (T_o - T_\infty)\,\frac{1}{r_o}\left[1 - \left(\frac{r_o}{R_z}\right)^{n\,x+1}\right]\frac{x^2}{n\,x+1}$$

$$- \frac{p_R^{\,2} - p_i^{\,2}}{p_s^{\,2}} = 0$$

If x is independent of z then T_o will also be independent of z in the thermally fully developed range. The influence of the pressure gradient on thermodynamic and transport properties of the transpirant is assumed to be negligible. Under this assumption the constant terms in Eq(B1) are separated from those which depend on z.

$$A_1 \, x \ln\left(\frac{R_z}{r_o}\right) - B\,\frac{T_\infty}{R_z}\,x^2 - (T_o - T_\infty)\left(\frac{r_o}{R_z}\right)^{n\,x}\left[A_2 + A_3\,(T_o - T_\infty)\left(\frac{r_o}{R_z}\right)^{n\,x} + B\,\frac{1}{R_z}\,\frac{x^2}{n\,x+1}\right]$$

$$+\frac{p_i^2}{p_s^2} = \frac{p_R^2}{p_s^2} - (T_o - T_\infty)\left[A_2 + A_3\,(T_o - T_\infty) + B\,\frac{1}{r_o}\,\frac{x^2}{n\,x+1}\right] - B\,T_\infty\,\frac{x^2}{r_o} = K_p \qquad \text{(B2)}$$

K_p is defined by Eq(B2), independent of z and strongly dependent on p_R. Rather than calculating K_p it is advantageous to give it implicitly by specifying the downstream boundary conditions at $\frac{z}{L} = 1$:

$$R_z(L) = R_1 \qquad\qquad p_i(L) = p_1$$

Eq(B2) then takes the form

$$\frac{p_i^2 - p_1^2}{p_s^2} = A_1\,x\,\ln\left(\frac{R_1}{R_z}\right) + B\,\frac{T_\infty}{R_1}\,x^2\left(\frac{R_1}{R_z} - 1\right) + (T_o - T_\infty)\left(\frac{r_o}{R_1}\right)^{n\,x}\left\{A_2\left[\left(\frac{R_1}{R_z}\right)^{n\,x} - 1\right] + A_3\,(T_o - T_\infty)\left(\frac{r_o}{R_1}\right)^{n\,x}\left[\left(\frac{R_1}{R_z}\right)^{2n\,x} - 1\right] + \frac{B}{R_1}\,\frac{x^2}{n\,x+1}\left[\left(\frac{R_1}{R_z}\right)^{n\,x+1} - 1\right]\right\} \qquad \text{(B3)}$$

If the whole constrictor is at room temperature T_∞ Eq(B3) reduces to

$$\frac{p_i^2 - p_1^2}{p_s^2} = A_1 \times \ln\left(\frac{R_1}{R_z}\right) + B \, x^2 \, T_\infty \left(\frac{1}{R_z} - \frac{1}{R_1}\right) \qquad \text{(B4)}$$

For small values of x, i.e. in the low flow rate range, the second term on the right hand side of Eq(B4) can be neglected, or in other words, the pressure drop across the wall is approximately given by Darcy's law, hence

$$R_z(z) = R_1 \exp\left(\frac{p_1^2 - p_i^2\,(z)}{A_1 \times p_s^2}\right) \qquad \text{(B5)}$$

The shape of the tube described in section 3.1.5 has been calculated from Eq(B5). A higher degree of accuracy short of solving Eq(B3) implicitly for $R_z(z)$ is achieved by using the approximation

$$\left(\frac{R_1}{R_z}\right)^{n \times} - 1 \approx n \times \ln\left(\frac{R_1}{R_z}\right)$$

Eq(B3) then can be brought into the form of Eq(26). The parameter K* depends on the transpirant mass flow rate and the inner wall surface temperature. Eq(27) allows to estimate the influence these parameters have on the uniformity of the transpirant flow rate distribution for a given axial pressure distribution $p_i(z)$.

BLANK PAGE

APPENDIX C

AXIAL PRESSURE DISTRIBUTION

As pointed out in Section 3.1.6, the axial pressure distribution can be calculated from Eq(28). By introducing the perfect gas law

$$p = \rho RT \quad \text{and} \quad \dot{w} = \rho v$$

one obtains

$$\dot{w}\, d\left(\frac{\dot{w}\, RT}{p}\right) + dp = 0$$

Executing the differentiation and rearranging yields Eq(29). In the thermally fully developed region the radial temperature distribution in the flow duct stays axially constant, and thus

$$\frac{d(\ln RT)}{dz} = 0$$

Eq(29)then reduces to

$$\frac{d(\dot{w}^2)}{d(p^2)} = \left(\frac{\dot{w}}{p}\right)^2 - \frac{1}{RT} \qquad \text{(C1)}$$

Integration of Eq(C1) yields

$$\dot{w}^2 RT = p^2 \ln \frac{C}{p^2}$$

In order to find the integration constant C it is useful to introduce the downstream boundary condition

$$p = p_1 \quad \text{and} \quad \dot{w} = \dot{w}_1 = \frac{\dot{m}_o + \dot{m}_T}{A}$$

One obtains

$$\ln C = \frac{\dot{w}_1^2 RT}{p_1^2} + \ln p_1^2$$

and hence Eq(31). It is possible to take the radial temperature distribution approximately into account by using the two channel arc model discussed in Section 3.1.7. Eq(31) then holds for each channel separately:

$$\left(\frac{p_1 \dot{w}_c}{p \dot{w}_{1c}}\right)^2 = 1 + \frac{2p_1^2}{R_c T_c \dot{w}_{1c}^2} \ln\left(\frac{p_1}{p}\right) \qquad \text{(C2)}$$

$$\left(\frac{p_1 \dot{w}_h}{p \dot{w}_{1h}}\right)^2 = 1 + \frac{2p_1^2}{R_h T_h \dot{w}_{1h}^2} \ln\left(\frac{p_1}{p}\right) \qquad \text{(C3)}$$

The subscript h refers to the hot core and the subscript c to the cold gas envelope. The pressure p is a function of z or implicitly of $\dot{w}_c$ and $\dot{w}_h$ respectively. The mass flow densities $\dot{w}_c$ and $\dot{w}_h$ as functions of z can be obtained from measurable quantities in the following way using Eq(32) through (36) given in Section 3.1.7. Combining Eqs(32) and (36) one finds

$$A_h = \frac{I}{\sigma E} \quad \text{and} \quad A_c = A - \frac{I}{\sigma E} \qquad \text{(C4)}$$

Combining Eqs(34) and (35) and by introducing (C4) one obtains

$$\frac{EIL}{\dot{m}_T} = \frac{\dot{w}_c (A - \frac{I}{\sigma E}) h_c + \dot{w}_h \frac{I}{\sigma E} h_h}{\dot{m}} \qquad \text{(C5)}$$

Similarly Eq(33) becomes

$$\dot{m} = \dot{w}_c \left(A - \frac{I}{\sigma E}\right) + \dot{w}_h \frac{I}{\sigma E} \tag{C6}$$

From Eqs(C5) and (C6) one can determine the two unknowns $\dot{w}_c$ and $\dot{w}_h$ as functions of measurable quantities.

$$\dot{w}_h = \frac{\dot{m}}{A_h^*} \tag{C7}$$

$$\dot{w}_c = \frac{\dot{m}}{A_c^*} \tag{C8}$$

$$A_h^* = \frac{I}{\sigma E} \frac{h_h - h_c}{\langle h \rangle - h_c} \tag{C9}$$

$$A_c^* = \frac{\left(A - \frac{I}{\sigma E}\right)(h_h - h_c)}{h_h - \langle h \rangle} \tag{C10}$$

In Eqs(C7) and (C8) $\dot{w}_h$ and $\dot{w}_c$ are functions of z; their boundary values at the downstream end of the constrictor are known:

$$\dot{w}_{1h} = \frac{\dot{m}_o + \dot{m}_T}{A_h^*} \tag{C11}$$

$$\dot{w}_{1c} = \frac{\dot{m}_o + \dot{m}_T}{A_c^*} \tag{C12}$$

If Eqs(C8) and (C12) are introduced into Eq(C2) and likewise Eqs(C7) and (C11) into Eq(C3), the quotient of the two resulting equations yields

$$A_c^{*2} R_h T_h = A_h^{*2} R_c T_c \qquad (C13)$$

Substituting Eq(C9) and (C10) into Eq(C13) one obtains Eq(37). The purpose of this equation is discussed in section 3.1.7. In order to obtain the axial pressure distribution Eq(37) is used to eliminate the term $I/\sigma E$ from Eq(C9) which is then substituted into Eq(C7) and (C11). The resulting equations are introduced into Eq(C3) which thereby becomes Eq(38) after rearranging. If one has a reliable measurement of the axial pressure profile for a given arc one can determine B from it using Eq(39). If one further has a plot of B vs $EIL/\dot{m}_T$ and AE/I vs $EIL/\dot{m}_T$ one can find the temperatures T_h and T_c.

UNCLASSIFIED

Security Classification

DOCUMENT CONTROL DATA - R&D

(Security classification of title, body of abstract and indexing annotation must be entered when the overall report is classified)

1. ORIGINATING ACTIVITY (Corporate author)
The University of Minnesota
Instute of Technology
Department of Mechanical Engineering
Minneapolis, Minnesota 55455

2a. REPORT SECURITY CLASSIFICATION
Unclassified

2b. GROUP

3. REPORT TITLE

EXPERIMENTAL STUDY OF A TRANSPIRATION-COOLED, CONSTRICTED ARC

4. DESCRIPTIVE NOTES (Type of report and inclusive dates)
Scientific. Interim.

5. AUTHOR(S) (Last name, first name, initial)
G. G. Gruber, E. Pfender, E. R. G. Eckert

6. REPORT DATE	7a. TOTAL NO. OF PAGES	7b. NO. OF REFS
February 1968	110	23

8a. CONTRACT OR GRANT NO.
AF 33(657)-7380 and F33615-67-C-1353

b. PROJECT NO.
7063

c. DoD Element 6144501F

d. DoD Subelement 681307

9a. ORIGINATOR'S REPORT NUMBER(S)

9b. OTHER REPORT NO(S) (Any other numbers that may be assigned this report)
ARL 68-0023

10. AVAILABILITY/LIMITATION NOTICES
1. This document has been approved for public release and sale; its distribution is unlimited.

11. SUPPLEMENTARY NOTES
TECH OTHER

12. SPONSORING MILITARY ACTIVITY
Aerospace Research Laboratories (ARN)
Office of Aerospace Research
Wright-Patterson Air Force Base, Ohio 45433

13. ABSTRACT

In this report, experimental work with a transpiration-cooled arc is described. An apparatus has been developed which verifies the analytical prediction that an electric arc can be confined and constricted by an entirely transpiration-cooled wall. The arc has been operated in argon atmosphere with currents ranging from 35 to 160 A. A porous ceramic (ALSIMAG 447) tube has been used as constrictor material. The investigations encompass basic trends of the arc, the constrictor performance, and the flow behavior with their mutual interactions. By introducing some simplifying assumptions, a number of formulae, containing observable quantities, have been derived which are useful for the representation of experimental results and which facilitate their comparison with analytical studies. Three different types of arc characteristics are plotted and used for a description of the transpiration-cooled arc. Results of spectrometric temperature measurements in the arc jet using the 5 mm ID constrictor tube are also included.

Details of an improved transpiration-cooled arc arrangement based on previous experience, are described and some preliminary results obtained with this apparatus are reported.

DD FORM 1 JAN 64 1473

UNCLASSIFIED

Security Classification

UNCLASSIFIED

Security Classification

14. KEY WORDS	LINK A		LINK B		LINK C	
	ROLE	WT	ROLE	WT	ROLE	WT
TRANSPIRATION-COOLED ARC ELECTRIC ARC ARGON ARC CONSTRICTED ARC						

INSTRUCTIONS

1. ORIGINATING ACTIVITY: Enter the name and address of the contractor, subcontractor, grantee, Department of Defense activity or other organization *(corporate author)* issuing the report.

2a. REPORT SECURITY CLASSIFICATION: Enter the overall security classification of the report. Indicate whether "Restricted Data" is included. Marking is to be in accordance with appropriate security regulations.

2b. GROUP: Automatic downgrading is specified in DoD Directive 5200.10 and Armed Forces Industrial Manual. Enter the group number. Also, when applicable, show that optional markings have been used for Group 3 and Group 4 as authorized.

3. REPORT TITLE: Enter the complete report title in all capital letters. Titles in all cases should be unclassified. If a meaningful title cannot be selected without classification, show title classification in all capitals in parenthesis immediately following the title.

4. DESCRIPTIVE NOTES: If appropriate, enter the type of report, e.g., interim, progress, summary, annual, or final. Give the inclusive dates when a specific reporting period is covered.

5. AUTHOR(S): Enter the name(s) of author(s) as shown on or in the report. Enter last name, first name, middle initial. If military, show rank and branch of service. The name of the principal author is an absolute minimum requirement.

6. REPORT DATE: Enter the date of the report as day, month, year, or month, year. If more than one date appears on the report, use date of publication.

7a. TOTAL NUMBER OF PAGES: The total page count should follow normal pagination procedures, i.e., enter the number of pages containing information.

7b. NUMBER OF REFERENCES: Enter the total number of references cited in the report.

8a. CONTRACT OR GRANT NUMBER: If appropriate, enter the applicable number of the contract or grant under which the report was written.

8b, 8c, & 8d. PROJECT NUMBER: Enter the appropriate military department identification, such as project number, subproject number, system numbers, task number, etc.

9a. ORIGINATOR'S REPORT NUMBER(S): Enter the official report number by which the document will be identified and controlled by the originating activity. This number must be unique to this report.

9b. OTHER REPORT NUMBER(S): If the report has been assigned any other report numbers *(either by the originator or by the sponsor)*, also enter this number(s).

10. AVAILABILITY/LIMITATION NOTICES: Enter any limitations on further dissemination of the report, other than those imposed by security classification, using standard statements such as:

(1) "Qualified requesters may obtain copies of this report from DDC."

(2) "Foreign announcement and dissemination of this report by DDC is not authorized."

(3) "U. S. Government agencies may obtain copies of this report directly from DDC. Other qualified DDC users shall request through _____."

(4) "U. S. military agencies may obtain copies of this report directly from DDC. Other qualified users shall request through _____."

(5) "All distribution of this report is controlled. Qualified DDC users shall request through _____."

If the report has been furnished to the Office of Technical Services, Department of Commerce, for sale to the public, indicate this fact and enter the price, if known.

11. SUPPLEMENTARY NOTES: Use for additional explanatory notes.

12. SPONSORING MILITARY ACTIVITY: Enter the name of the departmental project office or laboratory sponsoring *(paying for)* the research and development. Include address.

13. ABSTRACT: Enter an abstract giving a brief and factual summary of the document indicative of the report, even though it may also appear elsewhere in the body of the technical report. If additional space is required, a continuation sheet shall be attached.

It is highly desirable that the abstract of classified reports be unclassified. Each paragraph of the abstract shall end with an indication of the military security classification of the information in the paragraph, represented as *(TS), (S), (C), or (U)*.

There is no limitation on the length of the abstract. However, the suggested length is from 150 to 225 words.

14. KEY WORDS: Key words are technically meaningful terms or short phrases that characterize a report and may be used as index entries for cataloging the report. Key words must be selected so that no security classification is required. Identifiers, such as equipment model designation, trade name, military project code name, geographic location, may be used as key words but will be followed by an indication of technical context. The assignment of links, rules, and weights is optional.

UNCLASSIFIED

Security Classification